Injectable and Functionalized Tough Porous Hydrogels for Vocal Fold Repair

Sareh Taheri

Department of Mechanical Engineering
McGill University
Montréal, Canada

May 2022

A thesis submitted to the McGill University
in partial fulfillment of the requirements for the degree of
Doctor of Philosophy

To my Parents, Farah & Aziz

To my lovely niece Hana

To the victims of flight PS752, who will never be forgotten· · ·

Abstract

Many tissues in the human body are porous and tough. One treatment strategy for tissue repair and regeneration is the injection of biomaterials in the vicinity of the injured site. Most existing injectable biomaterials degrade over a short period of time and necessitate repeated injections, due in part to enzymatic reactions and fracture under mechanical load. Most biomaterials lack vascularization and are not perfusable, which hampers the recruitment of native cells in situ and leaves the cells in deeper layers starving for oxygen. It is postulated that injectable hydrogels that possess both a high permeability and mechanical toughness would improve outcomes in regenerative medicine. The synthesis of such materials has remained a long-standing challenge. Tissue-specific bioreactors provide a platform to investigate the long term outcome of engineered bio-materials in a bio-mimetic environment prior to animal and clinical studies. The mechanical stability and cellular response of new biomaterials can be investigated within bioreactors under mimetic bio-mechanical stimuli.

The extracellular matrix micro-structure such as void geometry and interconnectivity defines the hydraulic permeability of soft bio-materials and tissues. The hydraulic permeability measures fluid motion, thereby regulating nutrients delivery to encapsulated cells, and promoting cell proliferation and migration within the interconnected pores. The hydraulic permeability of hydrogels is thus an important feature that should be precisely measured and

monitored during scaffold development.

In the present study, novel injectable porous double-network hydrogels were designed and fabricated by orchestrating stepwise gelation and phase separation processes. The new gels feature porous double-networks, thereby termed PDNs. These gels improve upon previously reported injectable hydrogels that consist of either nanoporous or preformed porous networks. The fracture toughness and stretchability of PDNs is significantly better than that of nanoporous or porous single-network gels. PDNs are cytocompatible and support cell spreading and trafficking owing to their highly porous matrices which enable rapid media perfusion.

They can be easily delivered through fine needles and incorporated into 3D cell culture perfusion systems with complex mechanical loadings, such as microfluidic chips and bioreactors. Such perfusable hydrogels can support cell survival in organ-sized scaffolds with dimensions beyond 60 mm, the largest value reported so far in the literature. PDNs also possess great mechanical stability, and maintain their physical integrity when tested in biomimetic perfusion bioreactors ($>$ 6,000,000 cycles at 120 Hz), despite the presence of defect-like pores. The cells encapsulated within PDNs secrete more collagen I under dynamic loading, demonstrating their great transitional potential for vocal fold engineering as collagen is one of the main components of the extra cellular matrix. The novel method is generalizable to other material systems.

A novel setup was designed and fabricated to systematically measure the hydraulic permeability of PDNs. The setup was made of a syringe pump, pressure transducer and a 3D-printed customized t-shaped adaptor. The perfusion rate was monitored so that the shear stresses within the interior pores were negligibly small. The PDNs permeability was

then calculated using Darcy's law and the the obtained values were compared with that of other existing hydrogels and soft tissues. The permeability of PDNs was found to be within the range between 10^{-14} and 10^{-12} m^2, which is significantly higher than those of existing biomaterials.

The present study yielded new material systems and methods to generate porous double-network hydrogels combining of permeability, toughness, cytocompatibility, and injectability. The original meaurment methods offer a systematic platform to precisely measure the permeability of soft scaffolds. Overall, the described material systems and method may create new opportunities within regenerative medicine, and serve as biomimetic in vitro 3D cell culture platforms for a broad range of applications.

Résumé

La plupart des tissus du corps humain sont poreux et tenaces. Une stratégie possible de traitement pour la réparation et la régénération des tissus est l'injection de biomatériaux à proximité du site lésé. Mais, la plupart des biomatériaux injectables existants se dégradent sur une courte période de temps et nécessitent des ré-injections périodiqes. Ceci et du à la réaction enzymatique et aussi la fracture sous une charge mécanique élevée. De plus, les biomatériaux manquent souvent de vascularisation et ne sont pas perfusables, ce qui entrave le recrutement des cellules natives et laisse les cellules des couches plus profondes affamées d'oxygène. Il est postulé que des hydrogels injectables qui possèdent à la fois une perméabilité et une ténacité élevées auraint un impact certain dans la domain de la médecine régénérative et leus synthsis constitute, défi de longue durée.

La microstructure de la matrice extracellulaire, par exemple la géométrie des pores et l'interconnectivité, détermine la perméabilité hydraulique. Des biomatériaux, c'est a due leur résistance au mouvement de fluides. Le mouvement du fluide dans les hydrogels régule l'apport de nutriments aux cellules encapsulées et peut favoriser la prolifération cellulaire et la migration dans les pores interconnectés. Par conséquent, la perméabilité hydraulique des hydrogels est une caractéristique importante qui doit être mesurée avec précision.

Un nouvel hydrogel poreux injectable à double réseau a été conçu et fabriqué, sur un

processus de gélification et de séparation de phase par étapes. Les nouveaux gels sont dotés de réseaux poreux et doubles, appelés PDN. Ces gels améliorent le propriétés des hydrogels injectables précédemment signalés, qui sont constitués de réseaux poreux nanoporeux ou préformés. Les PDN sont résistants et leur ténacité à la rupture et leur extensibilité sont également supérieures à ceux de leurs homologues nanoporeux ou poreux à réseau unique. Les PDN sont cytocompatibles et soutiennent la propagation et le trafic cellulaires en raison de leurs matrices très poreuses qui permettent une perfusion rapide des milieux.

Ils peuvent être facilement injecté à l'aide d'aiguilles fines et incorporés dans des systèmes de perfusion de culture cellulaire 3D avec des charges mécaniques complexes, telles que des puces microfluidiques et des bioréacteurs. De tels hydrogels perfusables peuvent soutenir la survie cellulaire dans des échafaudages de la taille d'un organe d'une dimension supérieure à 60 mm, ce qui constitue une nette amélioration par apport aux gel non-poreux. Les PDN présentent également une grande stabilité mécanique et maintiennent leur intégrité physique lorsqu'ils sont testés dans des bioréacteurs de perfusion phonomimétiques (>6 million cycles à 120 Hz) malgré la présence de pores défectueux. Les cellules encapsulées dans les PDN ont également sécrété plus de collagène I dans un environnement sous-dynamique, démontrant leur potentiel de régénération. Notre méthode est également généralisable à d'autres systèmes de matériaux.

Une nouvelle méthode a été conçue pour mesurer la perméabilité hydraulique des PDN. La configuration consisté en une pompe à seringue, un transducteur de pression et un adaptateur personnalisé en forme de T en 3D. Le taux de perfusion a été surveillé de sorte que le nombre de Reynolds des pores intérieurs était suffisamment petit. La perméabilité des PDN a ensuite été calculée à l'aide de la loi de Darcy et les valeurs obtenues ont été comparées à d'autres

hydrogels et tissus mous existants. La perméabilité des PDN s'est avérée se situer dans la plage de 10^{-14} à 10^{-12} m^2, ce qui est significativement plus élevé que celui des biomatériaux traditionnels.

Les résultats de cette étude ont révéle de nouveaux systèmes de matériaux et une méthode pour générer des hydrogels poreux à double réseau combinaux de perméabilité, ténacité, cytocompatibilité, et d'injectabilité. La montage utilisé de fournit également une plate-forme systématique pour mesurer avec précision la perméabilité des hydrogel poreux. Dans l'ensemble, les systèmes de matériaux et la méthode décrits peuvent créer de nouvelles opportunités pour eu médecine régénérative et servir de plates-formes de culture cellulaire 3D biomimétique in vitro pour un large éventail d'applications.

Contributions and Claims of Originality

In this section a list of journal articles and conference proceedings published by the author during her doctoral studies is presented in chronological order.

- **Peer-reviewed journal articles**

1. **Taheri, S.**, Bao, G., He, Z., Mohammadi, S., Ravanbakhsh, H., Lessard, L., Li, J. and Mongeau, L., 2022. "Injectable, Pore-Forming, Perfusable Double-Network Hydrogels Resilient to Extreme Biomechanical Stimulations", *Advanced Science* 9(2), p.2102627. ***Contributions***: S.T. and G. B contributed equally to this work. S.T. and G. B, developed the materials and method for the hydrogels, carryied out the experiments, conducted the numerical simulations, analyzed the results and wrote the manuscript, with inputs from Z.He, S.M, H.R, L.R, J.L, L.M.

2. Mohammadi, S., Ravanbakhsh, H., **Taheri, S.**, Bao, G. and Mongeau, L., 2022. "Immunomodulatory microgels support pro-regenerative macrophage activation and attenuate fibroblast collagen synthesis", *Advanced Healthcare Materials*, p.2102366. ***Contributions***: Taheri, S contributed in carrying out the experiments and analyzing the Micro-CT results.

- **Patents and disclosures**

1. **Taheri, S.**, Bao, G., Li, J., and Mongeau, L., “Porous double-network hydrogel”, U.S. Provisional Patent No. 63/278,288, 2021.

- **Selected conference presentations**

1. **Taheri, S.**, Bao, G., Mohammadi, S., and Mongeau, L., "Injectable, Pore-Forming, Perfusable Double-Network Hydrogels Resilient to Extreme Biomechanical Stimulations", TERMIS, Canada, Toronto, July, 2022.

2. **Taheri, S.**, Bao, G., Mohammadi, S., and Mongeau, L., " Injectable Porous and Tough Hydrogels for Vocal Fold Repair", The Voice Foundation’s 51st Annual Symposium: Care of the Professional Voice, Philadelphia, USA, June. 2022.

3. Mohammadi, S., Ravanbakhsh, H., **Taheri, S.**, Bao, G. and Mongeau, L., "Sustained Release of IL-10 from Laponite-Loaded Microgels Modulate Macrophage Activation and Attenuate Vocal Fold Fibroblast Collagen Synthesis", The Voice Foundation’s 51st Annual Symposium: Care of the Professional Voice, Philadelphia, USA, June. 2022.

4. **Taheri, S.**, Bao, G., Mohammadi, S., and Mongeau, L., " Injectable porous double-network hydrogels with vocal fold-mimetic viscoelasticity", TERMIS World Conference, Maastricht, Netherlands, Nov. 2021.

5. Mohammadi, S., **Taheri, S.**, and Mongeau, L., "Effects of macrophage population on vocal fold fibroblasts regenerative behavior", TERMIS World Conference, Maastricht, Netherlands, Nov. 2021.

6. Ravanbakhsh, H., Mohammadi, S., Bao, G., Tang, G., **Taheri, F.**, Reyes, A., and Mongeau, L., "Microfluidic-based Fabrication of Hydrogel Microspheres with a Controllable

Size Using an Oil-free Approach", TERMIS World Conference, Maastricht, Netherlands, Nov. 2021.

7. **Taheri, S.**, Latifi, N., He, Z., and Mongeau, L., "Phonatory characteristics and cellular behavior of a perfusion vocal fold bioreactor", 35th Annual Meeting of the Canadian Biomaterials Society (CBS 2019), Quebec City, Canada, May. 2019.

Acknowledgements

First and foremost, I would like to express my deep and sincere gratitude to my Ph.D. supervisor, Prof. Luc Mongeau, whose guidance and support made this work possible. He convincingly guided and encouraged me to be professional and do the right thing even when the road got tough. He provided an environment in which I earned several new skills, learned many new concepts, followed ambitious interdisciplinary research objectives, collaborated with many researchers and graduate students with different backgrounds, and became experienced in leadership and team work. Thank you for all the supports you have given me over the course of my studies.

I would also like to extend my special thanks to Prof. Larry Lessard (School of Mechanical engineering, McGill Univeristy) for his kind guidance, support and motivation throughout my studies. I am also deeply thankful to Prof. Jianyu Li (School of Mechanical engineering, McGill Univeristy) for many constructive discussions and meetings on various aspects of my studies, particularly his valuable comments on our manuscript in *Advanced Science*.

Special thanks to my labmate, Guangyu Bao for his constructive criticism, suggestions, positive vibes and friendship throughout my studies. Working with him has always been one of the most rewarding and delightful experiences I have ever had. I would also like to thank the members of McGill Biomechanics Research Laboratory, Huijie Wang, Neda Latifi,

Zhengdong Lei, Mostafa Najafiyazdi, Hossein Ravanbakhash, Sepideh Mohammadi, Sara Nejati, Aria Hajimohammadi, Rayane Ait Oubahou, Alicia Reyes, Qiman Gao, Pooya Saberi, Alda Profka, Zixin He, Mitchell Strong, and Abigail Vikstrom. Being surrounded with such talented scientists was undoubtedly a great source of motivation. I would also like to thank all the people I met at McGill University and more generally in Montréal during this period of time; they made me grow as a person.

Words cannot express how grateful I am to my beloved mother, Farah, my dear father, Aziz, my lovely sister, Safoora, and my wonderful brother, Hossein, for their unconditional love, understanding and encouragement throughout the course of my life. The completion of this thesis would never have been possible without their constant support. Special thanks go to my lovely brother, Mohammadnaser, who has been always there to lend an ear to my concerns and complains. I am also thankful for his scientific recommendations over the course of my PhD. I would also like to thank my dear friend, Amir, who witnessed my progress in the PhD program and was always there to support and motivate me.

Lastly, I would like to thank, the National Institutes of Health (NIH grants: ROI DC005788 and ROI DC018577, Mongeau PI), Natural Sciences and Engineering Research Council (NSERC), McGill Engineering Doctoral Award (MEDA) and Optimisation du Potentiel Synergique et Interinstitutionnel D'équipes Interdisciplinaires Académiques Novatrices (OPSIDIAN). The content is solely the responsibility of the authors and does not necessarily represent the social views of the National Institutes of Health.

Abbreviations

2D two dimensional

3D three dimensional

APS Ammonium persulfate

BSA bovine serum albumin

CCM cell culture medium

CS chitosan

DMEM Dulbecco's Modified Eagle Medium

DN double-network

ECM extracellular matrix

FBS fetal bovine serum

FSI fluid-structure interaction

GC glycol chitosan

GelMA Gelatin-methacryloyl

GY glyoxal

HA hylauronic acid

HVFF human vocal fold fibroblast

LP lamina propria

MEM minimum essential medium

NDN nanoporous double-network hydrogel

NSN non-porous single-network

PAAm Polyacrylamide

PBS phosphate-buffered saline

PC pure chitosan

PDN porous double-network

PEG Polyethylene Glycol

PNIPAAm Poly(N-isopropylacrylamide)

PS phosphate solution

PSN porous single-network

SC sodium bicarbonate

SEM scanning electron microscopy

TEMED tetramethylethylenediamine

VF vocal fold

µCT micro-computed tomography

Contents

List of Figures

List of Tables

CHAPTER 1

Introduction

This chapter starts with a description of thesis organization and a brief summary of each chapter. It is then followed by a description of the problem of interest and a comprehensive review of the literature. The challenges and barriers that hamper the functionality of existing hydrogels in tissue engineering are discussed and the hypothesis underlying the proposed project to address the need for discoveries issues is explored. The sentences in quotations are verbatim from the author's publication (reference [1]).

1.1 Thesis organization

In general, this thesis includes five consecutive chapters namely introduction, methods, results and discussion, and conclusion. Chapter 1 focuses on the motivation behind studying the methodologies to develop injectable porous and tough bio-materials along with a deep survey of the existing literature. The current challenges in the design of tough and porous biomaterials are described and solutions to tackle those obstacles are proposed. The literature review is

divided into four main subsections. In the first part, the injectable hydrogels components, cross-linking chemistry, mechanical properties and biological performance are described. Existing pore-forming methods to fabricate micro-porous hydrogels as well as techniques to characterize their permeability are then summarized. The advantages and disadvantages of two pore-forming methods, namely pre-forming pores and in-situ pore-forming techniques are described in detail. The following subsection is allocated to the double-network (DN) hydrogels and the existing toughening methods. Lastly, an overview of the vocal fold (VF) mechanical environment as well as existing VFs bioreactors is presented.

Chapter 2 includes the experimental and numerical methods used throughout the thesis. The experimental methods are categorized into two subsections including non-biological and biological studies. The non-biological experiments consist of hydrogel synthesis, mechanical characterization, structural characterization, swelling and degradation tests, toughness measurements, permeability tests as well as bioreactors and microfluidics devices fabrication, while the biological tests include cell culture, viability, adhesion, penetration and immunostaining for collagen synthesis studies. Details about the numerical modelling and image processing are also provided in this chapter.

In chapter 3, the results of the experiments are presented, including the DN gels fabrication process, their mechanical and structural characteristics along with their biological performance. The methods to fabricate porous DN gels are discussed, followed by results showing the porous structure of the fabricated gels. The results from the permeability-porosity behavior of the DN gels are also depicted. It is demonstrated that the pores don't act as defects as the DN gels represent great stretchability and toughness compared to their nanporous counterparts. It is also shown that the DN gels have a great potential for cell culture as they

improve the cell adhesion and have a high cell viability.

The functionality and application of the DN gels is discussed in Chapter 4. It is shown that a DN can be used for three dimensional (3D) culture in microfluidics devices to model organs on a chip. The DN gel behavior in a phonomimetic perfusion VF bioreactor is presented, indicating that collagen synthesis is significantly improved due to the effect of mechanical stimuli and pores. The DN also depicts high mechanical stability under cyclic loading after one week of phonation. The experimental results of the mechanical studies are also supplemented by numerical models.

Finally, chapter 5 summarizes the main conclusions and highlights the outcomes of the thesis. The contributions to knowledge in the field of tissue engineering are discussed, and the perspective and the future research directions are presented.

1.2 Motivation

Primary and revision surgeries to replace damaged or loss tissues are nowadays frequent [2]. Statistics show that about 50 percent of medical therapy expenses are spent on implant devices in the USA. The substitution of organs costs about 350 billion USD around the world [3, 4]. In many applications, biomedical implants have successfully restored organ function but at limited lifespan, increased risk of infections by viruses, insufficient bonding, and allergic reactions caused by material abrasion [5]. The engineering of tissue substitutes *in vitro* may lead to new treatment strategies for restoring damaged tissues, addressing the limitations of conventional biomedical implants. This can be done through the use of biomaterials commonly known as hydrogels.

Hydrogels are a class of 3D polymer networks with biomimetic properties and the ability of retaining a noticeable amount of water or biological fluids. They have a broad range of application in many various areas of medicine such as drug delivery, tissue regeneration, bio-fabrication, organs-on-chips and wound healing as shown in Fig. 1.1 [6, 7]. Almost all native tissues are embedded by a vascular network, with every cell being located within 50-100 μm of a blood capillary. One major problem to generation of 3D tissues perfectly mimicking their native structures is the lack of angiogenesis. Mass transfer is needed to supply oxygen and nutrients to the cells. The 3D tissue structures engineered *in vitro* lack vascularization and cells are typically supplied through diffusion [8, 9]. Diffusion is limited to the superficial tissue layers (100 μm from the vessel wall) and leaves the cells in deeper layers starving to death.

Angiogenesis is pioneered by endothelial cells (ECs) and orchestrated by an important protein signal called vascular endothelial growth factor (VEGF). Under hypoxic conditions (shortage of oxygen) a protein named hypoxia-inducible factor 1α (HIF1α) is produced and activates VEGF production. VEGF in turn is secreted and diffuses away from the tissue undergoing hypoxia and signals to nearby ECs to start angiogenesis toward the VEGF gradient. Built on our understanding of the molecular mechanisms of angiogenesis, some efforts have been made to prompt angiogenesis in engineered tissues [10].

In one study, a functional 3D tissue with perfusable blood vessels was engineered using EC cocultured cardiac cells and a bioreactor harboring a vascularized tissue structure. The cardiac cells cocultured with ECs were layered upon the vascular bed. The culture medium was perfused into the vascular bed at 50 ml/min by connecting the bed artery to the inlet tube of the bioreactor pump. The medium was also supplemented with fibroblast growth

factor 2 (FGF-2) to enhance the vascularization process by endothelial cells [11]. In a more recent study, a step by step printing approach to vascularization was followed in which various tissue parts were layered on each other in a hierarchical manner using a 3D bioprinter. First, a 3D collagen I matrix was printed on the bioreactor flow chamber by polymerization of collagen precursor molecules in repeated reactions catalyzed by $NaHCO_3$. Two flow channels were placed on top and either side of the collagen matrix. Then, a sacrificial material was printed on the previously added collagen matrix and into the channels and allowed to solidify at 4 oC to increase the rigidity of the channels. In the next step, an amalgamation of ECs (labeled green), normal human lung fibroblasts (NHLF), thrombin and fibrinogen were layered between the two channels and fibrinogen was converted to fibrin by activated thrombin. Following the gelation of fibrin, several additional collagen layers were printed on the overall structure. Finally, ECs were injected into the flow channels to adhere to their inner surface and media was gently perfused through the channels using a peristaltic dispensing pump. The media was supplemented with VEGF and human Fibroblast Growth Factor - Basic with heparin (hFGF-B) to promote the process of vascular network formation within the cell bed between the two channels [12].

Although the existing method showing promises in developemnt of vasualrize tissuem, they are very complicated and time consuming. Also, to our best of knowledge, hitherto no efforts have been made to permit the formation of VF tissues with embedded vascular networks. A drawback which urges the need to develop new bio-materials that can harness and orchestrate *in vitro* the molecular mechanisms of angiogenesis to allow the formation of vascularized VF tissues mimicking their native structure with more precision. Therefore, strategies that prompt vascularization are needed for the generation of more native 3D tissue

structures.

One possible solution to get around the vascularization problem is to make scaffolds possessing interconnected pores within the size of cells (8-10 μm) to facilitate the irrigation of the deeper layers [13]. Unfortunately, most existing injectable hydrogels are not perfusable owing to their nanoporous structure [14]. As a result, the first objective of this study was to develop and fabricate novel biocompatible and porous hydrogels with the aim of improving their permeability characteristics to mimic that of the native tissue. For this purpose, a novel customized setup was designed and fabricated to characterize the permeability-porosity of hydrogels with different porous structures.

Numerous studies have demonstrated that mechanical cues (e.g., mechanical compression, hydrodynamic pressure, and fluid flow) lead to improved properties of engineered tissues, especially in mechanically active tissues such as the VF [15]. "Implants in the VF lamina propria (LP) are exposed to up to 50% strains at a fundamental frequency that is on the order of 100 Hz [16]. Currently, patients with VF injuries suffer from repeated hydrogel injections, due in part to the fracture-induced short lifetime of the implants under dynamic loading [17]. In contrast, many biological tissues are perfusable and yet tough to tolerate extreme biomechanical stimulations as part of their normal functions, as exemplified by the VF and heart [18, 19]." The second objective of this study is, therefore; to propose strategies to fabricate injectable hydrogels with a combination of high permeability and mechanical toughness. This would close the gap between injectable hydrogels and biological tissues.

Through the control of cell culture parameters, including pH, temperature, pressure, nutrient supply and waste removal, bioreactors provide a suitable environment for the development of biological and/or biochemical processes used for cell culture. One way to

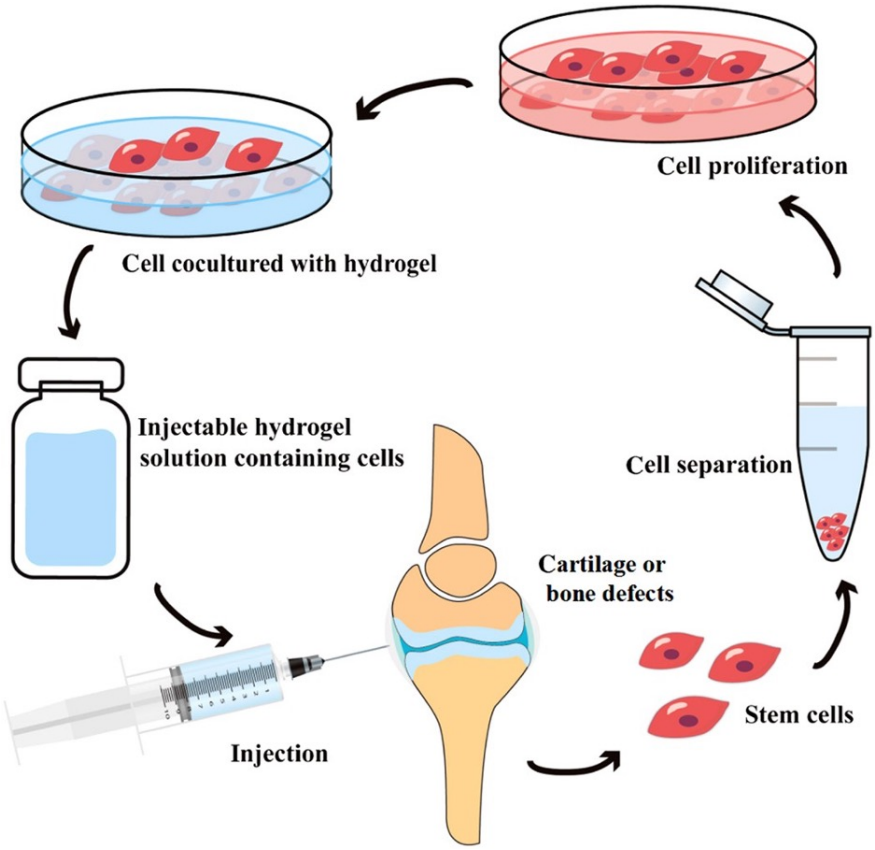

Fig. 1.1. Schematic illustration of approaches to make injectable hydrogels for cartilage- and bone tissue-engineering applications. (Adapted from [6] under the terms of the CC BY-NC 4.0 license.)

asses the functionality and performance of injectable hydrogels before the clinical use is via bioreactors. Due to distinct biological and engineering properties of tissues, bioreactors should be designed specifically for each individual tissue type. One example of such organ-specific tool is the human vocal fold bioreactors [8]. In the present study a phono-mimetic VF bioreactor with a secondary perfusion system was used to study the behavior of the biomaterials in a biomimetic environment. The last part of the present thesis investigates the phonatory characteristics of the bioreactor including the fundamental frequency, average static pressure,

supraglottal loudness, average subglottal dynamic pressure, and average supraglottal dynamic pressure. The developed hydrogels are injected to the perfusion bioreactor to investigate their mechanical stability and cellular behavior. Finally, a two dimensional (2D) computational model of the bioreactor was generated to study the failure of different groups of hydrogel under large mechanical stimuli and vibratory forces.

1.3 Literature survey

1.3.1 Injectable hydrogels

As a multidisciplinary field of study, tissue engineering covers a broad range of disciplines including biology, chemistry and medicine. The purpose of tissue engineering is to synthesize biological substitutes to restore, maintain or enhance tissue functionality [20–22]. In one of the most common strategies, 3D tissue structures are developed by cells within porous scaffolds and various drugs providing a suitable bio-mimic micro-environment for tissue generation [15]. As a result, scaffolding materials, cells, and biochemical/mechanical stimuli are among the three essential elements of tissue engineering.

Injectable hydrogels with three-dimensional cross-linked polymer networks are great candidates for scaffolding materials. Owing to their biomimeitc properties and capability of retaining noticeable amount of water or other fluids, hydrogel-based scaffolds have gained much attention over the past years [23]. Although conventional hydrogels are strong enough for engineering soft tissues like skin or brain, they suffer from poor mechanical properties for load-bearing tissues such as heart and vocal folds. Researchers are looking for solutions to address this issue and improve the mechanical performance of hydrogels. Increasing the crosslinking

concentration, incorporating insoluble additives such as fibers or nano-particles and reducing the swelling degree of hydrogel are some of the most common strategies to upgrade the mechanical properties of hydrogels [24–26]. Hydrogels can be categorized into different groups in terms of their fabrication methods, physical characteristics, biodegradability, cross-linking mechanism and ionic charges. A diagram showing hydrogels classifications is shown in Fig. 1.2 [27].

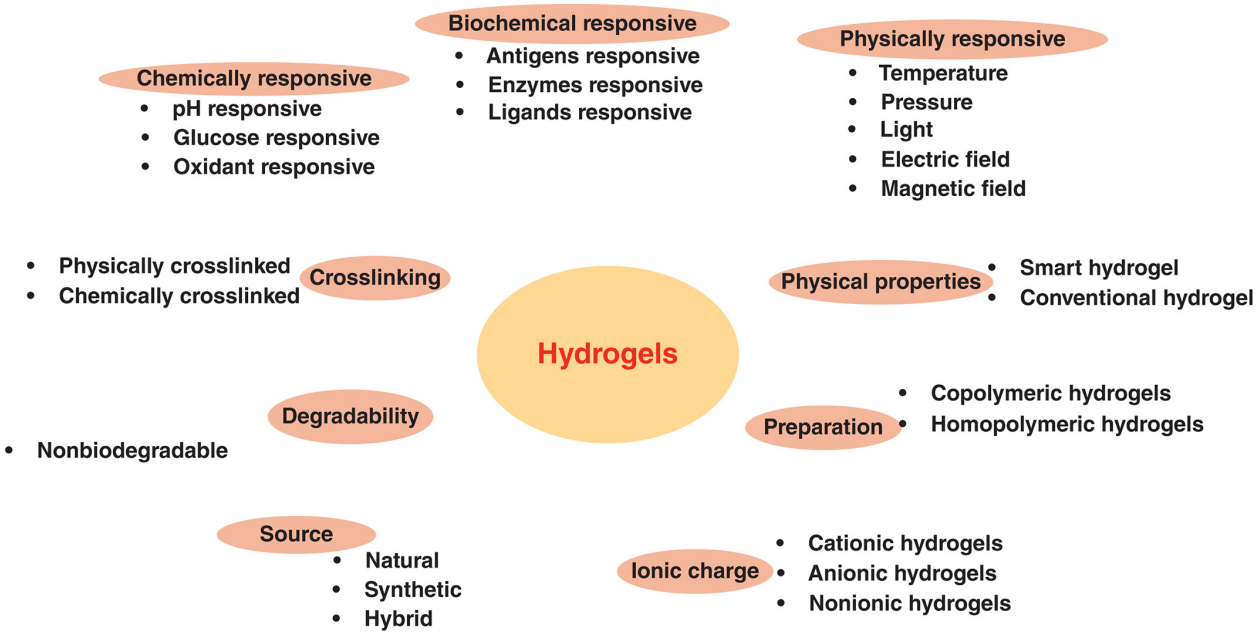

Fig. 1.2. Classification of hydrogels based on different properties. (Adapted from [27] under the terms of the John Wiley and Sons license, license number: 5257730819876.)

Herein, the classification of hydrogels according to their cross-linking methods, materials, biodegradability and preparation will be discussed.

1.3.1.1 Cross-linking Mechanism

Hydrogels can be categorized into two main groups in terms of their cross-linking mechanism. Chemical cross-linking involves polymer networks that are covalently crosslinked. Physical gelling occurs when there is a physical entanglement between the polymer chains such as van der Waals interactions, ionic interactions, hydrogen bonding, hydrophobic interactions, traces of crystallinity and multiple helices without any chemical reactions. In some hydrogels, both types of cross-linking may exist simultaneously [28, 29].

Chemical cross-linking can occur through radical polymerization, chemical reactions of complementary groups such as aldehydes, addition reaction, condensation reactions, high-energy irradiation and enzymes. Physical cross-linking, on the other hand, is obtained following reversible reactions, which can be initiated by ionic interactions, crystallization, amphiphilic block and graft copolymers, hydrogen bonds and protein interaction. Chemically cross-linked hydrogels are irreversible and more mechanically stable. The toxicity of many crosslinking agents has resulted in greater use of physical gels recently [30].

Ionic cross-linking involves a reaction between a water soluble and ionizable polymer and a soluble di-or trivalent opposite charge ion. Calcium-cross-linked alginate is the best-known example of ionic cross-linked gel, however; chitosan (CS)–polylysine, CS–glycerol phosphate salt, and CS–alginate hydrogels are also ironically cross-linked. Ionic cross-linking mechanism is that ionic bonds are stronger than the non-covalents bonds. Ionic cross-linking meanwhile they involves less toxic materials [31].

1.3.1.2 Materials Selection

Natural, synthetic and hybrid polymers have been widely used in the fabrication of biomaterials. Naturally derived hydrogels such as chitosan, alginate, hylauronic acid (HA), collagen and gelatin are very popular for soft tissue engineering due to their excellent biocompatibility and sensitivity to enzymatic degradation. Synthetic bio-polymers such as Poly(ethylene glycol) (PEG), poly(N-isopropylacrylamide) (NIPAAM), poly(vinyl alcohol) (PVA), poly(propylene fumarate) (PPF), and poly(hydroxyethyl methacrylate) (PHEMA) possess tunable chemical and physical properties, which are desirable when specific properties are required. Cell-material interaction and toxicity should be carefully monitored in the design steps of synthetic bio-polymer [32–36]. Chitosan (CS) is the second most abundant polymer in nature after cellulose. It is a linear polysaccharide, derived from chitin, with a wide range of biomedical applications due to its intrinsic bio-compatibility, minimal foreign body reaction, absence of chronic inflammatory response, immune enhancing effects, and low production cost. CS also presents a greater solubility and stronger reactivity compared to chitin due to its free amine group,. It can easily be processed to form hydrogels and its pH dependant behavior gives the polymer a phase separation ability. In other words, at natural pH and body temperature, it can separate into micro-phases and form hydrogen bonds for gelation [37, 38].

Unmodified CS possesses strong intermolecular hydrogen bonds, making it be only soluble in acidic solutions. To tackle this issue, different derivatives of CS has been developed such as glycol chitosan (GC) which is a 6-(2-hydroxyethyl) ether derivative of CS, proved to be soluble over any pH range. GC-based composite gels including carbon nanotube composite gels been developed recently, showing potential for biomedical purposes [39]. However, most of the

exisitng GC based hydrogels are nano-porous due to the strong covalent bonds between the polymers and crosslinkers. The introduction of CS with a phase separation characterstics to the GC network can influence the pore formation process and enhance the swelling capacity.

1.3.1.3 Biodegradability

Biodegradeble hydrogels can be formed by both natural and synthetic hydrogels. The biodegradable hydrogels should meet three main criteria namely cytocompatibility, mechanical stability and adaptability to the common sterilization techniques. Biodegradable hydrogels can be dissolved and/or absorbed by solubilization, chemical hydrolysis, enzyme-induced degradation and ion exchange. This behavior will reduce the risk of inflammation by the degraded products of the hydrogel over time. Natural polymers benefit from their cell friendly behavior and they can promote biological signaling, cell spreading and proliferation. They can also be degraded and remodeled by cells [40–42]. However, natural materials usually suffer from poor mechanical properties and they lack tunable structure and biodegradability [43]. Synthetic polymers have controllable degradation rates, mechanical strengths and micro-structures but they some of them are not cytocompatible and suitable for tissue regeneration [44, 45]. The fabrication of injectable hydrogels that combine natural and synthetic polymers has very active to search for better materials [46]. Significant challenges remain in development of injectable biomaterials which maintain high mechanical properties along with a reasonable degradation profile[47].

1.3.1.4 Hydrogel Preparation

Hydrogels can be categorized into: homopolymers, copolymers, semi-interpenetrating and interpenetrating networks according to their fabrication methods. In homopolymers the networks consist of identical monomer units. A cross-linked skeletal structure could be formed as a result of the nature of monomer and the polymerization procedures. The cross-linking of two co-monomer units results in co-polymer hydrogels. In this case, one of the monomers shows a hydrophilic behavior making the gel swell. Semi-interpenetrating networks are obtained when linear polymers entangle with a cross-linked network without the formation of any chemical bonds. Lastly, interpenetrating hydrogels are synthesized when a prefabricated network swells in another monomer solution followed by a monomer polymerization [27].

The different structure and composition of native tissues combined with the various biomechanical cues experienced by the cells within the tissues (specifically VFs and heart valves) have given rise to tissue-specific tissue engineering methods have been emerged. The current state of injectable hydrogels in tissue engineering will be discussed in the next section.

1.3.1.5 Skin Tissue engineering

Synthetic and natural hydrogels with superior bio-compatibility and mechanical strength can be great substitution for the repair and/or regeneration of damaged skin tissue as they can improve keratin synthesis and cells proliferation, which in turn stimulate the skin regeneration. There are numerous skin-specific cellularized scaffold systems either in a clinical or pre-clinical stage. Among them, modified collagens or resorbable polymers such as poly(glycollic acid) (PGA) or poly(vinyl alcohol) are the most frequently used gels [48]. In a study by Zhang et al. [49], it was observed that Gelatin-methacryloyl (GelMA) hydrogels with a co-culture

of mesenchymal stem cells and epithelial cells can increase the expression of angiogenic markers and the integration of exogenous skin substitutes and host tissues. In another study conducted by Boucard et al. [50], a CS-based hydrogel showed a great potential for the successful treatment of a third-degree burns. The developed gel made of only one material and, was found to be a convenient system to transfer and apply to wounds.

Despite recent progresses in the fabrication of skin-specific hydrogels and their success in providing micro-environment for the skin cells growth, there are still some remaining gaps to be addressed. In recently developed skin constructs, epidermal layer is usually combined with a dermal layer by introducing fibroblasts and keratinocytes into the respective layers of an acellular matrix [51]. Adding more layers resulted in the death of cells in further distance to the wound surface due to hypoxia. Therefore, vascularization, required for adequate healing of large wounds, is among the critical challenges in skin tissue engineering [52]. Use of growth factors, reactive oxygen species-inducing nanoparticles, stem cells to promote angiogenesis, and *in vitro* or *in vivo* prevascularization of skin grafts are some recent techniques to improve vascularization. It is challenging to accurately mimic the sequential release of different growth factors.

Recently, it was demonstrated that microvascular endothelial cells (ECs) migration and neovessel formation in full-thickness wounds were significantly improved by materials which were functionalized with the A13 and C16 sequence from laminin [53] and the RGD and the heparin-binding domain of fibrin (Fg β15–66(2)) [54]. However, these peptides created a competitive environment between angiogenic cells and other cells to adhere to them, which can be detrimental for local angiogenesis. Alginate hydrogels functionalized with peptides specific for α_4 β_1 integrin showed such behavior. Materials with the REDV showed potential

to improve the selective adhesion and proliferation of ECs *in vitro* and higher density of newly formed vessels after subcutaneous implantation in rats compared to those with the RGD or the YIGSR peptides [55]. HA hydrogels functionalized with the fibronectin fragment (Fn9-10) resulted in the non-leaky blood vessels formation as opposed to those with specificity for α_v β_3 [56]. The proliferation and migration of angiogenic cells within biomaterials such as HA relies on their byproducts degradation [57]. These materials are therefore suitable for addressing angiogenesis at early wound healing stages as their temporal control of angiogenesis is limited due to their quick degradation rates [57–61].

Overall, the speed of angiogenesis relies on the natural growth rate of blood vessels. This may be insufficient for the vascularization of large defects. Some of these challenges can be addressed by *in vitro* or *in vivo* prevascularization of scaffolds, resulting in functional vascular network within a few days. It is hypothesized that a combination of prevascularization and angiogenesis can improve wound healing. This necessitates a more comprehensive study on the development of such techniques in this field [62].

1.3.1.6 Cardiovascular Tissue engineering

Bio-materials fabricated for cardiovascular tissue engineering require the viscoelastic properties similar to those of cardiac tissues as well as the structural characteristics such as fibrosis arrangement to ensure that the gel can tolerate the physiological pressure from pulmonary artery and also improve the cell growth, histogenesis, and angiogenesis without thrombus. Natural and synthetic polymers have been used for development of cardiac-specific scaffolds. Collagen, gelatin, laminin, matrigel, hyaluronic acid (hyaluronan), alginate, and chitosan are among the most common natural polymers which have been used for cardiac tissue engineering.

Blackburn et al. [63] developed collagen hydrogels which can alter myocardial cytokine profile, improve angiogenesis, and decrease fibrosis and cell death when tested *in vivo* on an injured cardiac tissue of a MI mice model. However, collagen hyrdogels exhibited weak mechanical and electrical properties such as mechanical strength or stiffness and electrical conductivity, respectively. They can be easily compromised when exposed to a high temperature or different kinds of irradiation [64–66]. In a study by Christman et al. [67], the injection of fibrin scaffold with encapsulated rat skeletal myoblast into the infarct area on a rat MI model led to an increment in cell transplantation survival and a reduction in the infarct size when compared with the injection of bovine serum albumin (BSA) fibrin gel, and skeletal myoblast in BSA. Ryu et al. [68] also fabricated injectable fibrin matrix with bone marrow mononuclear cells. They found that their hydrogels promoted neovascularization in infarcted myocardium and cell survival compared to implantation of bone marrow mononuclear cells without the matrix. Fibrin hydrogels, however, suffer from low stiffness and slow gelation time [69, 70]. Alimirzaei et al. [71] fabricated a chitosan-based hydrogels. They dissolved chitosan in acetic solution and then tuned the pH to the neutral level, required for immediate gelation of the solution. The developed CS scaffolds with human bone marrow MSC (hBMSCs) were then tested *in vivo* and the results showed cell survival after 21 days. The degraded byproducts of the hydrogel were also cytotoxic. Lee et al. [72] micro-fabricated functional cardiovascular tissue composites by using a modular assembly hydrogel method in order to have a quantitative evaluation of micro-architecture effects on cellular functions. This can help study the relationship between structure and function in the heart. A nanocomposite hydrogel with photocrosslinkable microporous networks was successfully fabricated by Waters et al. [73], leading to a therapeutic system to treat the damaged cardiac tissue. Overall,

natural polymers demonstrated positive results for cardiac repair but they are limited by their poor mechanical stiffness and rapid degradation, long gelation times, insufficient electrical conductivity, and lack of inherent antioxidant properties [64]. To tackle this issue, synthetic polymers such as Polyethylene Glycol (PEG) and Poly(N-isopropylacrylamide) (PNIPAAm) have been developed [74–78]. For example, a degradable hydrogel with mechanical properties similar to the normal and infarcted myocardium was developed using functionalized PEG acrylate [74]. In another study, 3D PNIPAAM-gelatin based hydrogel was fabricated to investigate its capability for coculturing NRVMs and cardiac fibroblasts *in vitro*. Their findings illustrated that cell interactions and cytoskeleton organization were improved by co-culturing the cells [75]. Studies showed that synthetic hydrogels promoted mechanical and biochemical properties and they are generally more stable and reproducible than natural hydrogels. However, they are weak at biocompatiblity and natural cell adhesion sites.

In general, there are five key requirements that should be met for cardiac regeneration. These criteria include: 1) functional vascularization of large tissues, 2) successful electrochemical/mechanical cell coupling, 3) efficient maturation of cardiomyocytes, 4) balancing appropriate immune response, and 5) large-scale generation of constructs. For clinical purposes, cells should be electromechanically coupled with the host myocardium with synchronous contractile activity to ensure the reestablishment of the contractile function of the heart. The size and thickness of engineered cardiac tissue should be also clinically relevant, which necessitates vascularization within the graft. In addition to these scientific challenges, there are factors for reproducible fabrication of engineered tissue that should be met before clinical trials [79, 80].

In the next section a deeper review on the VF tissue engineering is studied as it is the topic

of interest in the presented thesis.

1.3.1.7 Vocal Fold Tissue engineering

The larynx is the organ in the body responsible for voice production. Voice is an essential part of speech and communication. The vocal folds are a pair of mechanically active soft connective tissues located in larynx. They have a layered structure including epithelium, LP and vocalis muscle. Vocal folds disorders leads to speech inability and impairs effective communication. According to statistics about 25 percent of the US workforce such as teachers and singers, rely on their voice in their daily occupation [81–83]. It has been confirmed that voice disorders have a detrimental impact on different aspects of human lifestyle from their social life to the professional area [84, 85].

High mechanical forces along with the environmental factors and pathological conditions during phonation can alter the structure and biomechanics of the VF tissue permanently, leading to VFs' scarring or fibrosis [86]. The loss of a part of soft LP or its replacement with a stiff fibrous tissue is among the most damaging voice-related disorders. Intubation, phonotrauma, chemical irritants in the environment, and la-ryngopharyngeal reflux are the main factors leading to VF disorders [87, 88].

Some of the current clinical treatment strategies for voice impairment are voice therapy, injection laryngoplasty, phonomicrosurgery and framework surgery [89, 90]. Mild voice damages can be treated successfully through voice therapy. Laryngoplasty and frame work surgery are the most common therapies for VF paralysis, while phonomicrosurgery is used for benign VF lesions treatment. However, these surgical methods may lead to scarring and inconsistency in results and would be effective only if they couple with the synthetic

superficial LP. Thus far, there is no long-term therapy which can successfully heal the VF scarring [86, 90].

Despite the noticeable progress in tissue engineering of VF, it still lags far behind the demonstrated need for VF repair [90]. Two main methods have been previously developed for VF tissue engineering. In the first method scaffolds with functional rheological properties are injected to damaged VFs to restore their rheological properties and form the extracellular matrix (ECM) *in vivo*. The second method is based on the regeneration of tissues *in vitro* through a proper combination of bioactive factors, injectable scaffolds, cells, and bio-mechanical and biological cues for partial or full replacement of the impaired tissue. The fabricated scaffolds for clinical treatments as a portion of the first method suffer from degradation over a longer period of time, necessitating a series of injections. A comprehensive descriptions of existing vocal fold specific hydrogels are discussed by Li et al. [86].

To date, most of the developed injectable hydrogels for vocal fold tissue regeneration have been made of hyaluronic acid (HA) derivatives and Col-I as they are the main components of the VF lamina propria extra cellular matrix [91–94]. The native HA, however, possess a rapid degradation rate which is not desirable for tissue regeneration purposes. Local hyaluronidase-mediated enzymatic degradation starts to degrade HA within 3-5 days after injection into the VF. As a result, HA derivatives have been developed though chemical modification of HA to improve the mechanical stability and degradation rate of developed hydrogels *in vivo*. In a study by Heris et al. [93], it was found that the modified HA has a lower degradation rate. In addition, HA also suffers from poor cell spreading and migration of human vocal fold fibroblast (HVFF). To address this limitation, gelatin, denatured collagen, was embedded into HA network. Despite the improvement in cell attachment and migration,

the degradation rate of the gelatin/HA hydrogel increased unfavorably [94, 95].

Thanks to their complex structural integrity and biocompatibility, ECM-derived natural materials including collagen and fibrin have been extensively investigated for different biomedical applications [96–98]. Injectable autologous mesenchymal stem cells encapsulated in 1% hydrochloric acid atelocollagen has been developed for the first time for treatment of injured canine vocal folds [99]. Modified atelocollagen was fabricated by Kanemaru et al. [99] and their investigations revealed that atelocollagen sheet is cell friendly with a proper degradation rate. Their adequate porosity also supported cell infiltration and increased residence time *in vivo*, required for ECM remodeling wihtin the damaged lamina propria tissue [100, 101]. Naturally-derived materials improved the VF function post-implantation. However, their long term *in vivo* outcome is limited due to gel resorption and/or compaction. The developed injectable collagen-based hydrogels did not offer a promising outcome in treatment of VF scaring due to unmatched biomechanical properties of collagen along with foreign body reaction and resorption response *in vivo*. As an example, the dynamic viscosity of collagen hydrogels is one order of magnitude higher than normal VFs [102–104]. Injectable collagen-based composite hydrogels with either HA or alginate were fabricated to study their ECM synthesis potential. These groups of hydrogels showed biocompatibility and favorable morphological behavior but alginate-based scaffolds didn't follow a regulated degradation pattern due to the absence of enzymes in mammals to break down alginate [105, 105, 106]. In spite of excellent biological properties of HA-based scaffolds and collagen hydrogels, their application is hampered by rapid degradation, scaffold compaction and poor mechanical properties such as toughness and stiffness *in vivo* [107–112]. Chitosan-based hydrogels and its derivatives have been recently studied for vocal fold tissue engineering [39, 107] and

showed great potential for the treatment of damaged VF tissues. However, their nano-porous structure have limited the proper transport of nutrient supply *in vivo* [1].

Overall, most of the available or prospective injectable hydrogels are poor at degradation, mass transport and mechanical properties. These shortcomings may be addressed by integrating techniques for the fabrication of vocal-fold specific biomaterials with desired characteristics including tunable porous architecture, high permeability, toughness, bio-mechanical stability and proper degradation rate [90]. Solutions to tackle these issues will be discussed in the following sections. In past works, the incorporation of porous structures within injectable hydrogels enabled medium perfusion in lieu of vascularization. In the next section, some of the in practice pore-forming techniques and methods to characterize the permeability of porous materials are explored. Existing methods for improving the mechanical performance of bio-materials are described further below.

1.3.2 Permeability

The creation of porous micro-structures is of paramount importance in many scaffold fabrication methods. Pore fabrication can regulate the ECM micro-structure in terms of micro-structural characteristics including void geometry, homogeneity, and interconnectivity. These characteristics can be demonstrated by hydraulic permeability, which is the resistance of the porous media to fluid flow. Hydraulic permeability can be affected by different parameters such as the physical and hydrophobic interactions. The permeability is usually modeled by Darcy's law and is dependant on the fluid viscosity, fluid velocity and pressure gradients over the thickness of the scaffold [113–118].

Here, some of the existing methods to measure permeability of gels are reviewed. Johnson

and Deen [119] developed a new technique to measure the hydraulic permeability of agarose gels. They mounted the gel membrane on a porous frit and used compressed nitrogen to perfuse phospahte/KCl buffer solution through the gel. The pressure drop was recorded using a pressure transducer and the flow rate was calculated by weighting the filtrate. Permeability was then determined for four different concentration of agarose gel and the reported values were within the range of 15 to 353 nm^2. In another study, the hydraulic permeability of gels was found from the curve-fitting of creep tests data to the biphasic model in confined compression condition. In specific, the gels were prepared in cylindrical shapes with 5 mm diameter and 3 mm height. The prepared samples were then subjected to a 10% compresssive strain, followed by a 2 hour creep test and a frequency sweep test (0.01-1 Hz). The obtained results were in a good agreement with literature [120]. Confined compression method was also used in another study to characterize the permeability of collagen hydorgels using biphasic theory [121]. Refojo [122] used a previously developed apparatus to measure the permeation of water through a series of hydrogels. A U-tube mercury manometer was used to record the pressure difference while the setup was immersed in a 25℃ water bath. The hydrogels' permeability varied from $0.075\times10^{-15}cm^2$ to $42\times10^{-15}cm^2$. Later, an apparatus consists of two porous screens, glass capillary, one pressure transducer and a MililQ2 system was used to predict the permeability. Water was forced through the membrane by pressurized nitrogen and buffer solution was filtered with 0.2 and 0.1 μm pore size polyester membranes. Validyne DP-15 transducers were used to measure the pressure difference while the flow rate was recorded by monitoring a bubble movement in a precision-bore capillary [123]. In a recent study, a series of samples were prepared by pouring the hydrogel solution into a 26.7 mm diameter syringe [124], making cylinders with around 20 mm thickness. Then, permeability

was directly measured by pumping fluid through the syringe containing the gel. Six different flow rate was applied with a Graseby 3150 syringe pump and a a pressure transducer. Finally, Miri et al. [113] designed and fabricated a new indentation-based apparatus to predict the hydraulic permeability of GelMA hydrogels. The experimental data were calibrated using biot's theory and numerical simulations.

In the next subsection, methods to fabricate porous scaffolds is elaborated.

1.3.3 Pore-forming methods

Porous structures can be preformed before injection or formed in-situ after placement in the human body. In a study by Bencherif et al. [125] a preformed macroporous scaffold was synthesized using cryotropic gelation technique. Ammonium persulfate (APS)/tetramethylethylenediamine (TEMED) initiator was mixed with the methacrylated alginate and then incubated in -20°C to allow the formation of ice crystals. This was followed by the cryogelation processes including the phase separation, cross-linking, polymerization and ice crystals thawing, leading to the formation of interconnected pores. The fabricated cryogel can be injected to the target site via conventional needles and can recover its original shape after deformation and injection. Various strategies, including extrusion-based 3D-printing, have been proposed recently to fabricate bioinks with the aim of bio-printing complex porous structures for different biological and biomedical applications. [126–128]. Ying et al. [129] synthesized a bioink by mixing an optimized ratio of cell-laded GelMA pre-gel solutions and a polyethylene oxide (PEO) solution using 3D extrusion bio-printing. The developed bioink was used to produce a porous hydrogel which can be printed in any desirable shapes and sizes. The cell-laden gel can regain its original shapes and showed a great cellular behavior after deformation

and injection. In another study an alginate-based macro-porous hydrogel was fabricated by incorporating gas bubbles within the scaffold and subsequently removing the gas bubble, resulting in interconnected pores [130]. "Preformed porous hydrogels can collapse to pass through a needle, and then regain their shape post-injection. However, to prevent damage to such hydrogels during injection, the use of oversized needles is necessary but increases the invasiveness of the procedure. In addition, the preformed method usually demands lengthy fabrication processes, such as cryogelation, lyophilization, or 3D printing, as well as prior knowledge about the shape and volume of the injection site to conform to the often irregular wound."

"Alternatively, in-situ pore-forming hydrogels are preferable as they can be delivered in liquid form through small-sized needles and undergo a sol-gel transition into porous scaffolds in the human body." Recently an injectable porous HA scaffold was developed using an in-situ bubble self-generation and entrapment process [131]. The pores were generated from the CO_2 bubbles as a result of the amine reaction between HA and cystamine dihydrochloride. The fabricated gel showed a clear porous structure along with a desirable gelling behavior. Similarly Tang et al. [132] proposed another novel gas foaming technique using magnesium (Mg) particle. The H_2 gas bubbles were released as the Mg particles were degrading over time, leaving interconnected pores within the scaffold. Photo polymerization and particle leaching are other methods of fabricating porous scaffold where the pores can be formed by leaching out the polymer micparticles [133]. Overall, in-situ pore forimg hydrogels have been developed using either porogen [131, 132], leachable particles [133], nanoclay [134], granular particles [135], self-assembly [136, 137], or polymer degradation [138]. As an example, Hsu et al. [135] developed an adaptable microporous hydrogel (AMH) composed of microsized

building blocks with opposite charges serves as an injectable matrix with interconnected pores and propagates gradient growth factor for spontaneous assembly into a complex shape in real time.

Bioprintable pore-forming formulas, such as aqueous two-phase emulsion system [129, 139, 140] and hydrogel microstrands [141] could be used for injection as well. "These hydrogels, however, suffer from limited pore size and low interconnectivity, which impair permeability and performance. Attempts to promote perfusion by enlarging the pores deteriorate their mechanical strength because pores essentially act as defects or cracks. This issue is particularly critical when the hydrogels are subjected to the biomechanical stimulations present in mechanically dynamic organs or tissues."

"Circumventing the inverse correlation between porosity and toughness while ensuring injectability and cytocompatibility proves to be a challenge. Recently, a variety of DN hydrogels have been reported to tolerate large defects and pores thanks to their high fracture toughness [142]." In the next section, the DN gels definition and applications for tissue engineering are reviewed.

1.3.4 Double-network hydrogels

Double-network hydrogels enable achieving exceptional mechanical behaviour (toughness and stretchability) which make them stand out among other single network hydrogels which are usually brittle and weak [143, 144]. The composite structure of DN hydrogel concurrently offers high stiffness, strength and ductility, where the former results from a brittle heterogeneous polyelectrolyte and the latter comes from a ductile neutral polymer [145]. The conventional DN gel formation is the chemical cross-linking in both networks

through a two-step polymerization method where the first covalent network is fabricated via polymerization of a single monomer. This is followed by a diffusion of the second network components into the first matrix and its large expansion. The second polymerization happens during the swelling process and form a weak corsslinked network within the first network. Molecular stent is another way of fabricating DN hydrogels from neutral polymers to form both networks similar to the two step synthesis method [146–148]. In general, postaddition and preaddition are two common ways of DN hydrogel fabrication. In the postaddition method, the preformed natural network is added to the monomeric electrolyte solution along with a linear polymerization of the monomers within the natural DN gel. In the preaddition method the polyelectrolytes are first formed and then polymerized with neutral first-network monomers. The second network is formed by adding the swollen gel into the second precursors solution to synthesize the tough DN hydrogel. Overall, the stent method is an optimum way of improving the mechanical performance (toughness) of DN gels.

Although the chemical cross-linking method is the most widely used mechanism of DN gel fabrication, there are DN gels synthesized via physically-chemically cross-linked method. Alginate-polyacrylamide is one example of a hybrid physically-chemically cross-linked DN gel in which alginate is physically cross-linked with Ca^{2+}, forming the first network along with the covalently cross-linked polyacrylamide chains as the second network. The developed Ca-Alginate/Polyacrylamide (PAAm) DN gel can undergo 20% tensile strain and have a fracture energy of around 9000 J/m^2. Agar-PAAm DN gel is another examples of a physical-chemical cross-linked networks fabricated from a one-pot strategy.

There are many studies in literature reporting the fracture energy G of DN gels measured from a tearing test. This value ranges from 100-1000 Jm^{-2} which is between 100-1000 folds

higher than that of the individual networks with the same concentration such as regular PAAm gels or PAMPS gels. Additionally, the fracture energy was reported to be independent of the crack speed V [149–153]. These behaviors cannot be explained with the normal mechanisms that increase the fracture strength of soft polymers such as viscous dissipation for chain pulling process around the crack tips and bulk rheological losses coming from the crack propagation [154, 155]. Researchers proposed several theories explaining the origin of high fracture strength of DN gels, however; the local yielding and hardening model at the crack tip is the most outstanding theory describing the exceptional behaviour of DN gels [156–160].

In separate studies by Brown [157] and Tirumala et al. [159], it was hypothesised that necking phenomena similar to the tensile test happens in the highly stretched area in front of the crack tip when there is a transition to a very soft from of the gel. This is followed by passing the crack tip through the softened region by extra stretching. In other words, after the breakage of the first, stiff network several cracks will formed due to the high stress level. The second network is responsible for holding the cracks together which results in a multiply crack zone formation. This is the reason behind the energy dissipation of the second network and around 40x increase in the hydrogel toughness.

Overall, "the pore-insensitivity of DN gels is attributed to the synergy between dissipative and stretchy networks, which are often denoted as primary and secondary networks, respectively. These strategies, however, cannot meet other requirements such as cytocompatibility for injectable perfusable hydrogels." Most of the DN hydrogels with high mechanical strength are fabricated over a multi-step process involving free radical polymerization, swelling, diffusion and second free radical polymerization. These methods suffer from a long processing

time, difficulty in monitoring the molar ratio of the components and preparing gels in various shapes, and free-radical polymerization process which leads to large hysteresis as result of a high degree of heterogeneity. Recently, hydrogels with only one-step process are fabricated by a combination of ionic and covalent cross-linking. This method still needs a time consuming high temperature process and free radical polymerization cross-linking. The limitation of all of these DN gels is the existence of toxic acrylamide monomer in their fabrication, making them impractical for 3D cell culture and tissue regeneration [161]. Overall, "while the dissipative primary network can be realized with biopolymers at mild conditions, there are concerns about the employment of the stretchy secondary network, which requires toxic precursors and/or harsh reaction conditions."

"To render the hydrogel precursor cytocompatible, synthetic and naturally derived polymers have been used as the secondary network components." Truong et al. [161] developed a novel DN gel using two orthogonal click chemistries including nucleophilic thiol-alkyne addition and tetrazine-norbornene (Tz-Nb) inverse-electron demand Diels–Alder cycloaddition. The gelling process occurs under physiological condition, which results in a tough and cytocompatible gel. Tandem supramolecular interactions and covalent cross-linking are among other techniques to form injectable and cytocompatibile DN gels. In this method a self-healing first network is formed via a supramolecular guest–host (GH) assembly while the second network formation occurs through an orthognal covalently cross-linked reaction between methacrylated HA and dithiothreitol (DTT) [162]. Another novel method was proposed to fabricate tough injectable DN gel made of CS and HA. In more details, β-glycerophosphate (BGP) was used as an ionic crosslinker as well as a weak polyol base to help tune the PH of CS and mix with HA. Genipin was used as the HA covalent crosslinker. Theses highly

tough, thermogelling and non-toxic DN gels supported the 3D cell culture and improved the Collagen II production compared to the single network HA or CS gels [163]. Later, Zhao et al. [164] presented a dual dynamic cross-linking strategy to develop an ultra-tough injectable cytocompatible DN gel. The hydrogel was formed via aborate bonding and ionic reaction between the Poly(vinyl alcohol) (PVA) and 4-carboxyphenylboronic acid (CPBA) as the crosslinker in the presence of calcium ions. This was followed by a self-reinforcing effect within the hydrogels as a result of the dynamic gathering of CPBA. The resulting DN cross-linked smoothly under physiological conditions which facilitates the 3D cell encapsulation and proliferation. In another study injectable bio-compatible and tough hydrogel were fabricated using a one-spot polymerization of polymerized PAAm and diacetone acrylamide (DAAm) under a dynamic crosslikning with acylhydrazone as the first and H-bond as the second cross-linker. The synthesized gel has fast-recoverable and re-healable properties along with a cell friendly behavior, suitable for biomedical application [165]. "All these resulting tough hydrogels are nonetheless nanoporous. Naturally derived fibrous networks, such as platelet-rich fibrin, have also been explored to form the secondary network but at the expense of significantly reduced stretchability [166]. It has also been shown that a high toughness often restricts activities for the cells that reside within and hinders their cellular functions [167]." Overall, literature shows that injectable hydrogels that possess both high permeability and toughness have profound impacts on regenerative medicine but remain elusive.

As mentioned before, bioreactors are used to investigate the functionality and lone term treatment effect of the scaffolds under controlled bio-mimetic environments [168]. The second phase of this thesis focuses on the behavior of bio-material in a VF bioreactor. Hence, Some of the the existing VF bioreactors are summarized in the next section.

1.4 Vocal Fold Bioreactors

Bioreactors lie at the heart of tissue engineering and organoid technology which offer the prospect of tissue replacement with minimal contamination risks, a characteristic that makes them an excellent tool for clinical applications [169]. Vocal fold bioreactors are generally categorized into mechanically or aerodynamically driven bioreactors.

Titze et al. designed the first mechanically driven VF bioreactor. Their bioreactor was capable of simulation of 3D-axial as well as the vibratory stresses generated in human VFs during phonation i.e. 0-1 mm amplitudes, 20-200 Hz frequencies, a variable on-off stress cycle. A 3D Tecoflex porous substrate was used to seed the human laryngeal fibroblasts. A 20% axial strain and 100 Hz vibratory strain were imposed to the substrates for 6 h. The results obtained from this study showed that mechanical stimuli enhanced the cell density as well as ECM production compared to the no tension/vibration or static condition [170]. Another mechanically driven bioreactor was built by Wolchok et al. [171] to study the behavior of human laryngeal fibroblasts in response to high- frequency vibratory stimuli. This bioreactor was able to impose a 100 Hz vibratory stimulation to the cells seeded in 3D Tecoflex substrate over a 21-day period (14 min per day). Results indicated that the density of collagen type I, ECM proteins and fibronectin increased noticeably in comparison with the non-stimulated controls but the cell viability was not studied. Branski et al. studied the rabbit VF response to 2D-cyclic tensile strains of various magnitudes. In this investigation, Collagen type I-coated Bioflex II was used to culture the cell monolayer subjected to equibiaxial tensile strain. The results collected 4 h per day over a period of 1-2 days, demonstrated that over 99% of cells remained viable. Although encouraging, the stimulation frequency was restricted to the range

of 0.005-0.5 Hz which does not capture the human phonation range [172].

Mechanically driven bioreactors offer several limitations in terms of loading scenarios that could be applied to the cells *in vitro*. These loads are generally idealized vibratory forces that are transferred to the cells mechanically and are not representative of capturing the realistic vibratory oscillations that occur in the human phonation system. To address the limitations of mechanically driven bioreactors, Farrant et al. developed a dynamic culture system that can produce vibratory stimulations within a frequency range of 60-300 Hz through a power amplifier, enclosed loud speaker and a function generator. In this study, the cells were seeded on a silicon membrane. The vibrations signals were aerodynamically transmitted to the membrane via an oscillating air pressure system [173]. To assess the functionality and performance of the bioreactor, neonatal foreskin fibroblasts (NFFs) attached to the membrane were subjected to a 1h vibrations at 60, 110 and 300 Hz frequency. The center of the membrane was also subjected to displacement varying in the range of 1-30 μm, followed by a 6 h rest. The results showed no morphological changes in the cell for different loading scenarios. An increase in cell proliferation was identified when cells were subjected to a 110 Hz oscillation with a normal displacement of 30 m. The normal displacement at the center of the membrane was 19.7 m at the driving frequency (110 Hz) while the displacements increased to 0.3 and 0.2 at 220 and 330 Hz, respectively. A phono-mimetic VF flow perfusion bioreactor with an enhanced physiological phonation environment, was designed by Latifi et al. [174]. This bioreactor used an airflow-induced self-oscillation system to generate realistic human phonations, namely mechanical loading and contact forces. The bioreactor was composed of two synthetic replicas located in a silicon body. A scaffold mixture from HVFF, HA, gelatin, and a polyethylene glycol cross-linker was injected into cavities within the replicas.

To ensure cell adaption, the bioreactor operated with no stimulation for 3 days following the injection process. A variable speed centrifugal bioreactor blower was used to induce phonation for 4 days (2 h per day). The results showed that cell viability was more than 90%. A significant increase in the amount of ECM proteins was observed in the phonated samples after a week compared to the non-phonated control. Recently, a phonomimetic bioreactor was developed and validated using a flexible silicone bottom and a loudspeaker to stimulate the cells with different kinds of phonatory stimuli. The viability of HVFF as well as gene expression of hyaluronan synthase 2, collagen III, fibronectin and TGFβ_1 were studied and there was a significant increase in their amount in the phonated samples. However, the study was performed in 2D [175]. In general, bioreactors showed the potential to be used as mimetic platforms to study the mechanical stability and cellular behavior of biomaterials under realistic stimulation. This approach allows the characterization of potential scaffold biomaterials *in vitro* at a lower cost before animal and clinical studies.

1.5 Research Objectives

The general goal of the present thesis is to develop long-lasting acelluar tough and porous injectable hydrogels for soft tissue engineering applications. To this goal, the hydrogels' composition and formation process were engineered. In more details, to make porous gels, CS-based DN hydrogels were fabricated to evaluate the efficacy of CS phase separation behavior on pore formation. Additionally, by incorporation of GC as the second network the mechanical stability and toughness of developed gels were enhanced. The presented DN gels are unique in terms of their porous structure and toughness as other existing injectable

hydrogels are either nanoporous or made of pre-formed pores. Furthermore, the developed gels were injected into a perfusion VF bioreactor to investigate the hydrogels' cellular performance along with their mechanical and biochemical stability under phonation-induced mechanical cues. The specific aims of this project were defined as follows.

Specific aim 1: The first aim was to develop, characterize and optimize injectable DN hydrogels that are porous, tough, and biochemically and mechanically more stable than previously used materials.

The design of porous double-network (PDN) was based on three main criteria including cytocompatibility, in-situ pore-forming mechanics; and DN framework. "To satisfy the first two criteria, we hypothesized that the phase separation of cytocompatible biopolymers at body temperature and physiological pH could both ensure cytocompatibility and generate porous structures in-situ." The initial phase of the project was then allocated to assess the biocomptability of the developed gels by conducting a series of viability tests to optimize each network concentration. Then, different imaging techniques were used to investigate the porous structure of the developed DNs. To meet the third criterion, the secondary network was made of covalently crosslinked biocompatible polymers.

Specific aim 2: The second aim was to investigate the effect of interconnected pores on the scaffold's permeability as well as cell adhesion and penetration in the DN gel.

The second phase of the project was to characterize permeability-porosity of the developed gel. A customized-setup was designed and validated to measure and characterize the permeability of hydrogels. In addition, cell adhesion and penetration were measures to demonstrate how interconnected pores can promote cell penetration and cell adhesion within the scaffold.

Specific aim 3: The third aim was to study the mechanical and cellular behavior of the

developed bio-material in a flow-perfusion VF bioreactor.

In the last phase of the project, the fabricated DN gels were injected in a vocal-fold perfusion bioreactor to test their resilience under complex physiological conditions to simulate biomechanical stimulations of the VFs. Also, the effect of phonation on ECM synthesis of the cells, encapsulated within the DN gels, were studied and compared to the single networks controls.

Finally, to better demonstrate the mechanical environment in the bioreactor, finite element analysis was conducted to quantify the mechanical loading applied onto the hydrogels.

CHAPTER 2

Materials and Methods

This chapter describes the experimental and numerical methods used throughout the thesis. The details related to materials selection, imaging techniques, mechanical tests, physical characterization, cell-related experiments, and finite element analysis are explained. The chapter is divided into three main sections including non-biological experiments, biological experiments, and numerical methods. The sentences in quotations are verbatim of the author's publication (references [1]).

2.1 Non-biological experiments

2.1.1 Hydrogel synthesis

Unless otherwise mentioned, all materials were purchased from Sigma-Aldrich. Different types of single network and double-network (DN) hydrogels were fabricated to study the effect of fabrication process and material components. "Chemicals used in the current work were

purchased from Sigma-Aldrich and used without further purification unless stated otherwise."

Single-network Hydrogels: Two types of non-porous single-network (NSN) hydrogels were fabricated using the same crosslinker. Glycol chitosan (GC) (molecular weight = 2000 kDa) and glyoxal (GY) 40% were both purchased from Sigma Aldrich Corporate. Pure GC powder was dissolved in phosphate-buffered saline (PBS) (Wisent Inc.) using a Fisher Scientific rotator to obtain the final concentration of 3.33%. A solution of 3.33% Chitosan-glycol and 0.0124% GY was then mixed to obtain the target concentrations of GCs (2%) and GY (0.005%). For the second NSN gel, a concentration of 4.17% (w/v) porcine skin gelatin-type A (G2500) solution was dissolved and stirred in PBS for 30 min at 37°C. Then, GY 0.0155% was added to the gelatin solution to obtain the final concentration of 2.5% gelatin and GY 0.006%. For the second single-network gel, "chitosan (CS) (DDA: 95%, medium and high molecular weight) was purchased from Xi'an Lyphar Biotech. Pure chitosan (PC) powder was dissolved and stirred in 0.2 M acetic acid to form a homogeneous chitosan solution. To prepare the gelling agents, a phosphate solution (PS) was firstly prepared by mixing 0.1 M sodium phosphate dibasic (Na_2HPO_4, S7907) and 0.1 M sodium phosphate monobasic (NaH_2PO_4, S8282) with a volume ratio of 50:3. The gelling solution was then completed by adding sodium bicarbonate (SC) (S233-500, Fisher Scientific) into the phosphate solution." To form the porous single-network (PSN) hydrogel, the chitosan solution was mixed with the gelling agent at a volume ratio of 3:2 using a syringe connector. For biological tests, a human vocal fold fibroblast (HVFF) cell solution (20×10^6 cells/ml) was encapsulated within the hydrogel immediately after adding the crosslinker to reach the final density of 2×10^6 cells/ml.

Double-network hydrogels. To form the porous double-network (PDN) hydrogel precursors, GC (G7753) was added to the chitosan solution at three different concentrations

of 0.84%, 1.67% and 3.34%. Also, three concentrations of GY were accordingly added into the same gelling agent solution prepared for the PSN gel. "Hydrogel precursor and its associated gelling agent were also mixed at a volume ratio of 3:2 using a syringe connector to yield hydrogels. The resulting hydrogels were denoted as PDN_x, where x stands for the w/v percentage of glycol-chitosan content." The detailed protocols for preparation of each PDN concentration are explained below.

To synthesize $PDN_{0.5}$, glycol chitosan and chitosan were first added and dissolved together into 0.2 M acetic acid solution at a concentration of 0.84% and 2.5%, respectively. The solution was used as the hydrogel precursor. Then a phosphate solution was prepared by mixing 0.1 M sodium phosphate dibasic solution with 0.1 M sodium phosphate monobasic solution at a volume ratio of 50:3. Sodium bicarbonate and GY were added to the prepared phosphate solution at a concentration of 0.445 M and 0.0031%, respectively. The resulting solution was used as the gelling agent. $PDN_{0.5}$ can be formed by mixing the hydrogel precursor and the gelling agent at a volume ratio of 3:2 using a syringe connector. To synthesize PDN_1 and PDN_2 the same steps were followed using the concentration shown in Table 2.1. Gelatin-Chitosan double-netwrok hydrogel was fabricated with the same proptocl by replacing GC with Gelatin as a control. Lastly, a non-porous DN gel was fabricated using alginate (ULV-L3G, KIMICA Corporation) and GC polymers. $CaSO_4$ (C3771) was used as the cross-linker for alginate with the ratio shown in Table 2.1.

2.1.2 Mechanical Characterization

"Gelation kinetics and frequency sweeps were measured using a torsional rheometer (HDR-2TM, TA Instruments) with parallel plates (upper plate diameter of 20 mm)." Trios software

Table 2.1. Hydrogel synthesis reagents

Hydrogel	Hydrogel precursor	Gelling agent
NSN	3.33% GC in PBS	0.0124% GY in PBS
PSN	2.5% PC in 0.2M acetic acid	0.445 M SC in PS
$PDN_{0.5}$	0.84% GC + 2.5% PC in 0.2 M acetic acid	0.445 M SC + 0.0031% GY in PS
PDN_1	1.67% GC + 2.5% PC in 0.2 M acetic acid	0.445 M SC + 0.0062% GY in PS
PDN_2	3.34% GC + 2.5% PC in 0.2 M acetic acid	0.445 M SC + 0.0124% GY in PS
Pure gelatin	4.17% Gelatin in PBS	0.0155% GY in PBS
Gelatin-PDN	1.67% Gelatin in PBS + 2.5% PC in 0.2 M acetic acid	0.445 M SC + 0.0062% GY in PS
NDN	1.67% GC + 2.5% alginate in water	0.1 M $CaSO_4$ + 0.0062% GY in water

(TA Instrument, DE) was used to control the and analyze the data. "The shear moduli of hydrogels were obtained from isothermal time sweeps at a frequency of 0.1 Hz and 0.1% strain at 37 ℃ for 2 hours. Frequency sweeps ranging from 0.01-100 Hz at 0.1% strain and 37 ℃ followed to determine the damping ratios."

Gelation: Gelation were measured from time-sweep experiments with a rotational frequency of 1 Hz and a shear strain of 0.1% firstly at room temperature, 24 ℃, to mimic the injection process and then increased to the human body temperature, 37 ℃. The gap size between the rheometer plates was adjusted to 1000 μm to provide a reproducible loading. Each sample was mixed using syringe and connectors and was immediately injected between the two plates to completely fill the gap over a period of 5000 seconds, covering the entire crosslinking period. The storage and loss moduli (G' and G", respectively) were recorded during the crosslinking period to monitor the gelation kinetics of the primary and secondary networks.

Stress Relaxation: "Relaxation moduli were obtained by holding a step compressive strain of 15% and strain rate of 1 mm/min using an InstronTM machine (Model 5965, 10 N load cell) and measuring the compressive stress-time profiles." The samples were prepared in hydrogel disks with 15mm diameter and 2mm thickness and then were equilibrated in Dulbecco's Modified Eagle Medium (DMEM) (without fetal bovine serum (FBS)) for 24 hours. Before starting the experiment, the samples were sealed with DMEM free and mineral oil to prevent dehydration. Stress relaxation was considered as the time when the compressive force relaxed to half of its initial value. Young's modulus was also calculated using the stress-strain curve between 5-10% of the strain.

2.1.3 Structural Characterization

The porous structure of the fabricated PDNs as well as controls were analyzed using three imaging techniques explained below.

2.1.3.1 Scanning Eletron Microscopy

A field emission scanning electron microscopy (SEM) (F50, FEI, Thermo fisher Scientific) under various magnifications was use the image the macro- and microscopic pores of the hydrogels. "Before SEM imaging, all samples were immersed inside 30, 50, 70, 80, 90, and 100% ethanol in sequence for dehydration. Ethanol inside the hydrogels was removed using a CO_2 super-critical point dryer (CPD030TM, Leica) to preserve the original pore size. Some of the samples were immersed in liquid nitrogen to become brittle and then were broken to reach the porous structure on the cross-section of the hydrogels. The dehydrated samples were coated 4 nm Pt using a high-resolution sputter coater (ACE600TM, Leica) to increase

surface conductivity."

2.1.3.2 Confocal Microscope

"The polymer network was imaged using a confocal microscope (LSM 710, Zeiss). Both chitosan and glycol-chitosan were conjugated with FITC fluorescent labels according to published protocols [176, 177]. Samples were prepared by mixing fluorescent-labeled polymer solutions and cross-linkers in a vial and transfering around 150 μL into a 35-mm Petri dish with a coverslip bottom (P35G-0-10-C, MatTek). Hydrogels were immersed under PBS and imaged as prepared. The polymer network was imaged with 10x and 20x objective lenses."

2.1.3.3 Micro-computed Tomography (µCT)

"Imaging with micro-computed tomography (µCT) was performed using a SkyScannerTM 1172 (Bruker) through a 360° flat-field corrected scan at 30 kV and 112 µA, with a rotational step size of 0.45°, a cross-sectional pixel size of 6.5 µm, and no filter. The samples were prepared and incubated at 37℃ for 24 hours. The volumetric reconstruction (NReconTM, Micro Photonics) was performed with a beam hardening correction of 40%, a ring artifact correction of 4, and an auto-misalignment correction. The two dimensional (2D) and three dimensional (3D) analyses were carried out using Dragonfly software and a grayscale intensity range of 50 to 70 (8-bit images) to remove background noise."

2.1.4 Swelling and Enzymatic Degradation

"The swelling ratios were determined by immersing the hydrogel disks (10 mm in diameter, 1.5 mm in thickness) in PBS (pH=7.4) at 37℃ with gentle mechanical stimulation (75 RPM).

The diameters of the disks were measured using a caliper at pre-determined time intervals using a pipette over 7 days. The swelling ratio was calculated by dividing the measured diameter size by the initial value."

"For biodegradation assays, all hydrogel samples were prepared with the same volume (500 µL). The average dry weight of the pristine hydrogels was used as the weight at Day 0. After that, an enzyme solution consisting of 13 µg/ml lysozyme (MP Biomedicals, 100831) in PBS was added to the gels. The samples were incubated at 37℃ with gentle mechanical stimulation over 28 days. The enzyme solution was changed every other day. At pre-determined time intervals, the enzyme solution was removed. The samples were then washed three times for 5 minutes with PBS. The samples were then lyophilized and the remaining polymer dry weight was measured. The remaining ratio of the polymer was calculated by dividing the dry weight of the remaining polymer by the dry weight of the initial gels."

2.1.5 Toughness Measurement

"The fracture energy or toughness of hydrogels was determined using pure shear tests. One pair of samples was used for each data point. One sample was unnotched, and the other sample was notched. In their undeformed state, each sample had a width W=40 mm and a thickness T=1.5 mm." 50mm.50mm acrylic sheets were prepared using the laser cutter and the hydrogels samples were glued to the acrylic sheet to perform the test. "The distance between the two PET clamps was H=5 mm. The unnotched sample was pulled by an Instron machine with a 10 N load cell at a strain rate of 2 min^{-1} to measure the stress-stretch S-λ curve. For the notched sample, a notch length of 10 mm was introduced using a razor blade. The notched sample was pulled until rupture to obtain the critical stretch (λ_c). The fracture

energy was calculated using the area under S-λ curve from the unnotched sample using the following equation:"

$$\Gamma = H \int_1^{\lambda_c} s \, d\lambda \tag{2.1}$$

2.1.6 Permeability Characterization

A simple setup was initially designed and tested using a 180 cm glass tube connected in series to another 72 cm glass with a stopcock at its end as shown in Fig. 2.1. To evaluate the feasibility of the test the samples were placed in a transwell and connected to the tubes. After opening the stopcock, water started to pass through the samples and collected in an erlenmeyer flask, placed below it. Using a stopwatch, time was recorded and the flow rate was measured accordingly. It was assumed that the pore Reynolds number is sufficiently small so that the inertia can be neglected and Darcy's law can be used to model the flow through the scaffold. However, the setup was not automated increasing the human errors and the pressure was not high enough to measure the permeability of materials with low porosity.

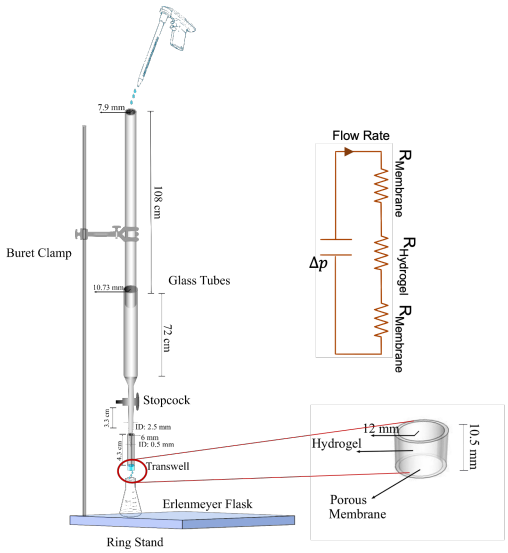

Fig. 2.1. Schematic of permeability setup.

As an alternative, "a customized t-shaped adaptor was 3D printed to fabricate an

automated system to measure the permeability of samples. Before testing, hydrogel samples was first cured inside a cylindrical container of 1 cm length and 1 cm in diameter at 37°C. The container was then enclosed by slotting it into the main body of the adaptor and screwing on the retaining cap. The pressure sensor was then connected, and the modified syringe connectors were opened. The schematic of the setup is shown in Fig. 2.2. A liquid-loaded syringe was then connected to the perpendicular port and the adaptor was slowly filled while ensuring all the air escapes. The air outlet was then sealed before the test began. During the test, the syringe pump was set to advance at a fixed rate and the pressure was measured. The fluid that passes through the hydrogel was collected and measured using the stopwatch and bucket method. The measured pressure and volume were used to calculate the permeability of the gel according to Darcy's law as follows:"

$$Q = \frac{k}{\mu}\Delta P, \tag{2.2}$$

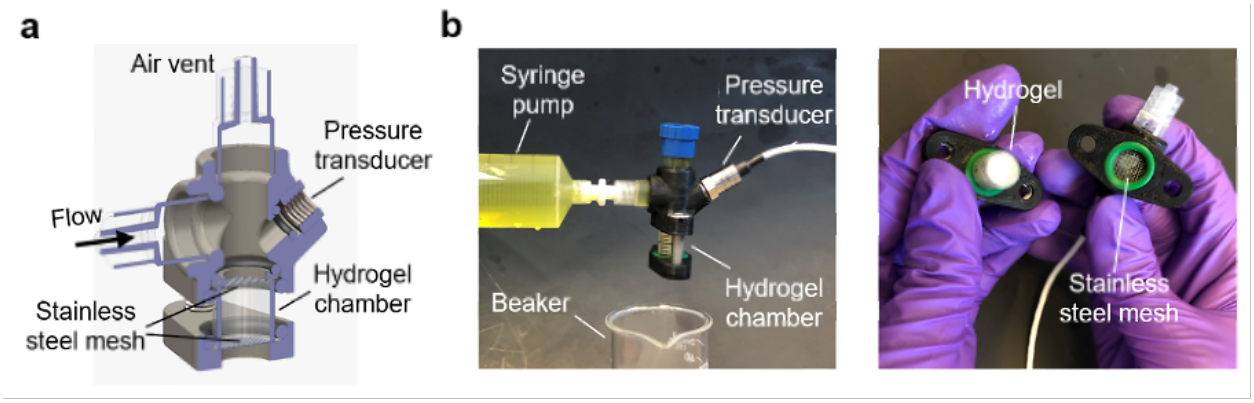

Fig. 2.2. Permeability setup. (a) "Schematics showing the internal structure of the perfusion chamber. (b) Digital photos showing the setup of the experiment."

2.1.7 Bioreactor Fabrication

"The bioreactor was made of two similar vocal fold (VF) replicas mounted on a custom build body. A CAD model of the VF replica mold with a cylindrical cavity (5 mm in diameter and 50 mm in length) was created for hosting the . A commercial 3D printer (Connex 500 multi-material 3D printer; Stratasys for a 3D World, Inc.,Eden Prairie, MN) was used to fabricate the mold. Two types of silicone rubber including Dragon skin 0030 and Ecoflex 0010 Platinum Cure Silicone Rubber (Smooth-On, Easton, PA) were used to fabricate the two layers of VF replicas. The collision contact between two human VF s in the larynx was mimicked by lateral contact of two replicas. Longitudinal stretch similar to that of human VF s during phonation was imposed using two sets of bolts, which could apply tensile force to the replicas. To fabricate the VF replicas, a mixture of two-part Ecoflex 0010; that is, part A, part B, and single- part silicone thinner with a mass ratio of 1:1:1.5, was used. The solution was molded and cured for 6 h, after being evacuated using a vacuum pump. Then, the cavity inside the cured replica was washed with 70% ethyl alcohol followed by deionized water to remove the residue of the release agent. The open side of the replica was sealed using additional Ecoflex 0010 mixture. The solution of Dragon Skin Part A, Part B, and silicone thinner (100-μm-thick layer) with a mass ratio of 1:1:1 was added on the superior surface of vibratory parts of the replicas. It is reported that the addition of an epithelial layer could result in lower tackiness and improvement of phonatory characteristic [174]. The bioreactor body was fabricated using a solution of two-part Ecoflex 0030 Platinum Cure Silicone Rubber (Smooth-On) (part A and part B) with a mass ratio of 1:1. After cleaning the mold parts with pure alcohol and applying a release agent, the parts were assembled and two sets of

bolts were placed on each side of the longitudinal and lateral axis of the mold before the preparation of the silicone solution. The VF replicas were then gently placed in the body mold and a thin plastic sheet was used between the contact surface of the replicas to avoid adhesion. The Ecoflex 0030 mixture was then carefully poured in the mold to prevent the formation of air bubbles. The bioreactor body was then taken out from the mold after being cured for 12 h at room temperature. The entire bioreactor was autoclaved to sterilize the inner cavity. The detailed bioreactor fabrication steps can be found in Fig. 2.3."

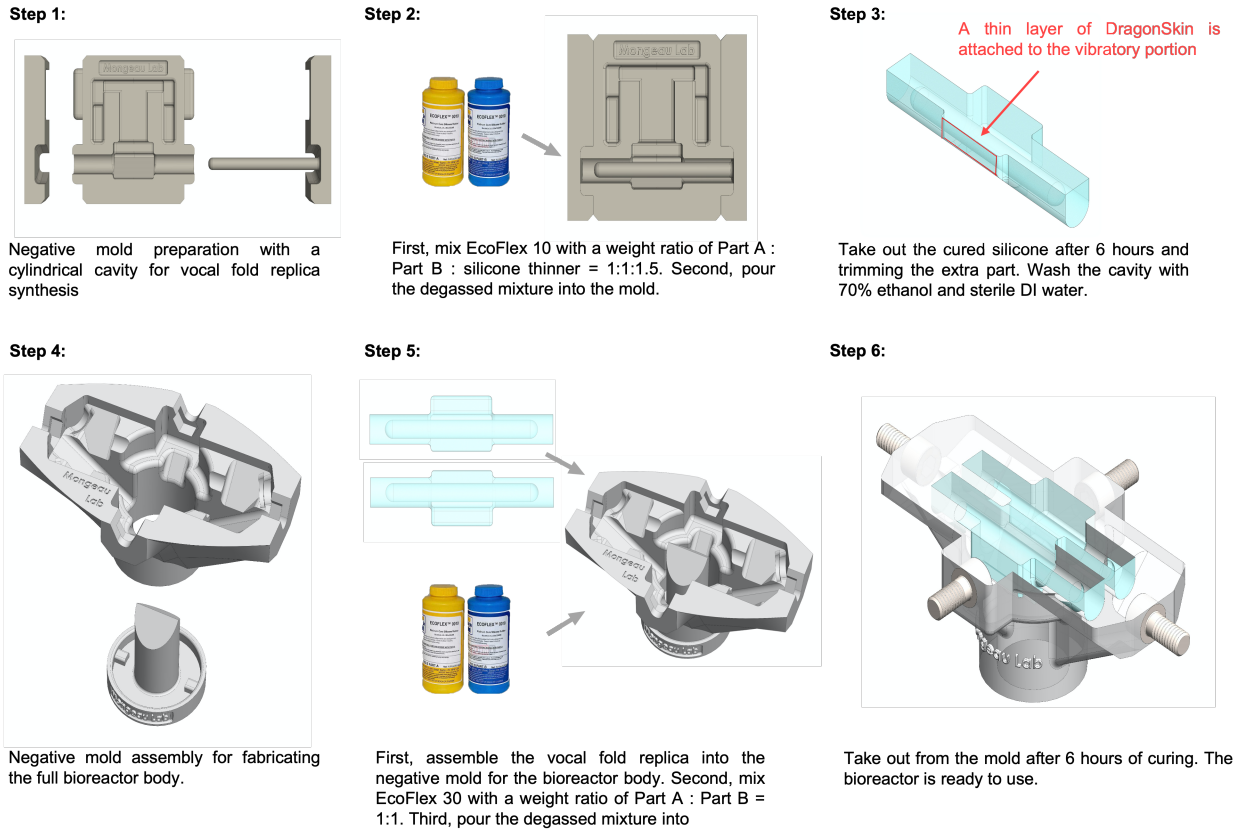

Fig. 2.3. Bioreactor fabrication

2.1.8 Microfluidic Devices

"The body of the microfluidic devices was fabricated using soft lithography. In brief, a negative mold was created by printing a PluronicTM F-127 ink (37 wt% in water, P2443) inside a Petri dish into predefined patterns with a bioprinter (BioAssemblyBot, Advanced Solutions). PDMS (SYLGARD 184, Dow) was prepared by mixing the base to cure at a weight ratio of 10:1. PDMS was degassed and poured into the Petri dish to cover the printed constructs. After curing at 60℃ overnight, the cured PDMS was taken out of the mold. Pluronic F-127 was removed by washing in cold water. The surfaces of the PDMS body and glass slide were treated with oxygen plasma before bonding to form the complete device. A 2-mm biopsy punch was used to create openings for the inlets and outlets. Devices were repeatedly sterilized with 70% ethanol before washing with PBS. Hydrogels were injected to fill the microfluidic channels. The devices were incubated at 37℃ for 30 mins before flow perfusion."

2.1.9 Measurement of the pH

The pH values of hydrogel solutions were measured using an electronic SevenEasy pH meter (Mettler Toledo) at room temperature.

2.2 Biological Characterization

2.2.1 Cell Culture

"Immortalized HVFF were cultured in Completed DMEM (Life Technologies Inc.) containing sodium pyruvate and supplemented with 10% FBS (Sigma- Aldrich Co., St. Louis, MO), 1% penicillin/streptomycin (P/S, Sigma-Aldrich Co.), 1% sodium pyruvate (Life Technologies, Inc.), and 1% minimum essential medium (MEM) nonessential amino acids (MNEAA; Sigma-Aldrich Co.) at 37℃, in a 5% CO_2 humidified atmosphere." Volume- to-volume percentages (%v/v) was used for expressing the concentration of all cell culture medium (CCM) ingredients. CCM was replaced every three days. Cells were ready for encapsulation within the hydrogel when the cell confluency reached 70% (about 7 days). The 0.25% trypsin-EDTA was used to disassociate cells as the sufficient confluency is reached.

2.2.2 Bioreactor Injection

"Sterile needles (305198, BD Medical) were first inserted from the two sides of the bioreactor body until reaching the empty hydrogel chamber. Hydrogel precursors and their associated gelling agent were quickly mixed, followed by mixing in a cell suspension to reach a final concentration of 2 million/ml. The cell-laden hydrogel precursors were then injected through pre-inserted needles to fill the chambers. While the was slowly injected into one side of the replicas, air bubbles were removed from two needles on the other side of the replicas. The injection was conducted under the laminar hood to prevent any contamination. A peristaltic pump (Ismatec, Wertheim, Germany) and an air blower were used for cells feeding

and phonation, respectively. All equipment was placed in a tissue culture incubator CO_2 incubator (NU AIRE Model NU-5510; NuAire, Inc., Plymouth, MN) as shown in Fig. 2.4a to keep a temperature and relative humidity of 37°C and 95%. Hydrogels were left to crosslink for 2 hours before cell culture media was perfused. A combination of the CCM with a mixture of filtered oxygen and 5% carbon dioxide was perfused through the along the longitudinal direction of the replicas. The perfusion system has a secondary loop as shown in Fig. 2.4b. Using the loop, a portion of the used medium was collected as waste byproduct while the remaining was mixed with the fresh media inside the tubing system for re-perfusion into the replicas. The average perfusion flow rate was 5 µL/min. The bioreactor was phonated for 2 hours per day over 7 days. Dynamic subglottal and supraglottal pressure was monitored using two pressure transducers (130D20, PCB Piezotronics) placed 10 cm below and above the bioreactor lips, respectively. The microphone was connected to a conditioning amplifier (Brüel and Kjær) that connected to a data acquisition system (National Instruments). Digital readouts for flow and pressure were displayed on a PR 4000F (MKS Instruments). Hydrogels were harvested after pre-determined time points for various assays."

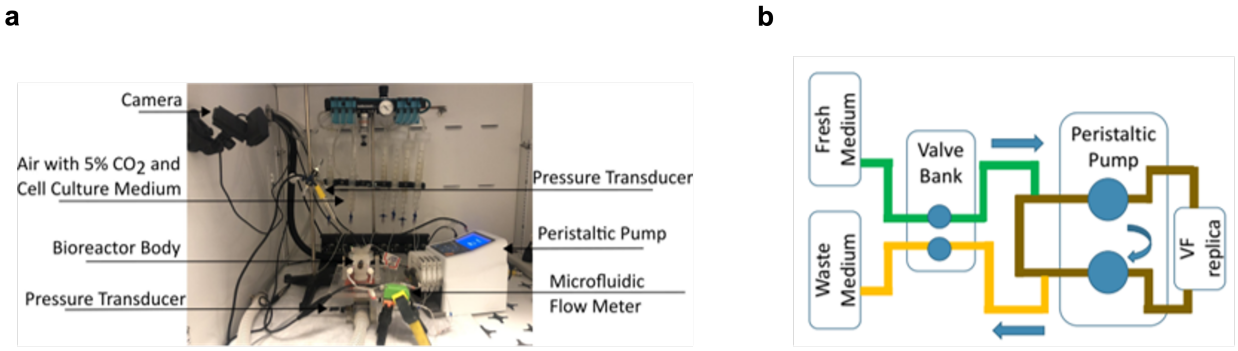

Fig. 2.4. Schematic and digital photo showing (a) the arrangement of the complete bioreactor setup and (b) the configuration of the control loop.

2.2.3 Cell Viability

"To evaluate the cytocompatibility of hydrogels, HVFF s were suspended in hydrogel mixtures immediately after the precursors and gelling agents were mixed. The final cellular concentration was 1 million/mL. The mixtures were then injected into Petri dishes to form hydrogels. Complete DMEM with 10% FBS was used as CCM and changed every day. HVFF s were stained by a LIVE/DEAD viability kit (L3224, Invitrogen) inside 3D matrices on Day 0, 3, 7. Imaging of fixed HVFF s was conducted using a confocal laser scanning microscope (LSM710TM, Zeiss, Germany). Live cells were shown in green fluorescence and dead cells were shown in red."

2.2.4 Cell Penetration

"To evaluate the cell penetration into the hydrogels, HVFF s cultured in 2D flasks were firstly starved in serum-free DMEM for 6 hours. Cells were then detached and suspended in serum-free DMEM at a concentration of 50,000 cells/mL. 200 µL of cell-free hydrogels were coated to cell culture inserts (08-771-10, Fisher Scientific) to evenly cover the permeable membrane of 0.45 μm pore size. Serum-free cell suspension (0.8 mL) was added on top of each hydrogel.The cell inserts were then placed into a 12-well plate. Serum-rich DMEM containing 10% FBS was then added to the wells and outside of cell culture

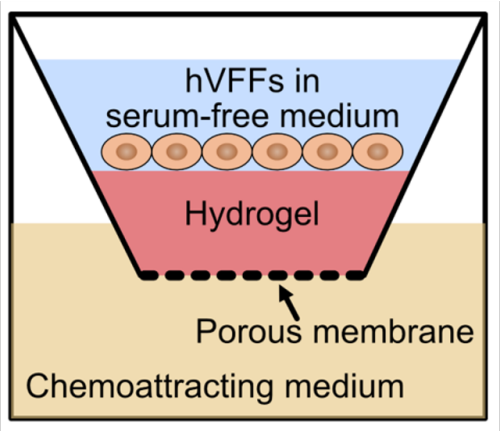

Fig. 2.5. "Schematic of cell penetration experimental setup."

inserts to form a chemoattractant gradient across the permeable membrane. The Schematic of the experimental setup is depcited in Fig. 2.5. Cells were cultured for 2 days before being counterstained with DAPI (D1306, Invitrogen) using a 1:5000 dilution for 5 min, followed by rinsing twice with PBS. Z-stack imaging of cell penetration into the hydrogels was conducted using a confocal laser scanning microscope (LSM800TM, Zeiss, Germany)."

2.2.5 Immunohistochemistry

"Hydrogels were first washed with pre-warmed PBS twice and then fixed in 3.7% formaldehyde solution for 15 mins. The fixed samples were washed with PBS again twice and permeabilized with 0.1% Triton X-100 in PBS for 5 minutes. The samples were blocked in 1% bovine serum albumin (BSA)(A1595) for 1 hour.

To conduct F-actin staining, 10 µL of Alexa Fluor 633 Phalloidin (A22284, Invitrogen) was diluted into 200 µL PBS containing 1% BSA . The samples were incubated inside the staining solution at room temperature for 30 mins followed by three times PBS wash.

To conduct collagen staining, rabbit polyclonal antibody of collagen-I (1:200, ab34710, Abcam) was added to PBS containing 1% BSA . The samples were incubated inside the staining solution at room temperature for 30 mins followed by three times PBS wash. The samples were blocked again in goat serum and then incubated for 1 hour with the Alexa Fluor 488 goat anti-rabbit IgG secondary antibody (1:1000, A11034, Invitrogen) followed by three times PBS wash. The nuclei were counterstained with DAPI using a 1:5000 dilution for 5 min, followed by rinsing twice with PBS."

2.2.6 Statistical Analysis

"A sample size of $N \geq 3$ was used for all experiments. Data are shown as Mean ± SD. Statistical analysis was performed using one-way ANOVA and post hoc Tukey tests for multiple comparisons or Student's t-tests for comparison between two groups (Prism 9, GraphPad Inc.). P values <0.05 were considered statistically significant."

2.3 Numerical Simulation

"COMSOL Multiphysics (Stockholm, Sweden) was employed to simulate the phonation in the VF bioreactor. A two-dimensional fully coupled fluid-structure interaction (FSI) model was developed using the unsteady Navier-Stokes equations for the fluid domain. The solid domain consisted of three parts representing the lamina propria (LP) (hydrogels), vocalis muscle (Ecoflex 00-10), and a thin epithelium layer (Dragon Skin). The hyperelastic Ogden material model was used for the solid domain. The strain energy density for the Ogden model is given by

$$\psi_D = \frac{\mu}{\alpha}(\lambda_1^\alpha + \lambda_2^\alpha + \lambda_3^\alpha - 3) \tag{2.3}$$

where ψ_D is the strain energy density, μ and α are the fitting coefficients, and λ_i is the ith principal stretch. The nominal stress S for a pure shear test is given by

$$S = \mu(\lambda^{(\alpha-1)} - \lambda^{-(\alpha+1)}) \tag{2.4}$$

The Ogden parameters for the hydrogels were determined by fitting Equation (2.4) to the loading paths in the pure shear test results of the hydrogels. The Ogden parameters for the Ecoflex 00-10 and Dragon Skin were extracted from our previous measurement [174].

Rayleigh damping model was used for the hydrogels. A dynamic system can be described by

$$[M]\frac{\partial^2 x}{\partial t^2} + [C]\frac{\partial x}{\partial t} + [K]x = F_{static} + F_{dynamic} \tag{2.5}$$

where [M] is the mass matrix, [C] is the damping matrix, [K] is the stiffness matrix, x is displacement as a function of time, and F_{static} and $F_{dynamic}$ are static and dynamic loads, respectively. The system damping matrix is defined by

$$[C] = \delta[M] + \beta[K] \tag{2.6}$$

where δ and β are the mass and stiffness proportional Rayleigh damping coefficients, respectively. The Rayleigh damping coefficients were determined by the different damping ratios ξ at different response frequencies ω in rad/s according to

$$\xi = \frac{1}{2}(\frac{\delta}{\omega} + \beta\omega) \tag{2.7}$$

The damping ratios, $\xi = \frac{1}{2}\frac{G"}{G'}$, were measured from frequency sweep between 0.1 to 100 Hz using a rheometer, where G' and G" are the storage and loss moduli, respectively. Damping in the two other solid bodies was modeled using the isotropic loss factor to account

for the intrinsic damping properties of the materials. For the fluid domain, the no-slip boundary condition was applied on the surface of the elastomers. The inlet airflow was defined as an incompressible fully developed laminar flow at room temperature. To reduce the computational cost, a symmetric one half-body of the M5 VF model was designed from a canonical model ([178]) for glottal airflow simulation. Dynamic free triangular fine meshes were used to allow for the FSI modeling. An implicit time-dependent fluid solver with a step size of 0.001 s was used in conjunction with a physically controlled tolerance. The stress distribution within the elastomers and the hydrogels were obtained from the simulations. Tables 4.10 and 2.3 present the material properties and simulation parameters, respectively."

Table 2.2. "Simulation parameters used in the numerical model"

Parameters	**Value**
Inlet average velocity of air ms^{-1}	2.66
Outlet pressure	0
Half of the initial glottal gap size (mm)	1
Epithelium thickness (mm)	0.1
Minimum mesh size(mm)	0.0075
Maximum mesh size (mm)	1.33
Dragon Skin density kgm^{-3}	1070
Dragon Skin dynamic viscosity ($Pa \cdot s$)	20
Dragon Skin Young's modulus (Pa)	592 949
Dragon Skin Poisson's ratio	0.49
Dragon Skin isotropic structural loss factor	0.24
Ecoflex 00-10 density kgm^{-3}	1 040
Ecoflex 00-10 Young's modulus (Pa)	9693
Ecoflex 00-10 Poisson's ratio	0.49
Ecoflex 00-10 isotropic structural loss factor	0.53

Table 2.3. "Material parameters of the hydrogels used in simulation"

Parameter	**NSN**	**PSN**	**PDN**
Density kgm^{-3}	1000	1000	1000
Poisson's ratio	0.49	0.49	0.49
Ogden parameter α	3.24	1.91	2.79
Ogden parameter μ (Pa)	1913.57	2526.60	3 159.89
Mass damping parameter δ s^{-1}	0.0093	0.027	0.026
Stiffness damping parameter β (s)	0.0029	0.0021	0.0048

CHAPTER 3

Porous Double-network hydrogels

In this chapter, a novel strategy to fabricate porous double-network (DN)s with different concentration of the glycol chitosan (GC) is presented. The fabricated DN gels were studied in series of mechanical, rheological, and biological tests. The pore size of the hydrogels were measured based on three different imaging techniques to evaluate the porous structure and measure the pore size and porosity of the DNs. A new setup was designed and fabricated to characterize the permeability of DNs. Then, the effect of porosity on the cellular performance of DN, such as the cell viability and penetration of human vocal fold fibroblast (HVFF) were investigated. The viscoelastic characteristics of the DNs were investigated using rheometry tests while the mechanical properties, such as toughness, stretchability, stiffness and stress relaxation are measured using Instron machine. Water absorption capacity and degradation rate of the developed gels were also discussed using swelling and enzymatic degradation tests over specified time. The results support the potential of using DN hydrogels as a synthetic scaffold for tissue engineering applications. The sentences in quotations are verbatim of the author's publications (references [1]).

3.1 Rheological Characterization

3.1.1 Thermal Gelation Kinetics

"The gelation of injectable, pore-forming hydrogels involves three coordinated processes: initial solidification, phase separation and further crosslinking. The initial solidification should occur in a controlled manner and ensue fast enough to avoid dilution by body fluids. The phase separation and further crosslinking should be separated in time to allow both to proceed independently, leading to interconnected and mechanically stable pores. Our porous double-network (PDN) hydrogels meet these design criteria. The precursors and gelling agents reacted and partially crosslinked immediately upon mixing, followed by a gradual stiffening process over time. The initial solidification is reliant on the thermogelling behavior of chitosan (i.e., part of secondary network) [179]. At room temperature, gelation was slow and steady, allowing time for cell encapsulation and injection (Fig. 3.1a). After injection and placement at 37℃, gelation accelerated, quickly yielding a strengthened hydrogel (Fig. 3.1a). Accompanying the initial solidification, phase separation also took place within seconds. Sequentially, the GC needed around 15 minutes before starting to crosslink (Fig. 3.1b). The disparate kinetics of the fast phase separation and relatively slow covalent crosslinking ensures the mobility of polymer chains before they are immobilized by chemical bonds, which is essential to the formation of a polymer-poor phase for the porous structure. The viscosity at room temperature was also low, which is beneficial for injection with reasonable processing time. The viscosity graph is shown in Fig. 3.2."

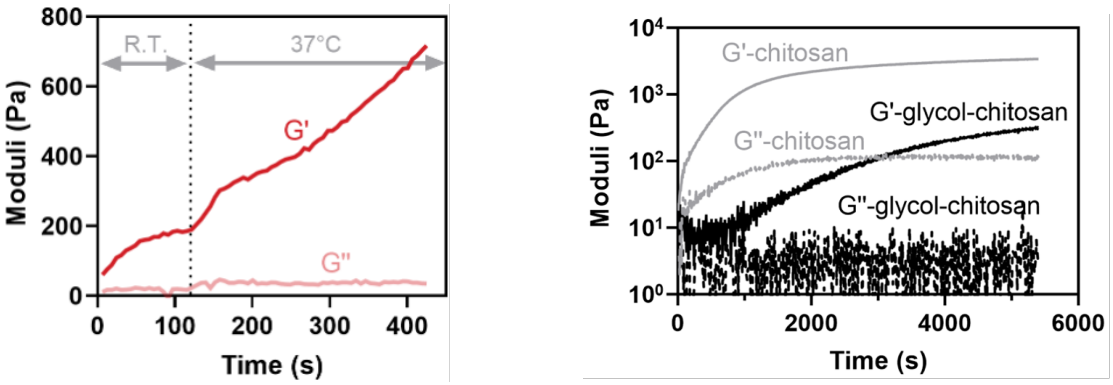

(a) (b)

Fig. 3.1. (a) "Thermal gelation kinetics of PDN mixture when the temperature is raised from room temperature (R.T.) to 37 ℃ (b) Gelation kinetics of chitosan and GC. The primary network (chitosan) crosslinks within seconds, while the secondary network (GC) did not occur within 15 mins. The disparate kinetics provides a sufficient time window for pore formation."

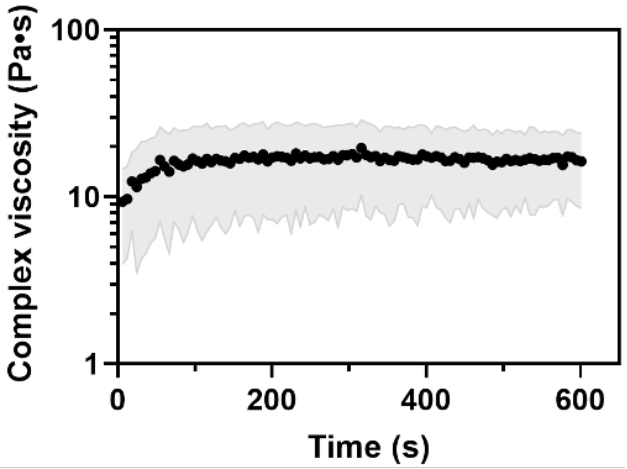

Fig. 3.2. "Viscosity of PDN_1 as a function of time after mixing at room temperature. Black dots denote the mean value, and the grey area denotes the standard deviation. Sample size, N = 3."

3.1.2 Stiffness

Time-sweep tests were conducted to study the viscoelastic characteristics of the hydrogels. "The resulting PDNs showed a favorable viscoelastic response that resembles that of biological tissues. In terms of stiffness, the storage moduli of $PDN_{0.5}$ and PDN_1 were both around 3.5 kPa and comparable to that of porous single-network (PSN). Additional covalent network polymers further increased the storage moduli to $\sim$ 9 kPa as depicted in Fig. 3.3a. The stiffness range spans the range of various biological tissues, such as the vocal fold (VF)s, lungs, heart, and gastrointestinal tract [180]".

3.1.3 Young's Modulus

Young's modulus data were calculated from a series of compression tets using an InstronTM machine. "Young's moduli of PDNs were significantly higher than non-porous single-network (NSN) and PSN (Fig. 3.3b). Several possibilities could have contributed to this finding. First, the formation of pores concentrates the polymers and crosslinkers at the solid phase, leading to higher crosslinking density and higher moduli. The potential crosslinking between the chitosan and the GC networks by glyoxal (GY) could further amplify this effect; Second, the polymer concentration of PDN is marginally higher among the three conditions tested, which could contribute to the concentration effect as well. Third, the Young's moduli were measured at small-strain ranges, whereas the pores mainly affect the large-strain behavior (i.e., because of pore collapse). The synergy of those effects strengthens the PDNs despite their high porosity."

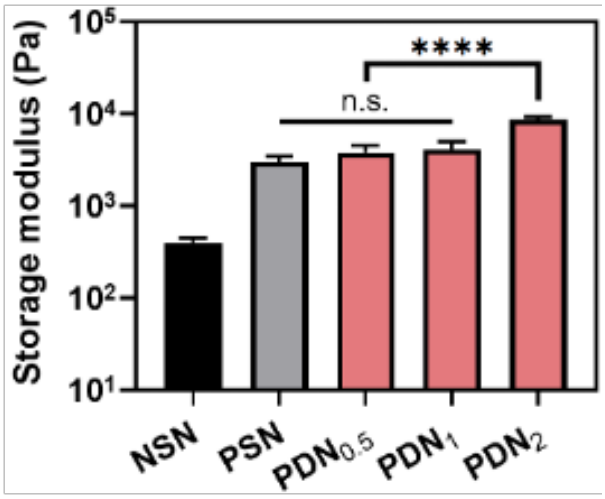

(a)

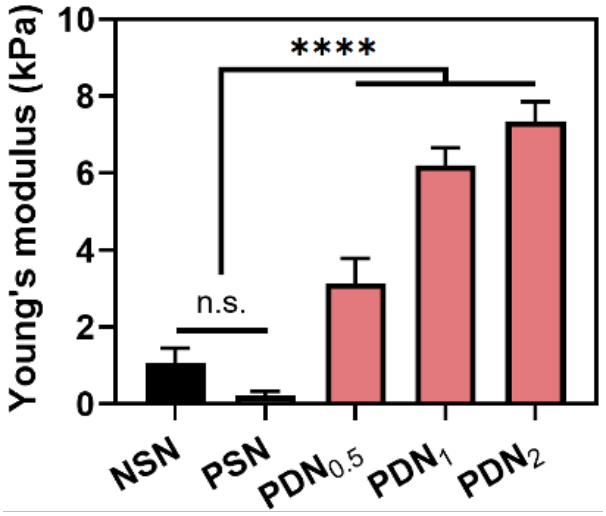

(b)

Fig. 3.3. (a) "Storage moduli of NSN, PSN, and PDNs." (b) "Young's moduli of NSN, PSN, and PDNs calculated from compression tests. Sample size, N = 4. **** $P < 0.0001$, n.s. means $P \geq 0.05$."

3.1.4 Stress Relaxation

All PDNs exhibited a quick stress relaxation behavior. "We quantified stress relaxation behavior using the half-life time, $\tau_{1/2}$, a matrix to relax to one-half of its peak value under a constant compressive strain (15%). Stress relaxation time using the stress retention of 1/e was also evaluated (Fig. 3.4b). Notably, all the PDNs relaxed within 10^1 to 10^2 s (Fig. 3.4a). This fast stress relaxation response is comparable to that of organs and native extracellular matrix, such as collagen [181]. We attribute this behavior to the stress-induced rupture of hydrogen bonds in the dissipative network, and the fast water migration enabled by the interconnected porous structures, described in a later section. Prompt stress relaxation is beneficial for cell proliferation and migration; it can also help regulate the fate of stem cells [182]."

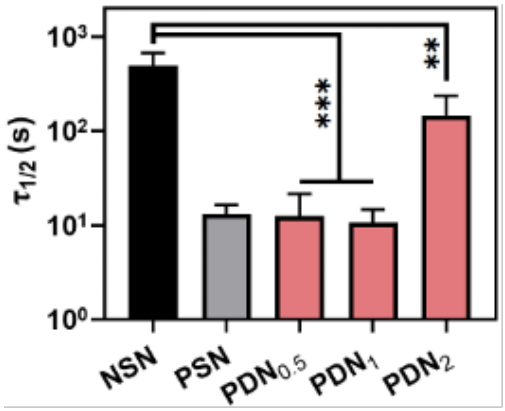

(a)

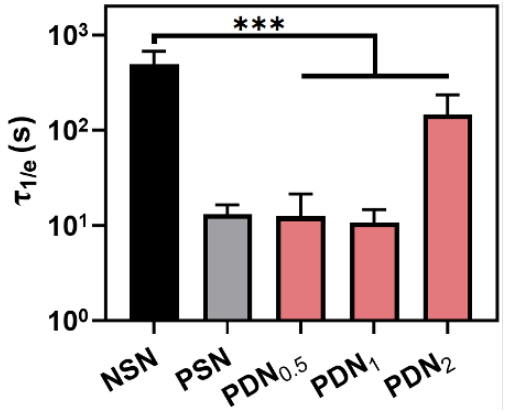

(b)

Fig. 3.4. (a) "Half-life time of stress relaxation ($\tau_{1/2}$) of NSN, PSN, and PDNs." (b) "Stress relaxation time of different hydrogels. Stress relaxation was evaluated by the stress retention of 1/e."

3.2 Porous Structure

The porous structure of the hydrogels were studied using three different methods. The results of each experiment are depicted below.

3.2.1 Confocal Microscopy

"A salient feature of PDNs is their interconnected microporous structure. To characterize the structural properties, we synthesized and visualized the three types of hydrogels (NSN, PSN, and PDN) containing FITC-labeled macromolecules with a confocal microscope at wet state. This process involves no drying or lyophilization treatment. The confocal images are shown in Fig. 3.5. As expected, NSN displayed no detectable pores. The mesh size of NSN and most existing injectable hydrogels is on the order of 10 nm, therefore well below the resolution limit of the confocal microscope. In contrast, PSN and all PDNs displayed micrometer-sized pores resulting from the phase separation of chitosan, which was further confirmed by the fluorescence intensity distribution. A single peak was observed for NSN, indicating a homogenous network. PSN and PDNs displayed a wide intensity distribution that included areas with low or even no fluorescence."

3.2.2 Scanning electron microscopy (SEM)

The second imaging method to analyze the structure of hydrogels was SEM. "For SEM, the samples were dehydrated with a CO_2 supercritical dryer to minimize artifacts." The obtained data were in great agreement with the confocal images. The confocal and SEM images for all concentration of PDNs, NSN and PSN are shown in Fig. 3.6.

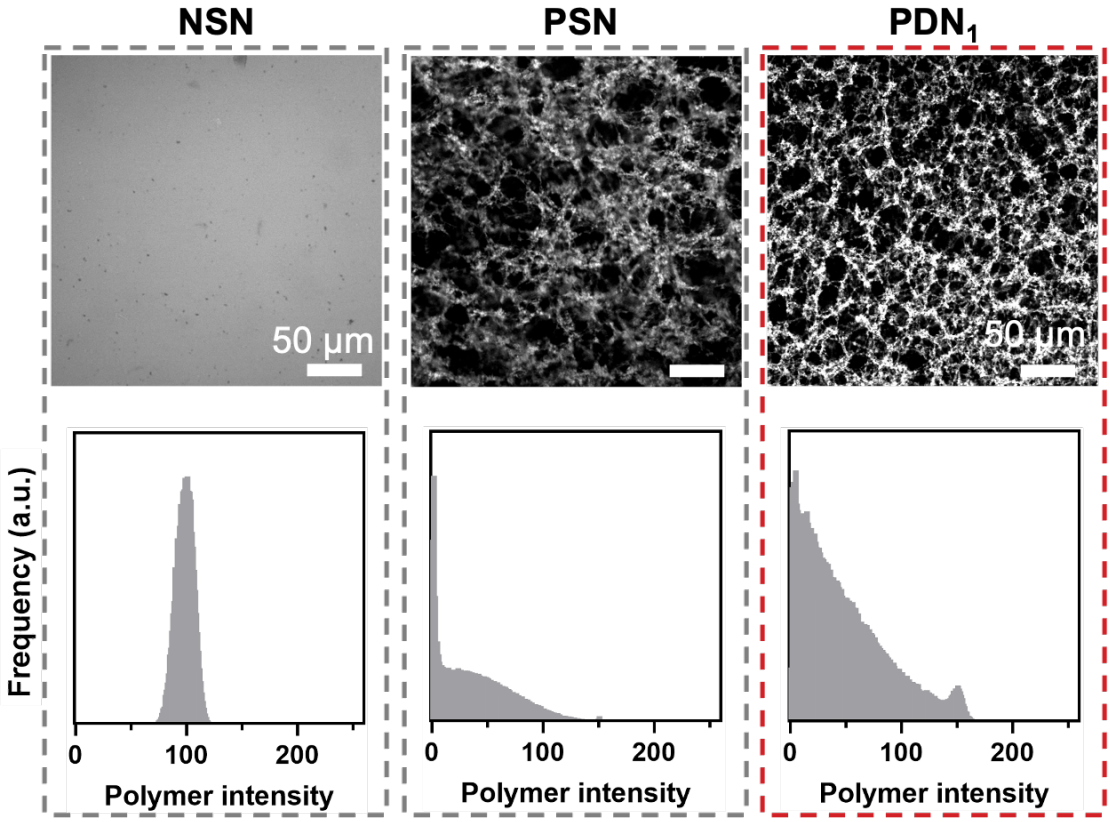

Fig. 3.5. "Confocal images (top) and fluorescent signal distribution (bottom) of hydrogels containing FITC-labeled chitosan and GC, showing the network configurations."

3.2.3 Micro-computed tomography (µCT)

Lastly, "we also verified the porous structures of hydrogels using µCT." As mentioned previously, the µCT samples were prepared in 0.5 ml Eppendorf vials and were scanned in hydrated condition. As it can be seen in (Fig. 3.7), NSN does not have any micropores while the PDN_1 has a micro-porous structure. Hence, "µCT results also confirmed the presence of an interconnected porous structure within PDNs, concluding the pore-forming capacity of our hydrogels."

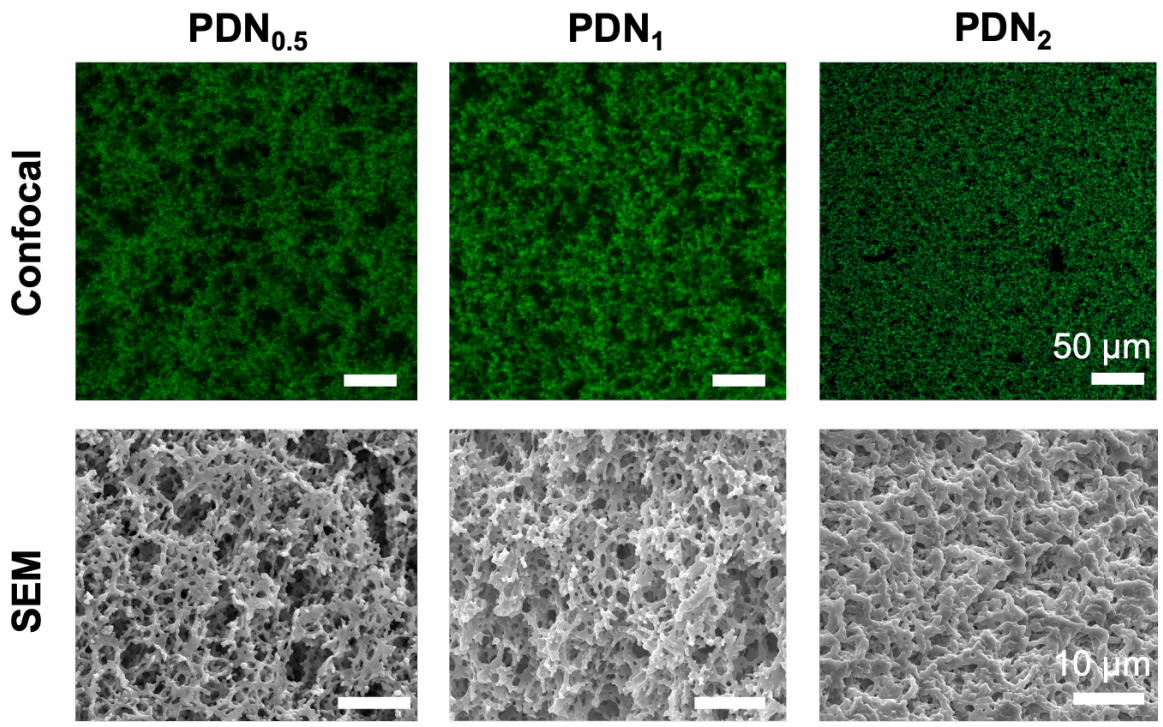

(a)

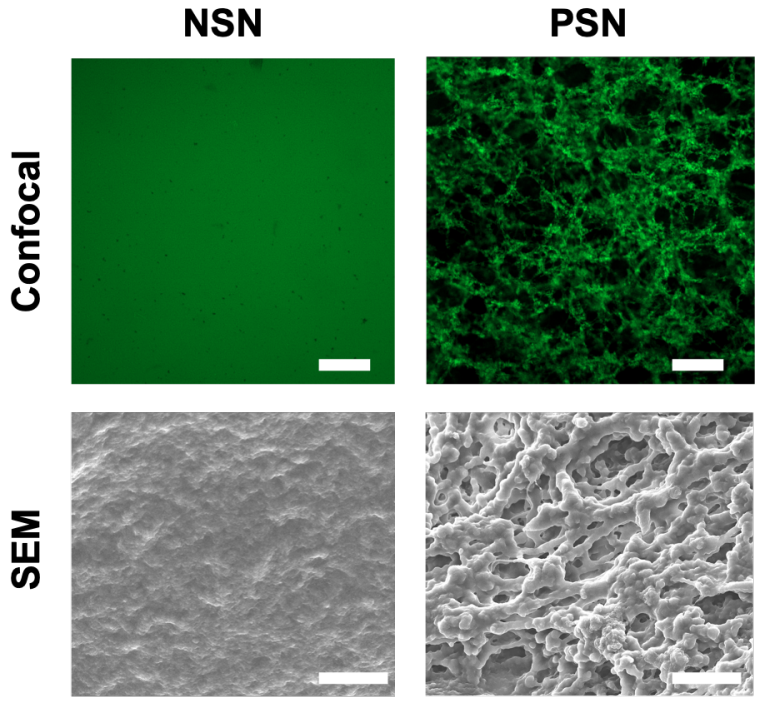

(b)

Fig. 3.6. "Confocal and SEM images showing the porous structures of (a) PDNs. (b) NSN and PSN. Sample size, N = 3."

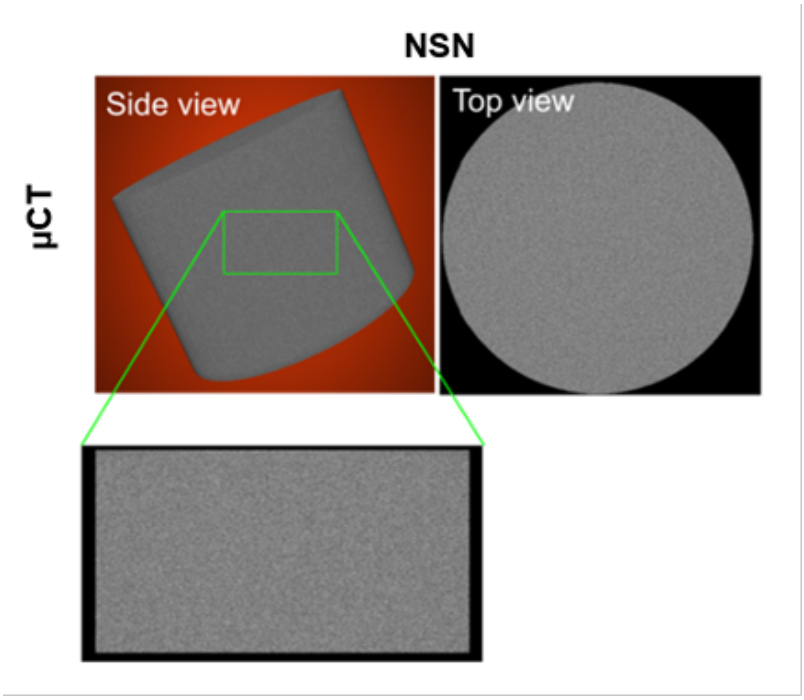

(a)

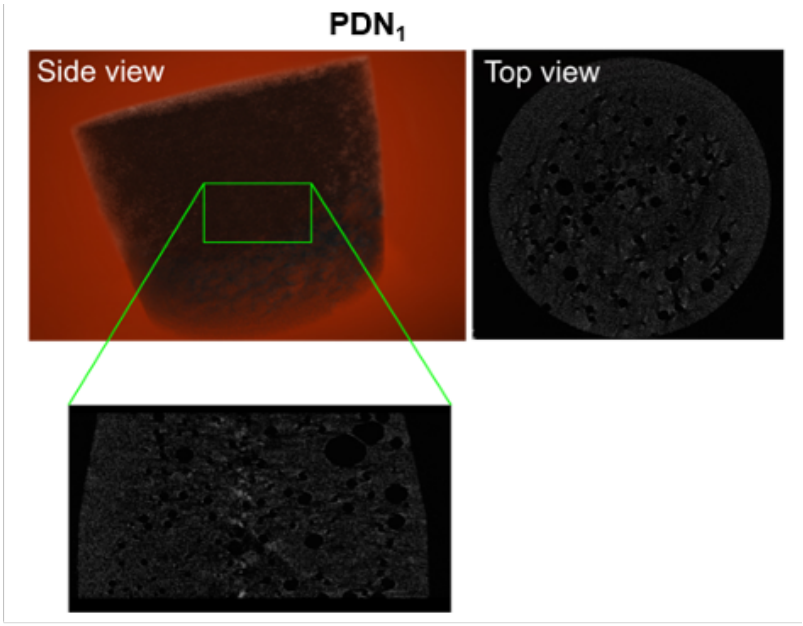

(b)

Fig. 3.7. "μCT images showing the porous structures of (a) NSN. (b) PDN_1. Sample size, N = 3."

3.2.4 Pore Size and Porosity

The pore size and porosity of samples were measured by processing the obtained images in ImageJ software. "Both the pore size and porosity are tunable by adjusting the concentration of the secondary network polymer–GC. The average pore size varied between 6 to 10 μm, comparable to the size of cells (Fig. 3.8a). The porosity can be tuned over a range of $\sim$ 21-54% (Fig. 3.8b). The concentration of GC is inversely proportional to the average pore size and porosity. We attribute this relationship in part to the interplay between the phase separation and the crosslinking of GC. With increasing GC concentration, the crosslinking of GC accelerates, and thus reduces the mobility of the chitosan and the time window for the phase separation. As a consequence, the proportion of the polymer-poor phase, i.e., pores and porosity, is decreased. The results further

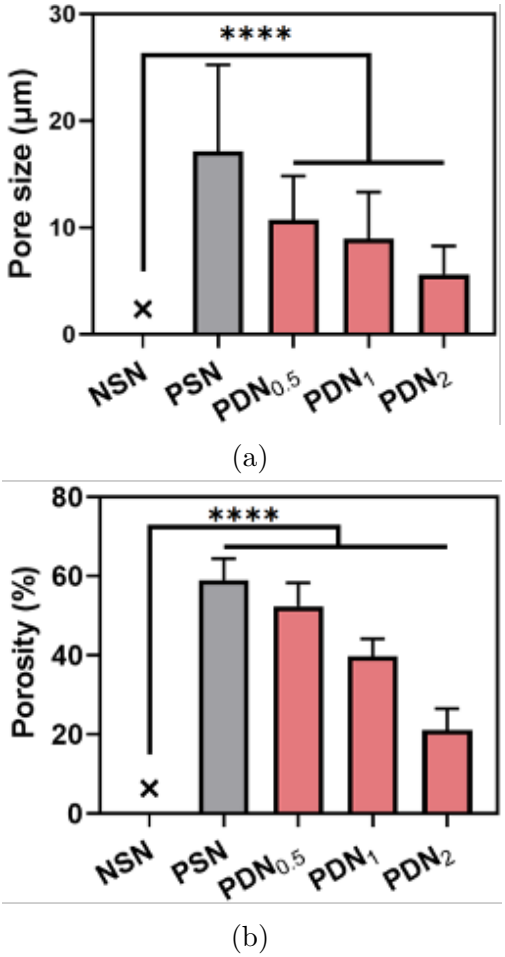

Fig. 3.8. "(a) Pore size and (b) porosity of NSN, PSN, and PDNs. Sample size, N = 4; ** represents $P < 0.01$, *** $P < 0.001$, **** $P < 0.0001$, n.s. means $P \geq 0.05$."

underscore the importance of orchestrating the gelation and phase separation processes for desired porous structures."

3.2.5 Permeability

"The interconnected porous structures of PDNs enable superior permeability. Permeability governs fluid transport within a hydrogel and mass exchange with the surrounding environment. High permeability supports the survival, activities, and function of cells in deep layers of hydrogels by ensuring adequate nutrient and oxygen delivery. This is especially important when immediate vascularization is lacking. To characterize the permeability, k, of PDNs, we perfused cylindrical hydrogel samples with media at various flow rates Q, while measuring the pressure drop, $\Delta P = P_0 - P_1$ using a pressure transducer as it is shown in Fig. 2.2 and Fig. 3.9.

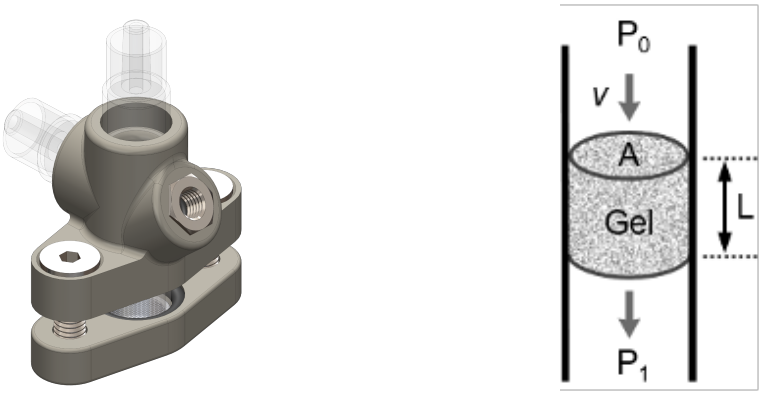

(a) (b)

Fig. 3.9. Schematics of the permeability measurement. (a) Full Assmebly. (b) Cylindrical hydorgel Sample. "The height and cross-sectional area of the gel are denoted as L and A, respectively. The flow velocity, up- and down-steam pressures are denoted as v, P_0, and P_1."

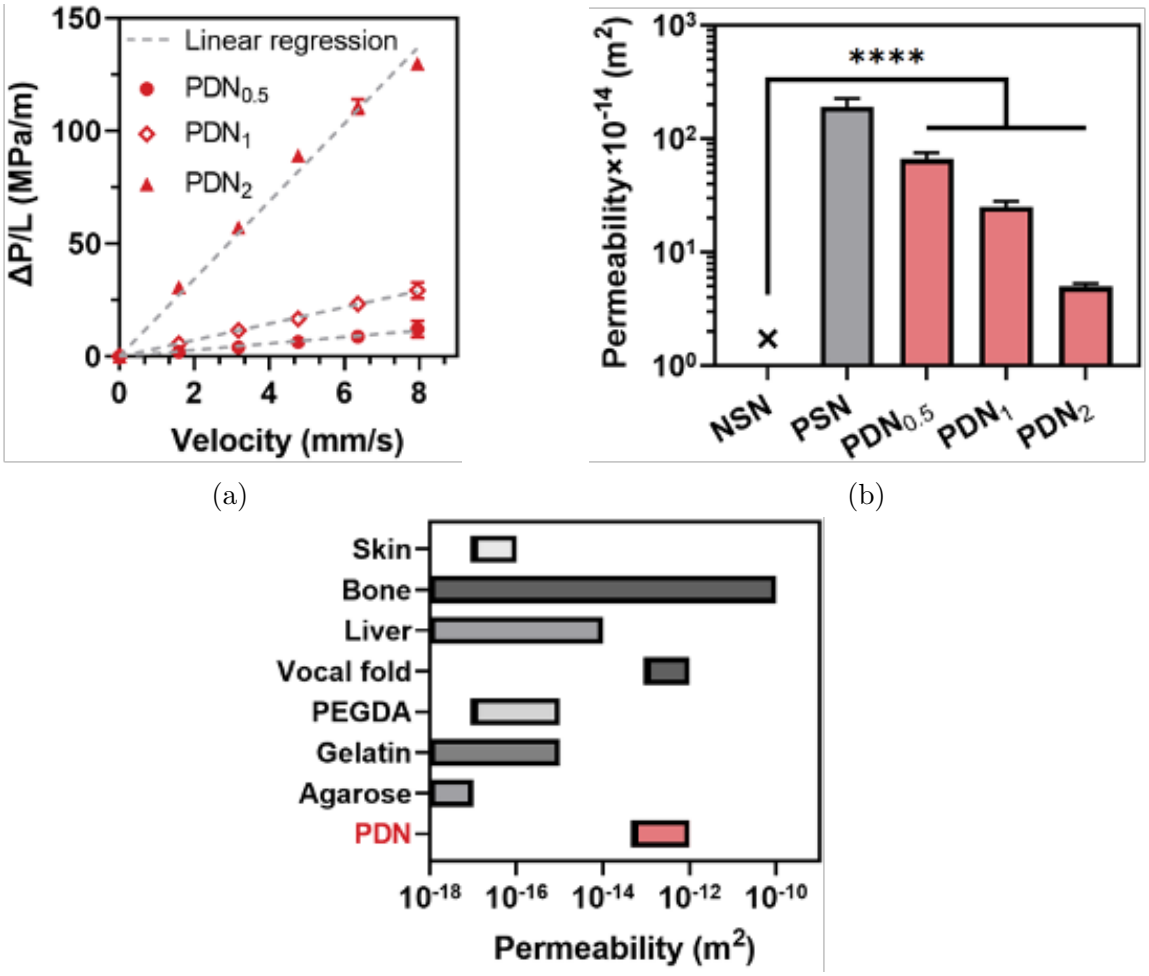

Fig. 3.10. "Permeability of PDNs. (a) Pressure gradient-velocity relations of different gels. (b) Permeability of different hydrogels. (c) Permeability of different hydrogels and biological tissues."

"Following Darcy's law, we calculated $k = \mu \frac{L}{A} \frac{Q}{\Delta P}$, where μ is the dynamic viscosity of the media (8.90×10^{-4} Pa $\cdot$ s for water), and A and L are the cross-sectional area and thickness of the hydrogel, respectively. The normalized pressure drop ($\frac{\Delta P}{L}$) across the PDN sample was linearly proportional to flow velocity, confirming an ideal porous material flow resistivity

behavior (Fig. 3.10a). The permeability of PDNs was on the order of 10^{-14} to 10^{-12} m^2 as shown on Fig. 3.10b . In contrast, it was not possible to perfuse media through NSN without fracturing the hydrogel due to its low permeability. We also compared the permeability results with values for commonly used hydrogels and biological tissues (Fig. 3.10c). PDNs exhibited at least 2 to 4 orders of magnitude greater permeability than most existing hydrogels. The measured permeability demonstrates that the PDN s contain highly interconnected porous structure, enabling rapid convection of transport fluid within the matrix."

3.2.6 Toughness and pore-insensitivity

"Despite the highly porous structure, PDNs are mechanically tough and insensitive to pores (Fig. 3.11a). We measured the toughness with pure shear tests (Fig. 3.11b). The area under the stress-stretch curve before a critical stretch, which was measured with a notched specimen, is the critical energy release rate to drive crack propagation (Fig. 3.12a). The toughness of NSN and PSN was $\sim$ 1 and 5 Jm^{-2}, respectively. These values agree with past reports on the toughness of single-network hydrogels (1 to 10 Jm^{-2}) [183]. In comparison, $PDN_{0.5}$ and PDN_1 exhibited a fracture toughness of 20 and 39 Jm^{-2}, respectively, corresponding to 20- and 40-fold increases compared to NSN (Fig. 3.12b).

The stretchability of PDN_1 was also twice higher than that of NSN (Fig. 3.12c). The enhanced toughness and stretchability of PDNs are attributed to the double-network configuration. Presumably, the physical crosslinks of chitosan break to dissipate energy under strain, while the covalent crosslinks of GC retain structural integrity. Notably, the toughening performance from the phase separation of chitosan was more significant compared to commonly used dissipative network, such as calcium crosslinked alginate. We prepared nanoporous

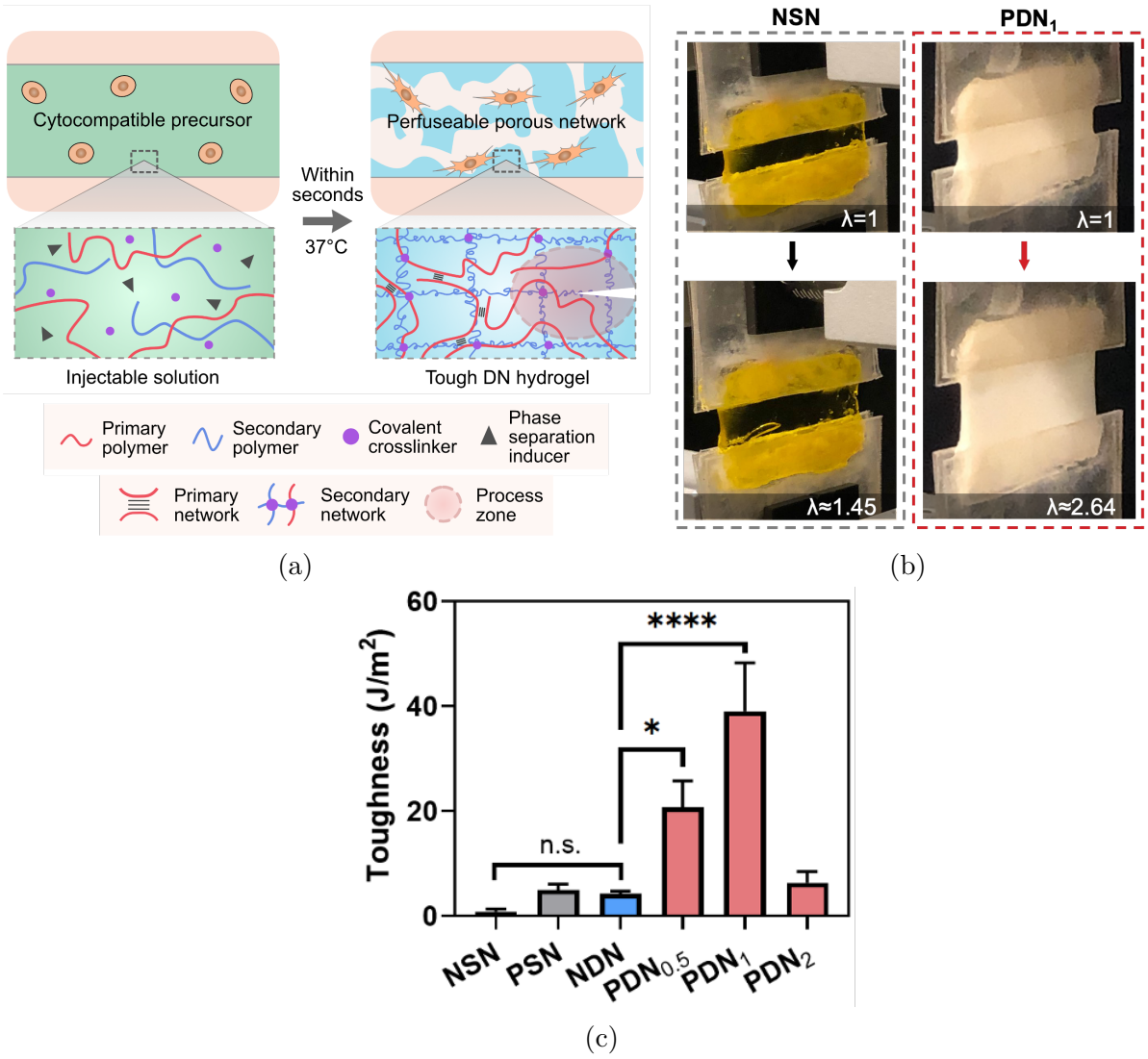

Fig. 3.11. " Toughness of PDNs. (a) PDNs form a tough matrix with micropores in-situ in a cytocompatible fashion. (b) Photos showing the stretchability of NSN and PDN_1. (c) Comparison of toughness among NSN, PSN, NDN, and PDNs."

double-network hydrogel (NDN) by replacing chitosan with calcium-alginate within PDN. Although NDN improved the toughness by 5-fold compared to NSN, the achieved toughness was still one order of magnitude lower than that of PDN_1 (Fig. 3.11c). To evaluate the

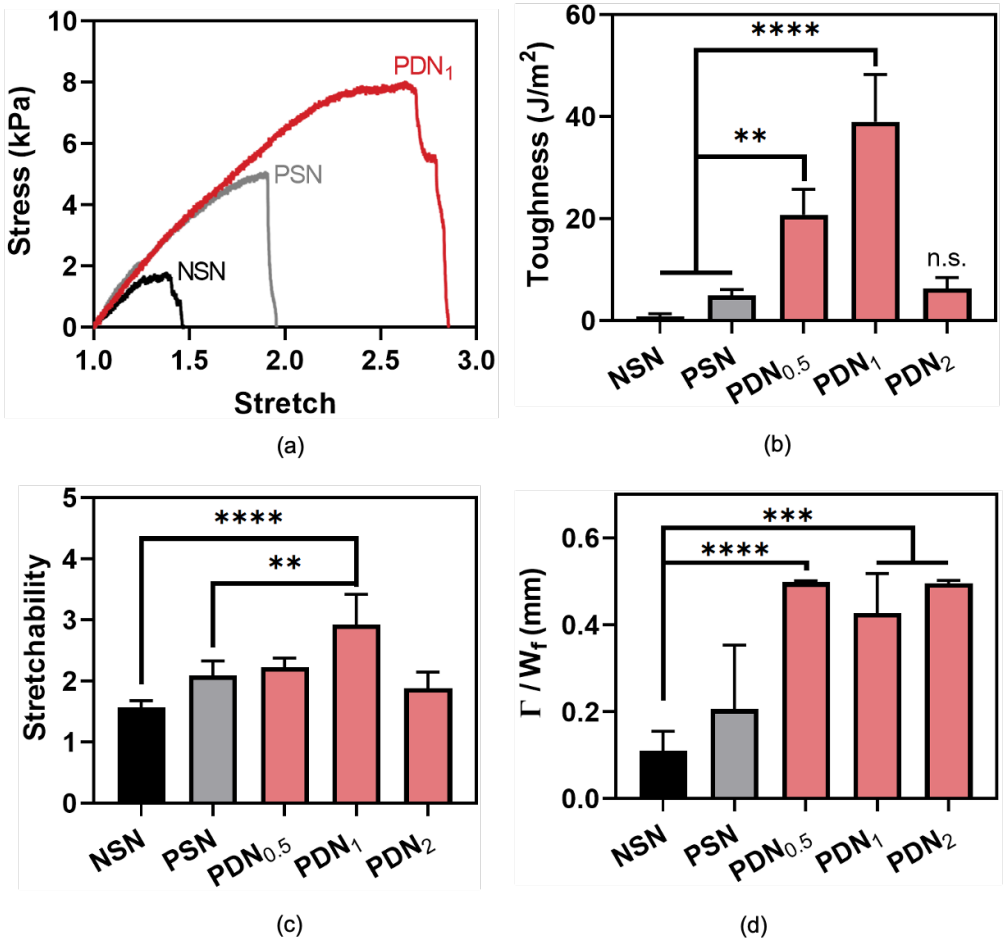

Fig. 3.12. "(a) Stress-stretch curves of NSN, PSN, and PDN_1. (b) Toughness, (c) stretchability, and (d) fractocohesive length of NSN, PSN, and PDNs. Sample size, N = 4, n.s. represents P$\geq$ 0.05, ** P $<$ 0.01, *** P $<$ 0.001, **** P $<$ 0.0001."

pore-sensitivity of the hydrogels, we compared their fractocohesive lengths, characteristic crack lengths below which a material is insensitive to its presence. Unlike single-network hydrogels, for which pores act as defects, our PDNs demonstrated a fractocohesive length of up to 0.5 mm (Fig. 3.12d). Owing to this high flaw-insensitive threshold, the pores within the PDNs did not degrade their toughness or act as defects."

A detailed summary of toughness,permeability, pore size, porosity, and stress relaxation data is shown in Table 3.1.

Table 3.1. Summary of structural and mechanical properties of representative hydrogels and biological tissues.

Hydrogels	Pore Size (μm)	Porosity (%)	Toughness Γ (J m^{-2})	Permeability (m^2)	$\tau_{1/2}$ (s)	Cyto-compatible synthesis?
This work	6-10	$\sim$ 21-54	Γ: 5-39 W^a: $\sim$ 14 λ^b: $\sim$ 3	10^{-14} - 10^{-12}	10^1 - 10^2	Yes
MethGH-HA hydrogel [162]	N/A	$\sim$ 0	Γ: N/A W^a: 9-14 λ: $\sim$ 3	N/A	N/A	Yes
Dual-click tough hydrogel [161]	N/A	$\sim$ 0	N/A	N/A	N/A	Yes
PVA-CPBA/Ca [164]	N/A	$\sim$ 0	N/A	N/A	N/A	Yes
PVA-Bioglass [165]	N/A	N/A	N/A	N/A	N/A	Yes
Fibrin-gelatin nanoparticles [166]	$\sim$10	$\sim$ 35	Γ: N/A W^a: 9-10 λ^b: $\sim$ 1.5	N/A	N/A	Yes
Alginate [106, 183, 184]	0.005-0.017	$\sim$0	1-10	N/A	10^2 - 10^4	Yes
Agarose [119, 185, 186]	0.08-0.4	N/A	15	10^{-17} - 10^{-16}	10^2 - 10^3	Yes

Table 3.1 continued from previous page

Chitosan [186]	<0.1	∼0	1-10	N/A	10^4	Yes
Gelatin [113, 187–189]	0.012-0.03	N/A	0.5-5	10^{-18} - 10^{-15}	10^3 - 10^4	Yes
Hylaurnic Acid [190, 191]	0.005-0.012	N/A	N/A	N/A	10^2 - 10^4	Yes
PEGDA [192, 193]	0.007-0.025	∼0	N/A	10^{-17} - 10^{-15}	N/A	Yes
Polyacrylamide [123, 183]	∼0.01	∼0	10-500	10^{-18} - 10^{-16}	$>10^4$	No
Collagen gel [194]	1.1-2.2	N/A	N/A	10^{-16} - 10^{-15}	10^0 - 10^2	Yes
Bioprinted GelMA [129]	18-53	∼10-50	N/A	N/A	N/A	Yes
Alginate cryogel [125]	∼30-100	∼70	N/A	N/A	N/A	No
Collagen sponge (freeze-dried) [195]	95-150	>99	N/A	10^{-13}	N/A	No
Bioglass foam [196]	∼300	∼90-95	N/A	10^{-9}	N/A	No
Polycaprolactone scaffold [197, 198]	∼1000	∼30-70	N/A	10^{-10} - 10^{-8}	N/A	No
VF [199, 200]	∼1-100	∼90	160-450	10^{-13} - 10^{-12}	∼60	NA
Liver [184, 201, 202]	0.1	∼20	160	10^{-18} - 10^{-14}	500	
Skin [203–205]	5-500	∼80	1000-20000	10^{-17} - 10^{-16}	N/A	
Tendon [205–207]	4-12	∼60-70	N/A	10^{-21} - 10^{-17}	∼1	

Table 3.1 continued from previous page

Intervertebral disc [208]	0.0015	N/A	N/A	AF: 10^{-17} NP: 10^{-18}	∼1 (NP)
Bone [209, 210]	6-300	∼3-80	400-30000	10^{-25} - 10^{-10}	N/A
Small-intestinal submucosa [210, 211]	1-10	∼87	N/A	10^{-17}	N/A
Articular cartilage [180, 212]	∼0.006	∼75	690-1300	10^{-17}	1500

3.3 Physical Characterization

3.3.1 Swelling

"As swelling affects the mechanical and physical robustness, the swelling profile of PDNs was evaluated next. Due to difficulties in accurately measuring the weight of hydrated porous materials, we quantified the swelling by monitoring the dimensional change of PDNs upon immersion in phosphate-buffered saline (PBS). PDNs maintained their original sizes with less than 10% size change while swelling greater than 30% was observed in NSN over a 7-day period (Fig. 3.13). Good physical stability in a liquid environment helps hydrogels maintain their shape, which is important in ensuring that surrounding tissues are not subjected to undue compressive stresses."

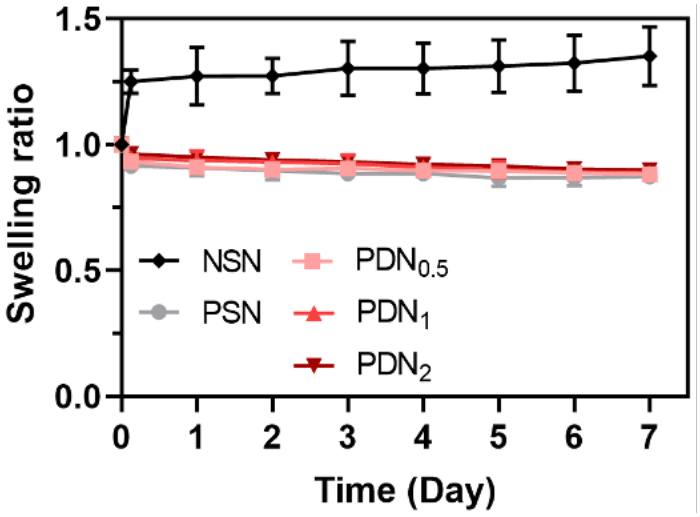

Fig. 3.13. "Swelling ratio of different hydrogels immersed in PBS for 7 days. N = 4."

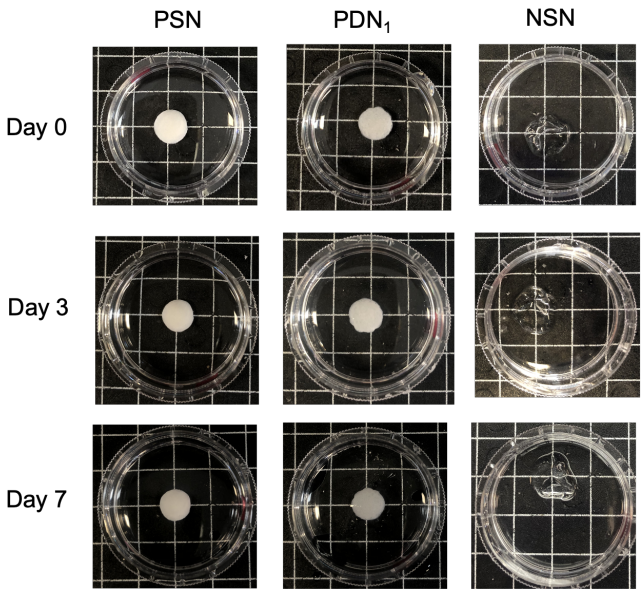

Fig. 3.14. "PSN, PDN_1 and NSN swelling samples immersed in PBS. sample size, N = 4."

3.3.2 Degradability

"PDNs are also biodegradable by enzymes. They showed a slow degradation profile over 28 days when exposed to lysozyme at the physiological level (Fig. 3.15). Such a degradation rate is helpful in supporting the growth of encapsulated cells while they secrete their own matrix to form new tissue."

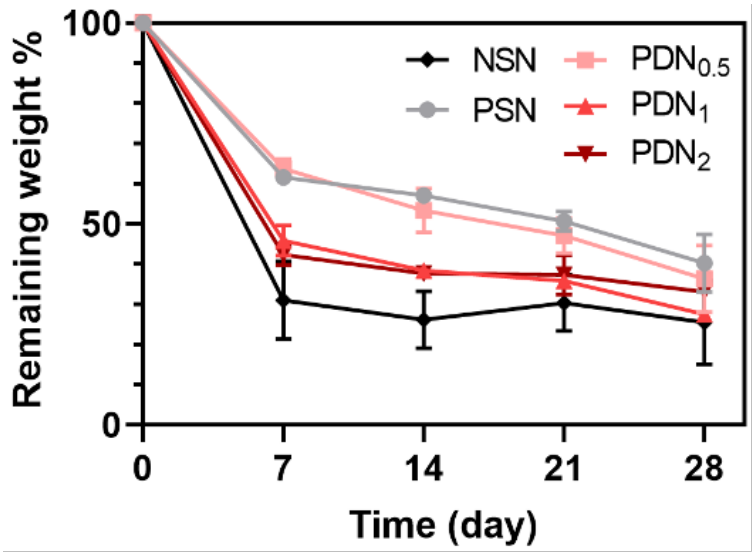

Fig. 3.15. "Biodegradation assay showing the remaining weight of different hydrogels when exposed to an enzyme solution over time. Sample size, N = 4."

3.4 Biological Experiments

3.4.1 Cytocompatibility

"Injectable hydrogels for cell encapsulation and delivery must be cytocompatible and supportive of cell growth. These biological characteristics of PDNs were evaluated with HVFFs,

one of the main cell types found in mechanically dynamic VF tissues [213]. The cells were encapsulated within the hydrogels during a 7-day culture. LIVE/DEAD assays showed that all the NSN, PSN, and PDNs are cytocompatible. The cell viability for PDNs exceeded 85% in all cases and was consistently higher than that of NSN (Fig. 3.16a, Fig. 3.16c and Fig. 3.17); Hydrogels used here were not fluorescently labeled and thus not visualized. Substantial HVFFs proliferation further confirmed that PDNs provided a cell-friendly three dimensional (3D) environment (Fig. 3.16b). In contrast, cells cannot proliferate in NSN, likely due to the nanoporous matrix imposing excessive mechanical constraints that restricted cellular activities."

3.4.2 Cell Adhesion

" A similar conclusion was drawn from assessments of cell morphology. The HVFFs elongated within the 3D porous matrices of PDNs, while those cultured in NSN maintained spherical shapes (Fig. 3.18a and Fig. 3.19). Fig. 3.18b shows a substantial difference in cell circularity between the nanoporous and porous gels, supporting the importance of porous structure in promoting cell spreading."

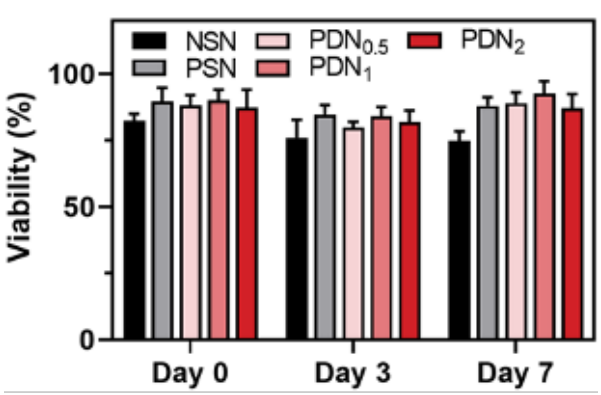

(a)

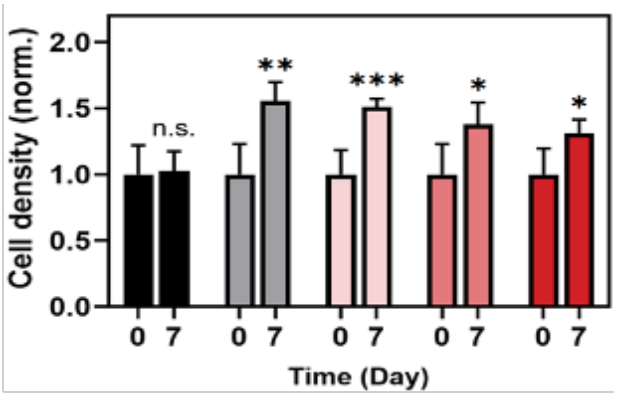

(b)

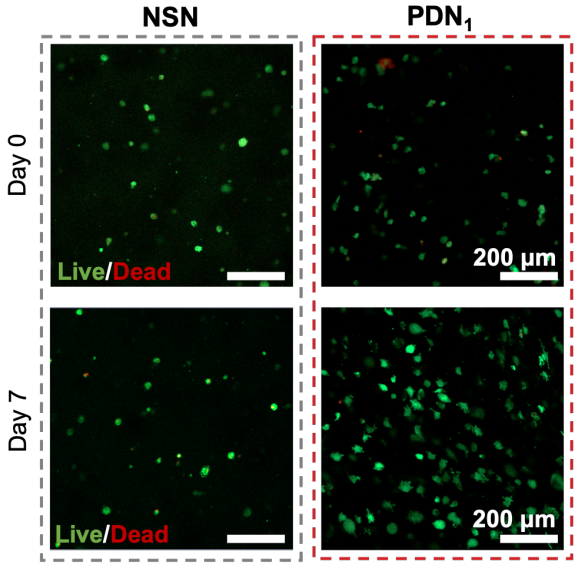

(c)

Fig. 3.16. "Biological properties of PDNs. (a) Cell viability over time. (b) Normalized cell density over time. (c) Confocal images of live/dead cells cultured within hydrogels on Day 0 and 7. *** represents $P < 0.001$, **** represents $P < 0.0001$. Sample size, $N = 4$."

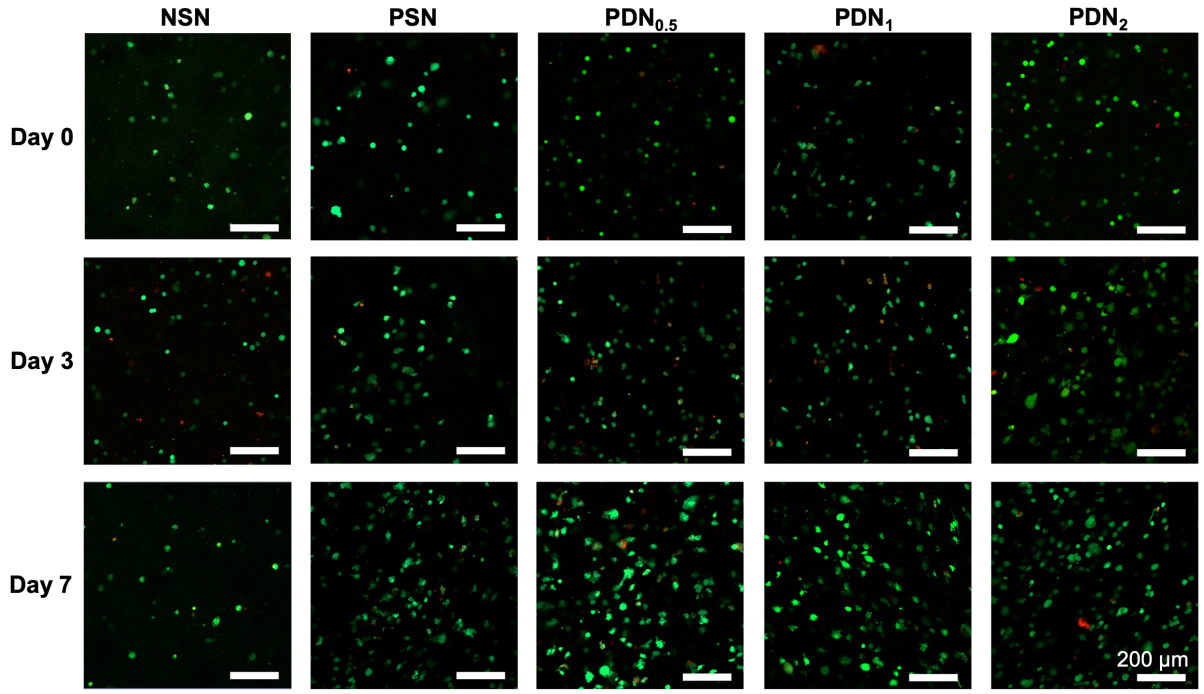

Fig. 3.17. "Viability of HVFFs encapsulated inside different hydrogels at Day 0, 3, and 7. Live cells are shown in green and dead cells in red. Sample size, N = 4."

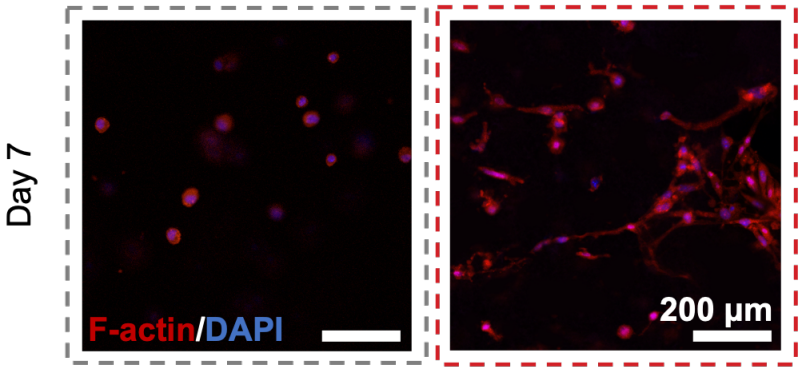

(a)

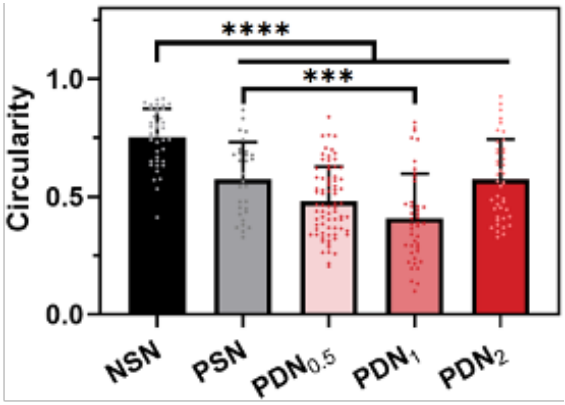

(b)

Fig. 3.18. "Cell adhesion. (a) Confocal images showing the morphology of cells cultured within hydrogels on Day 0 and 7. (b) Circularity of cells cultured within different hydrogels on Day 7. *** represents $P < 0.001$, **** represents $P < 0.0001$. Sample size, $N = 4$."

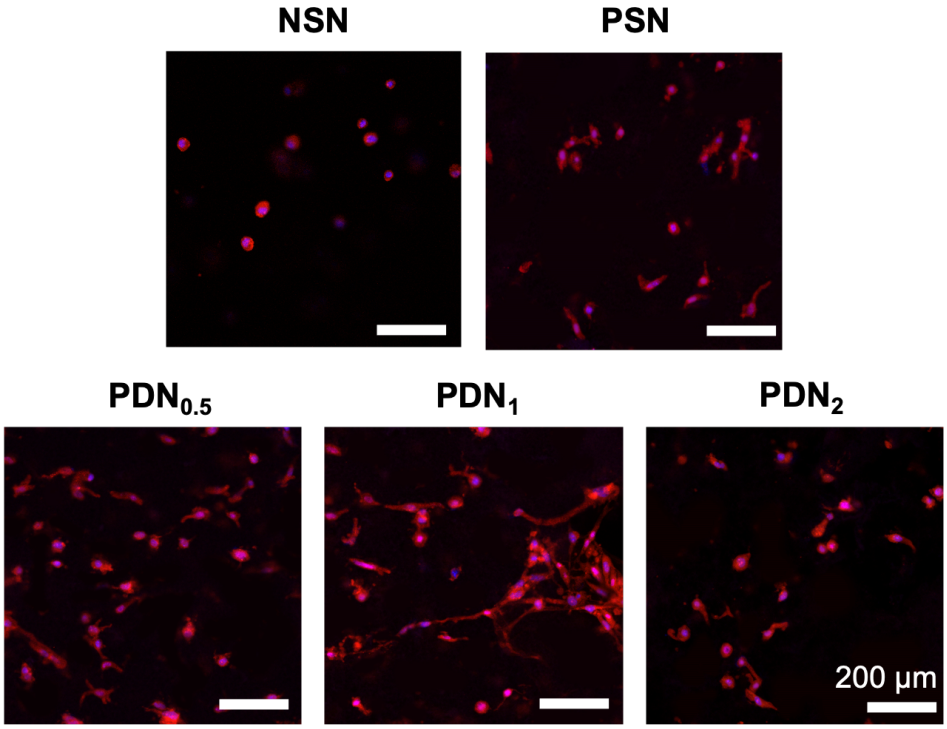

Fig. 3.19. "Morphology for HVFFs encapsulated inside different hydrogels at Day 7. F-actin is shown in red and nuclei in blue. Sample size, N = 4."

3.4.3 Cell penetration

"Cells were also found to penetrate into PDN_1 matrix within a 2-day culture period under a chemoattractant gradient but not NSN (Fig. 3.20). The result demonstrates the function of pores in facilitating cell recruitment and migration. Considering its excellent mechanical, structural, and biological properties, PDN_1 was chosen for the subsequent investigations, unless otherwise specified."

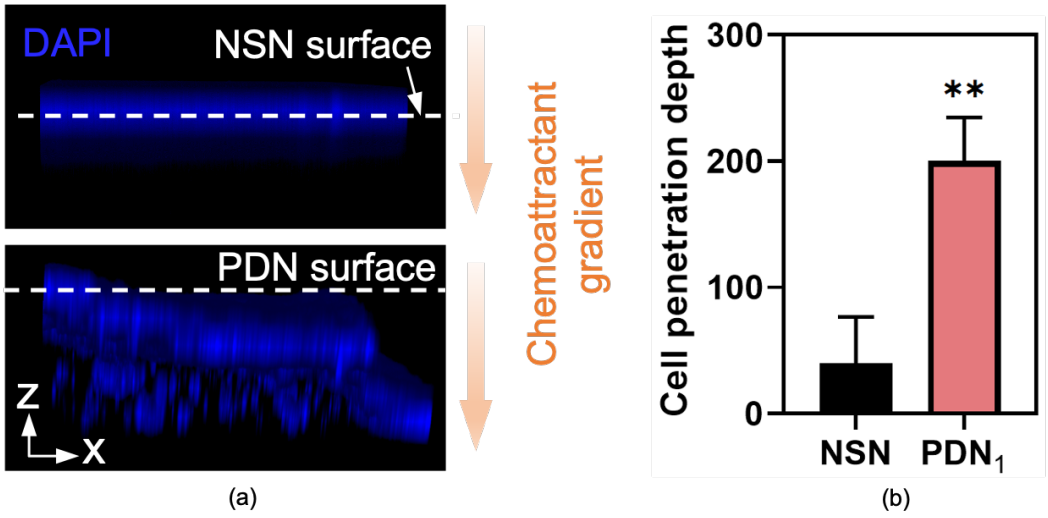

Fig. 3.20. "Comparison of cell penetration in NSN and PDN. (a) Confocal imaging showing HVFFs penetration into different hydrogels. Cells were counterstained with DAPI. (b) Penetration depth of HVFFs into different hydrogels. Sample size, N = 3. ** $P < 0.01$."

3.5 Discussion

"The design of PDN proceeded according to the following criteria: i) cytocompatibility, ii) in-situ pore-forming mechanism; and iii) double-network framework. To satisfy the first two criteria, it is hypothesized that the phase separation of cytocompatible biopolymers at body temperature and physiological pH could both ensure cytocompatibility and generate porous structures in-situ. Chitosan, a polysaccharide that exhibits phase separation behavior and finds wide uses in biomedical applications, was selected as an example to test this hypothesis. When the pH of an acidic chitosan solution is raised above its pK_a, 6.5, bicontinuous polymer-rich and polymer-poor phases emerge [38]. When the polymer-rich phase is crosslinked, the polymer-poor phase, comprised mainly of water, results in interconnected open space. This pore-forming mechanism occurs at physiological conditions, without additional chemical

reagents, and is suitable for cell encapsulation and delivery [179, 214]. Meanwhile, the primary amine groups [NH_3^+] of the chitosan deprotonate and are converted to [NH_2], which can bond with the hydroxyl groups [OH] of the chitosan [215]. This self-crosslinking behavior can stabilize the polymer-rich phase and thereby reinforce the already-formed porous structure. Notably, the structure contains a large number of hydrogen bonds and other intermolecular interactions that can be exploited for energy dissipation as the dissipative primary network [180]. To satisfy the third criterion, we constructed the secondary network with covalently crosslinked biocompatible polymers. In principle, any polymer that does not affect the phase separation of the dissipative network can be used. Here we used a combination of GC and GY. GC is a derivative of chitosan with improved solubility at neutral pH. It can be crosslinked by dialdehydes such as GY through a Schiff Base reaction to form a secondary network [39, 216]."

The mechanical charactersitics of the developed PDNs were also evaluated. It was found the PDN gelation behavior was temperature dependant and similar to the existing injectable pore-forming hyrogels. It started with a controlled and fast gelation to avoid mixing with body fluids while the phase separation and additional cross-linking happened as the next two processes. This leades to the formation of strong and interconnected pores. The stress relaxation as well as the viscoelastic properties of the developed PDNs were also comparable to that of the native soft tissues. We also explained the quick relaxation response of the PDNs by the stress-induced fracture of hydrogen bonds in the dissipative network and also the quick water migration, thanks to the interconnected pores. The porous structure of the PDN was evaluated using three different imaging methods and all of them confirmed the existence of cell-sized pores, leading to high permeability values for the PDNs. However, the pores didn't affect the stability of the PDNs as they showed Superior stretchibility and

toughness compared to other injectable gels. Swelling profile of the PDNs also demonstrated their good physical stability while their slow degradation rate supported the cell growth and extracellular matrix (ECM) synthesis.

Additionally, PDNs exhibited viability rate of higher than 85% afters seven days of culture with the cells elongated within the scaffold. Lastly, it was demonstrated that the interconnected pores improved the cell penetration depth more than twice of the nonporous control.

CHAPTER 4

PDNs' application: Microfluidics and Bioreactor Study

In this chapter, the application of developed PDNs is investigated. As mentioned in Chapter 3, $porousdouble-network(PDN)_1$ was selected for the subsequent studies owing to its excellent mechanical and biological behavior, unless otherwise specified. Firstly, cell-laden PDN_1 was injected into the microfluidic device channel and then perfused for a day while a control chip was prepared with a standard culture condition but without the perfusion. Secondly, the phonatory characteristics of a perfusion vocal fold (VF) bioreactor was evaluated and then the bioreactor was used to study i)the mechanical stability of hydrogel under extreme cyclic loading and ii) the biological performance of the cell-laden PDN_1 in a biomimetic environment. A two dimensional (2D) computational model was also developed to further analyze the behavior of hydrogels. (references [1]).

4.1 Use of PDN in Microfluidics

"We first explored the use of PDN in a miniaturized perfusable three dimensional (3D) culture device, where PDN was injected into a microfluidic channel (Fig. 4.1a). Their injectability eliminates the need for high-precision prefabrication of tight-fitting inserts for microfluidic devices. To visualize the function of the device, we prepared FITC-labeled hydrogels (green) and added rhodamine dyes into phosphate-buffered saline (PBS) to simulate perfusion media (red). Fig. 4.1b shows the direct media perfusion through the PDN matrix, thanks to its interconnected porous structures and high permeability. No channel blockage or media leakage was observed. By examining the distribution of the fluorescent signals, we confirmed that media perfused through the entire channel. In contrast, non-porous single-network (NSN) blocked the microfluidic channels and prevented media flow."

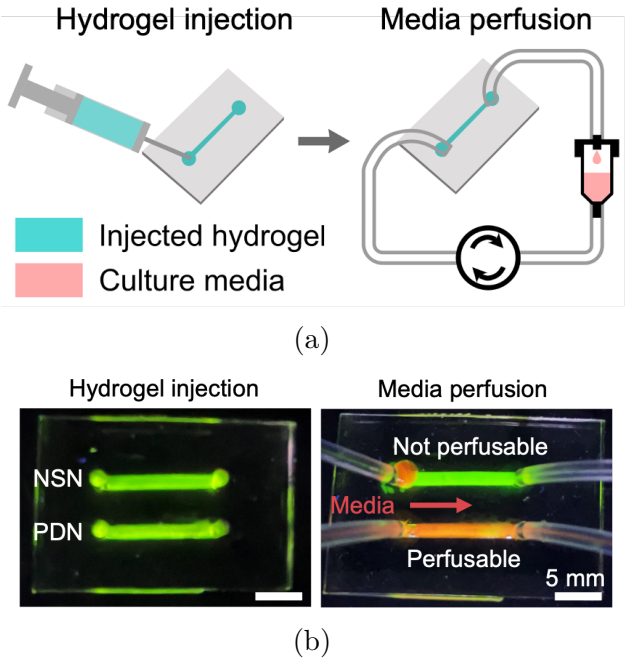

Fig. 4.1. "Injectable PDN for microfluidics. (a) Schematics showing the delivery of PDNs to microfluidic channels through injection. and (b) Perfusion of media through injected hydrogels."

"To demonstrate the cell culture with PDN in microfluidics, we cultured human vocal fold fibroblast (HVFF)s in the PDN-laden devices. The HVFFs were mixed into the hydrogel

precursors and injected into the device's channels. The cell-laden device was then perfused with cell culture media for 24 hours. A standard culture condition without perfusion was included as control. Viability assays confirmed perfect cell viability throughout the PDN channel, including the inlet, the middle, and the outlet (Fig. 4.2a and Fig. 4.2b). In contrast, most cells were dead in the control due to a lack of oxygen and nutrients."

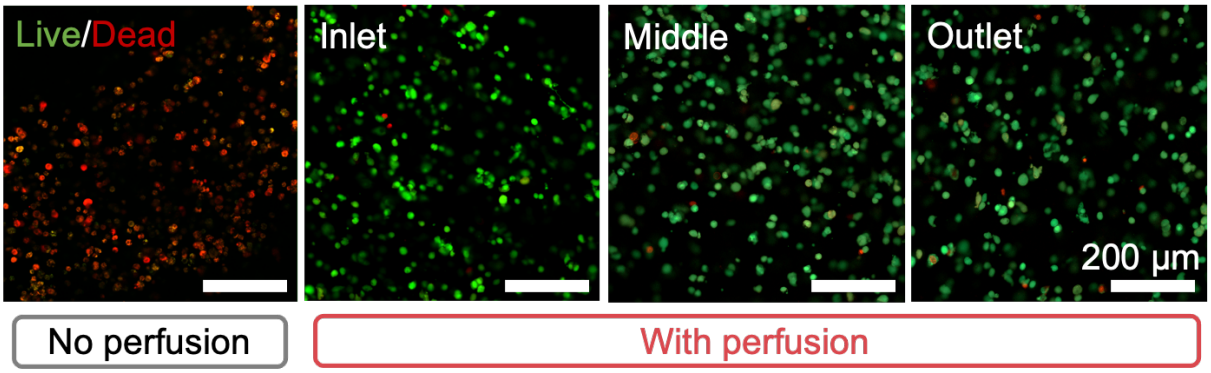

(a)

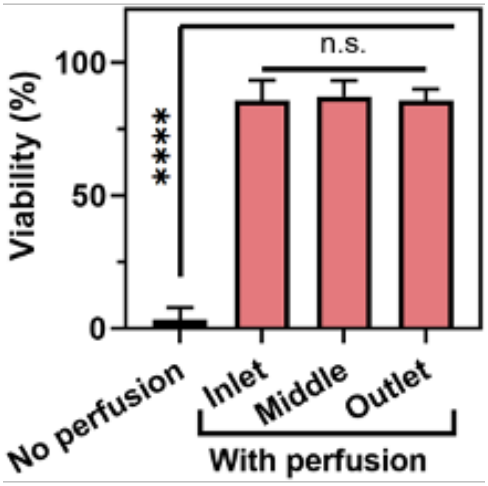

(b)

Fig. 4.2. "Cell-laden PDN in microfluidics. (a) Confocal images showing live/dead cells within PDNs with and without perfusion after 24 hours. (b) Cell viability. **** represents $P < 0.0001$, n.s. represents $P \geq 0.05$. Sample size, $N = 3$."

"The setup is also readily useable in well plates, similar to those used in microfluidic devices (Fig. 4.3a). Notably, the high permeability and low flow resistance of PDNs allow the perfusion of multiple channels connected in series with a single syringe input (Fig. 4.3b). This enables a modular design for the coculture of multiple cells in different compartments."

(a)

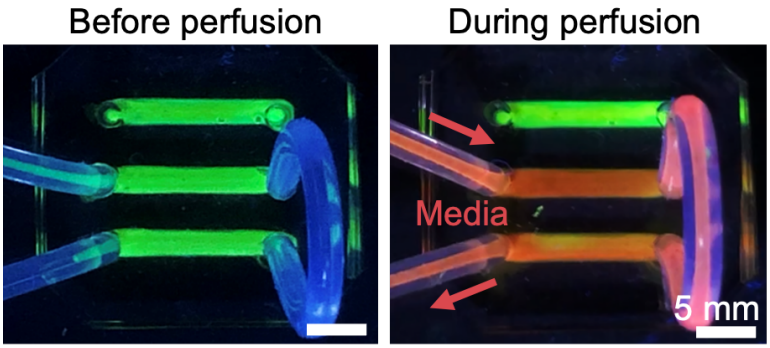

(b)

Fig. 4.3. "Cell-laden PDN in microfluidics. (a) Confocal images showing live/dead cells within PDNs with and without perfusion after 24 hours. (b) Cell viability. **** represents P < 0.0001, n.s. represents P$\geq$0.05. Sample size, N = 3."

"The PDN can aslo be injected in a controlled manner from two sides of a chanel (Fig. 4.4a). Confocal images of the junction area of the two materials shows that the two materials are

well connected together (Fig. 4.4b). Additionally, owing to their mechanical toughness, the injected PDNs can be easily harvested and manipulated after their maturation (Fig. 4.4c). Overall, they can be sectioned to perform multiple assays in parallel, such as different immunochemistry staining tasks. PDN shows promise in simplifying the design and operation of 3D cell culture microfluidics.

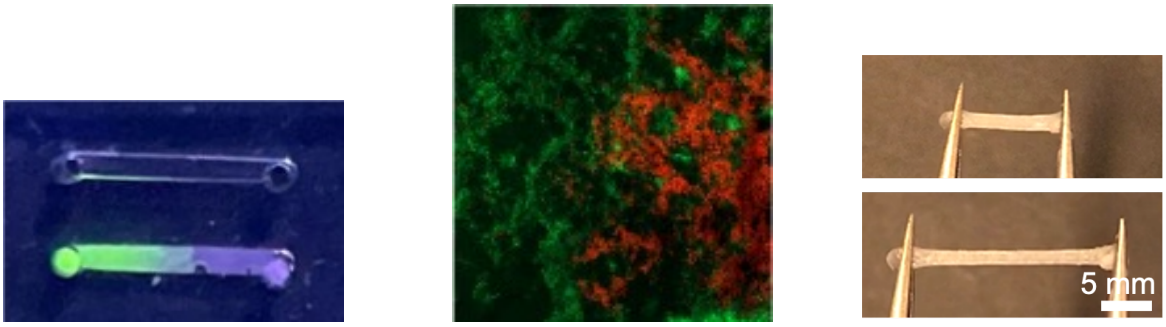

(a) (b) (c)

Fig. 4.4. "(b) Multi-material Injection demo. (b) Confocal images of multi-material junction. (c) Injected PDNs can be taken out from the microfluidic channels and handled easily without rupture. **** represents $P < 0.0001$, n.s. represents $P \geq 0.05$. Sample size, $N = 3$."

4.2 Bioreactor Study

4.2.1 Phonatory Characteristics of Bioreactor

"Fig. 4.5 illustrates the structure of the bioreactor, which contains a pair of elastomer-based VF bodies covered by a thin outer layer, representing the lamina propria and the epithelium of the real tissue. Each VF body contains a cavity where the PDN can be easily injected, perfused, and be subjected to phonation stresses thereafter."

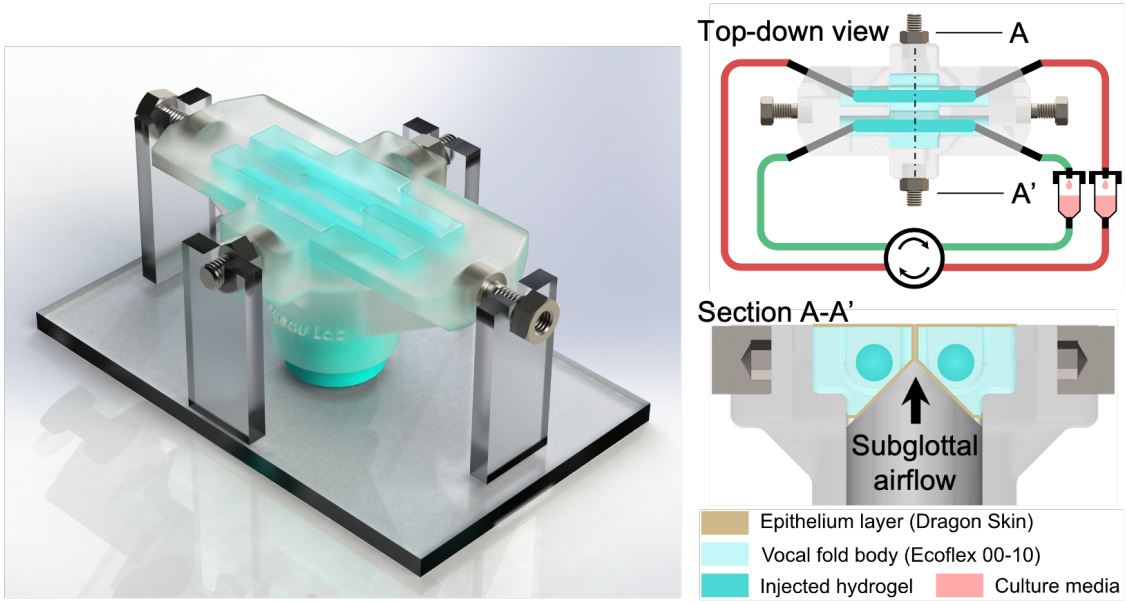

Fig. 4.5. "Bioreactor schematics showing the design and setup of a phonomimetic bioreactor."

"Medium is perfused through hypodermic needles inserted through the elastomer to reach the cavity and ensure a hemetic seal (Fig. 4.6)."

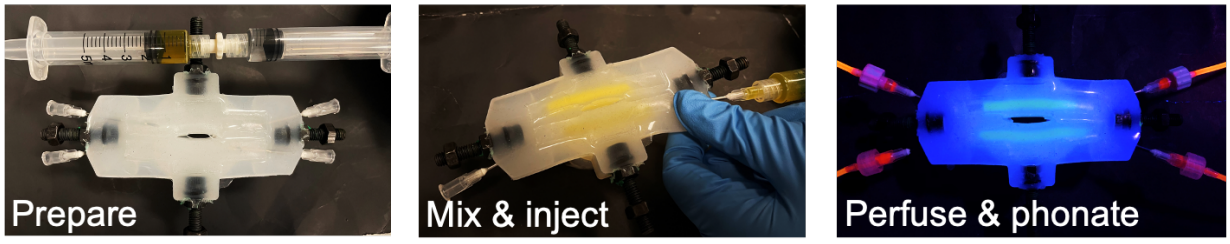

Fig. 4.6. "PDN being injected into the bioreactor."

"Phonation is achieved with controlled airflow across the subglottal area that induces self-oscillation of the VF bodies (Fig. 4.5, section A-A'). The phonation frequency and subglottal pressure were controlled to within physiologically relevant range (Fig. 4.7a). In particular, the frequency was kept at $\sim$ 120 Hz, similar to the fundamental frequency of

humans when voicing." The average values of phonatory characteristics during phonation are shown in Table 4.1. As can be observed, the static pressure of the normal human phonation is around 13.7 cmH_2O [217], which is close to the value obtained from the bioreactor. Fig. 4.7b shows the phonation map of one of the bioreactor. Theoretical studies have demonstrated a hysteresis phenomenon for non-linear systems, resulting from the energy loss incidence [218]. As can be observed in Fig. 4.7b, less energy is required to sustain phonation of the VFs compared to initiating it.

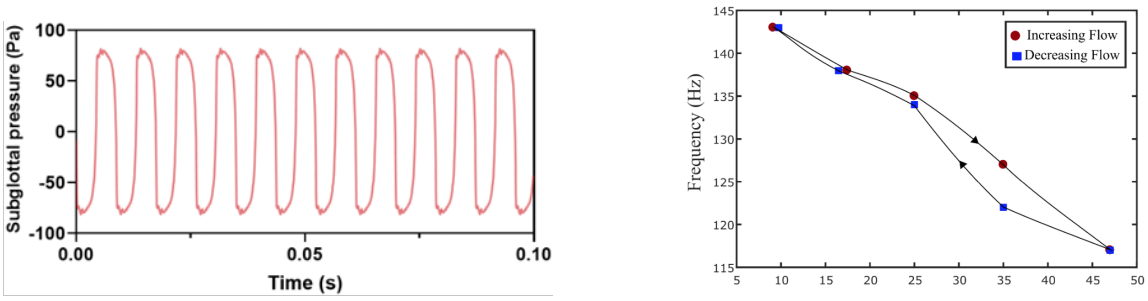

(a) (b)

Fig. 4.7. "(a) Close-up view of subglottal pressure profiles applied on the injected hydrogels." (b) Phonation Map (Frequency vs Flow Rate).

Table 4.1. Phonatory Characteristics of the Bioreactor.

Static subglottal pressure (cmH_2O)	**Dynamic Subglottal pressure**(cmH_2O)	**Supraglottal Loudness (dB)**	**Fundamental Frequency (Hz)**
12.88	0.22	79.18	120

4.2.2 Performance under Extreme Biomechancial Stimulations

"To test the resilience of PDN under complex physiological conditions, the phonomimetic perfusable bioreactor was used to simulate biomechanical stimulations of the VFs as shown

in Fig. 2.3 [174]. The injected hydrogels were phonated for 2 hours/day for 7 days, inducing a total of over 6,000,000 cycles of vibrations (Fig. 4.8a). The lips of the bioreactor close, collide, and open during each phonation cycle that lasts 0.008 s (Fig. 4.8)."

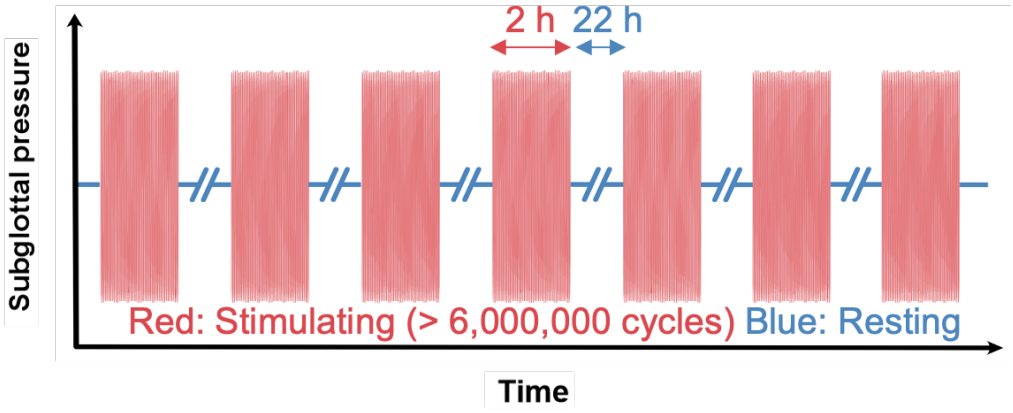

(a)

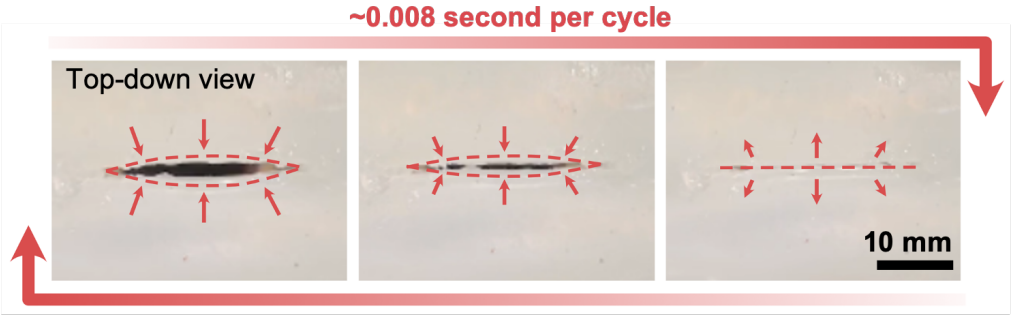

(b)

Fig. 4.8. "(a) Injected hydrogels experience more than 6 million high-frequency cyclic mechanical stimulations. (b) The movement of bioreactor lips within one cycle from the top-down view."

"After the completion of biomimetic stimulations, we harvested the hydrogels from the bioreactor and found that PDN withstood the extreme biomechanical environment and maintained their integrity (Fig. 4.9a). We also verified experimentally that the stiffness of PDN was not affected by the cyclic mechanical stimulations (Fig. 4.9b). The porous structure

was also found similar to the pristine state after cyclic loading under perfusion (Fig. 4.9c). In contrast, NSN disintegrated into small particles that were washed away by the perfusion media, and porous single-network (PSN) fractured into multiple disjoint chunks."

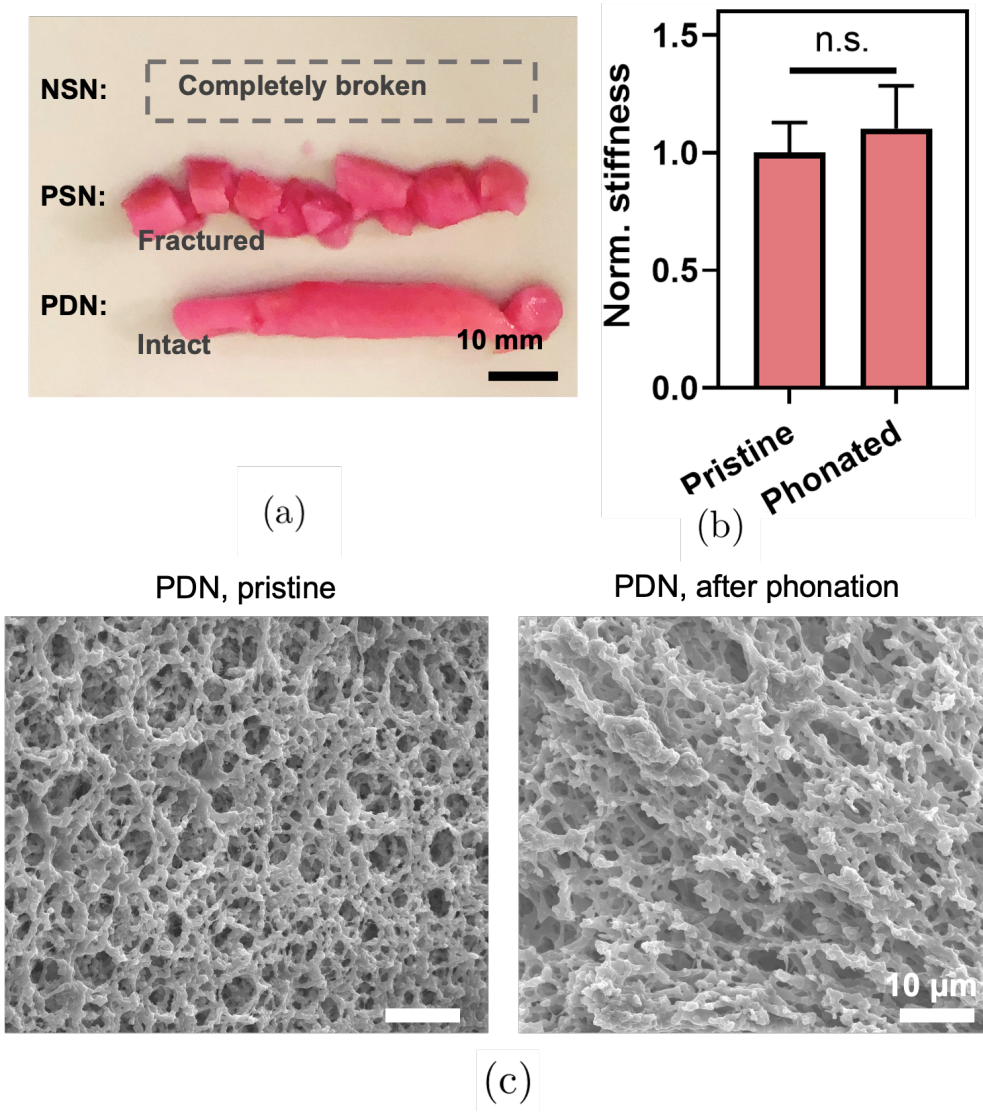

Fig. 4.9. Mechanical stability of PDN. "(a) Digital photos showing the morphologies of injected hydrogels after mechanical stimulations. (b) Stiffness and (c) Porous structure of the pristine PDN and the PDN after being stimulated in the bioreactor for 7 days."

4.2.3 Numerical Simulation

"To further reveal the mechanical environment in the bioreactor, we conducted finite element analysis to probe the mechanical loading applied onto the hydrogels (Fig. 4.10a and Fig. 4.11). Both elastomers and hydrogels were treated as hyperelastic materials with the Ogden model and conjugated with damping. The PDN model has the lowest maximum von Mises stress and the most homogenous stress distribution among the three conditions, due to its excellent energy dissipation under stress (Fig. 4.10b)."

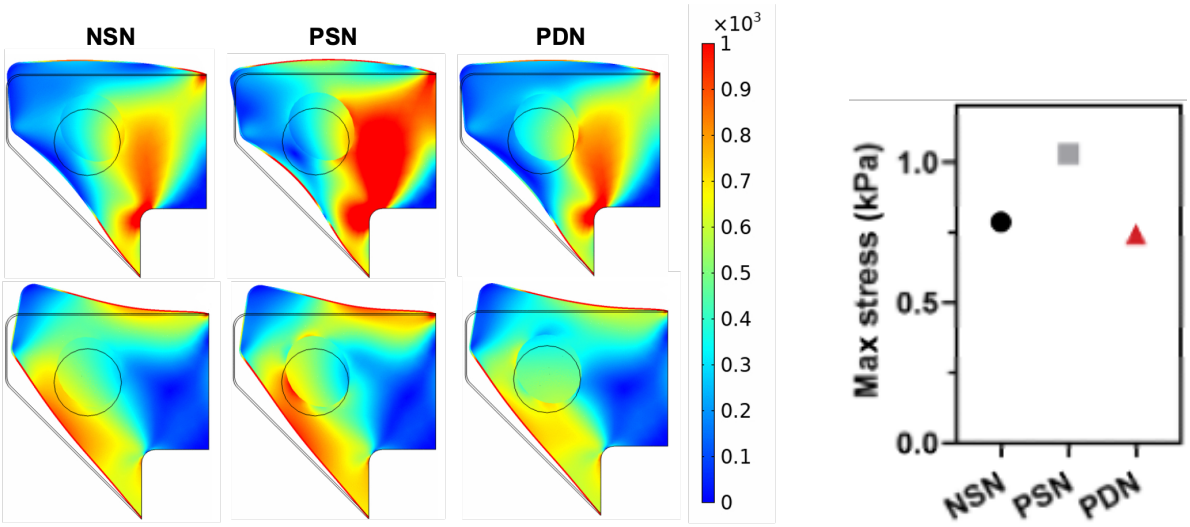

(a) (b)

Fig. 4.10. "(a) Finite element simulations showing the stress distribution within the solid phases of the bioreactor and the injected hydrogels. Black contours indicate the undeformed shape and the inner circle refers to the hydrogel. The two rows represent the two positions during one phonation cycle where the hydrogel experiences the highest stresses. (b) Maximum stress experienced by different hydrogels."

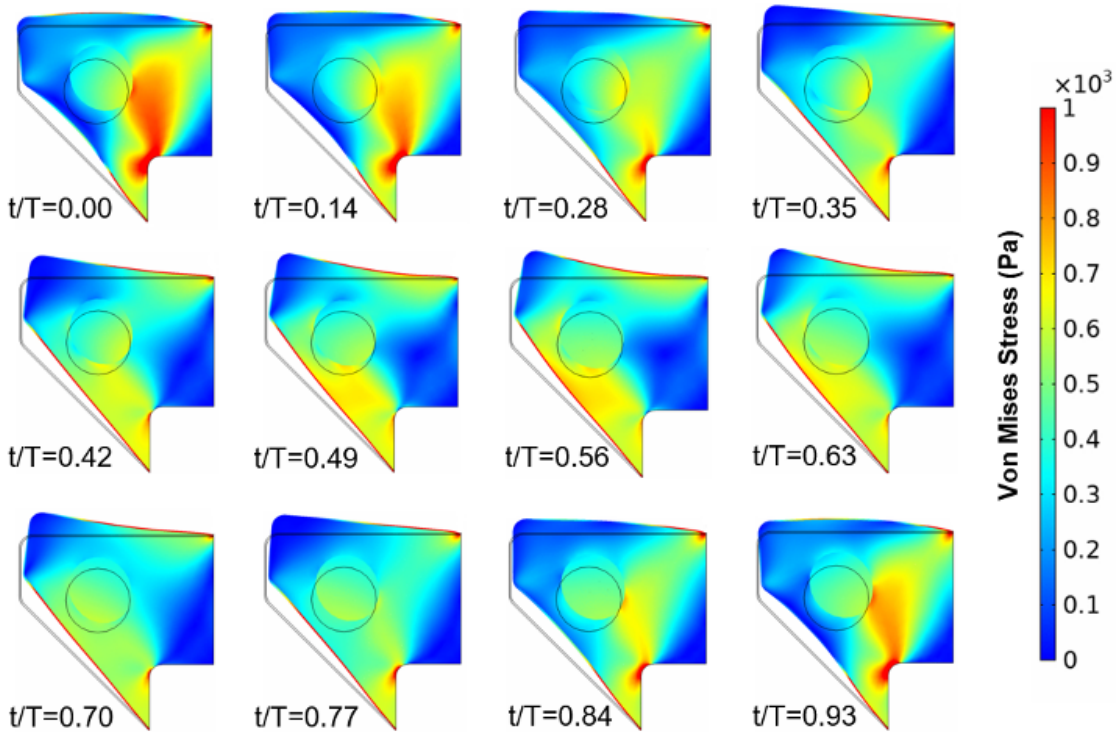

Fig. 4.11. "Finite element simulations showing the stress distribution of PDN and the elastomeric parts of the bioreactor during one period of oscillation. t/T represents the normalized time during one period. Black contours indicate the undeformed shape and the inner circle refers to the hydrogel."

4.2.4 Biological Study

"Despite the complex loadings within the bioreactor, PDN was found to support cellular viability and proliferation for the encapsulated cells throughout the 7-day culture period (Fig. 4.12a). Cell culture media were able to penetrate the entire 6 cm-thick scaffold thanks to its exceptional permeability. To our knowledge, this is the first material reported to support cell viability in a centimeter-scale avascular construct. PDN also shows great translational potential. We found that encapsulated HVFFs secreted more collagen content under dynamic

stimulations compared to cells that cultured statically, indicating the stability of PDN could help activate encapsulated cells to produce a functionalized tissue (Fig. 4.12b)."

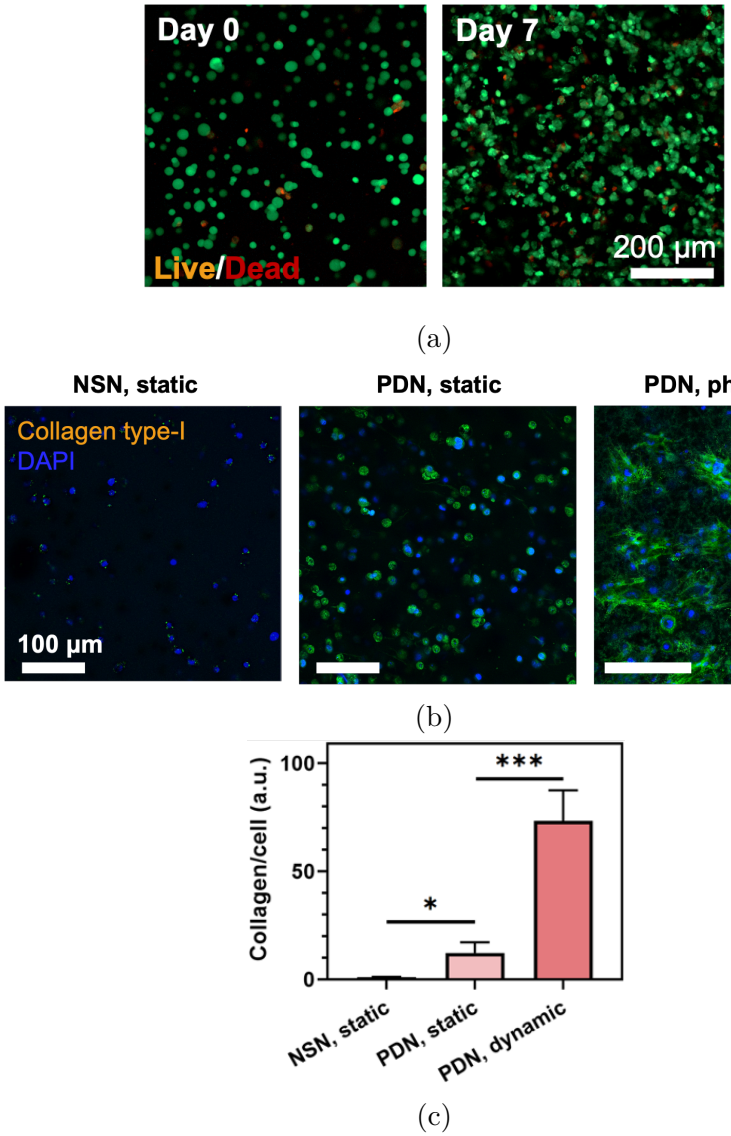

Fig. 4.12. "(a) Confocal images showing the live/dead cells cultured within injected PDNs after phonated for 7 days. (b) Collagen secretion by HVFFs within different hydrogels with and without mechanical stimulations at Day 7. (c) "

4.3 Animal Study

"In addition, we demonstrated that PDNs can be easily injected into animals subcutaneously to form a porous hydrogel in situ without leakage (Fig. 4.13a). The collective evidence supports the hypothesis that PDNs can be used to repair mechanically active tissues such as VFs after lesion removal and calls for future investigations (Fig. 4.13b). It is also be valuable to explore and expand the use of PDN for other cell systems such as stem cells and organoid in future studies."

(a)

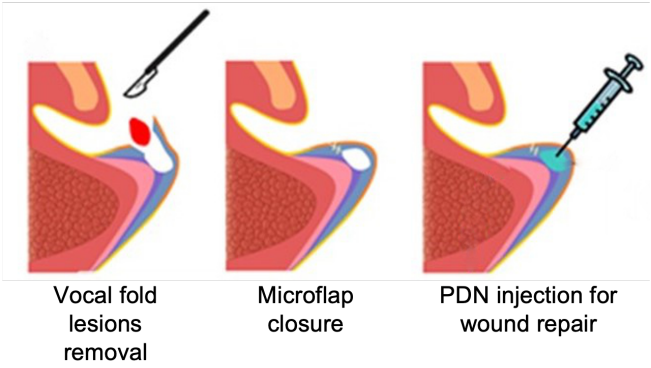

(b)

Fig. 4.13. "Use of PDN in animals. (a) Injection of PDN (0.85 mL) into a rat cadaver subcutaneously through a fine needle (21G). PDN formed in situ without leakage. (b) Schematic illustration showing the potential use of PDN for VF repair and regeneration."

4.4 Generalizability

"We next discussed how our design strategy of PDN hydrogels could be extended to other material systems. Since the phase separation of chitosan occurs under mild conditions, our strategy could be compatible with other materials and polymer crosslinking strategies, including free-radical polymerization. As an example, we replaced glycol chitosan (GC) with gelatin, another widely used biopolymer, for the secondary network. We prepared a gelatin-based PDN precursor by dissolving gelatin and chitosan in an acetic acid solution while keeping the same gelling condition. In the new material system, the gelatin can also be crosslinked by glyoxal and the chitosan still ensues phase separation. As expected, the resulting gelatin-based PDN showed an interconnected porous structure (Fig. 4.14). The toughness of the resulting PDN was also higher compared to that of pure gelatin hydrogel. Chitosan could be potentially substituted with other thermogelling polymers such as poly(N-isopropylacrylamide) [219].

It is worth noting that although PDNs are relatively weak in comparison with traditional tough hydrogels, they provide significantly improved toughness and fatigue-resistance compared to existing injectable hydrogels and perform stably under the most extreme conditions present in the human body. Given the diversity of polymer systems, the present work may well give rise to a new class of injectable microporous hydrogels that are tough, perfusable, and easy to use."

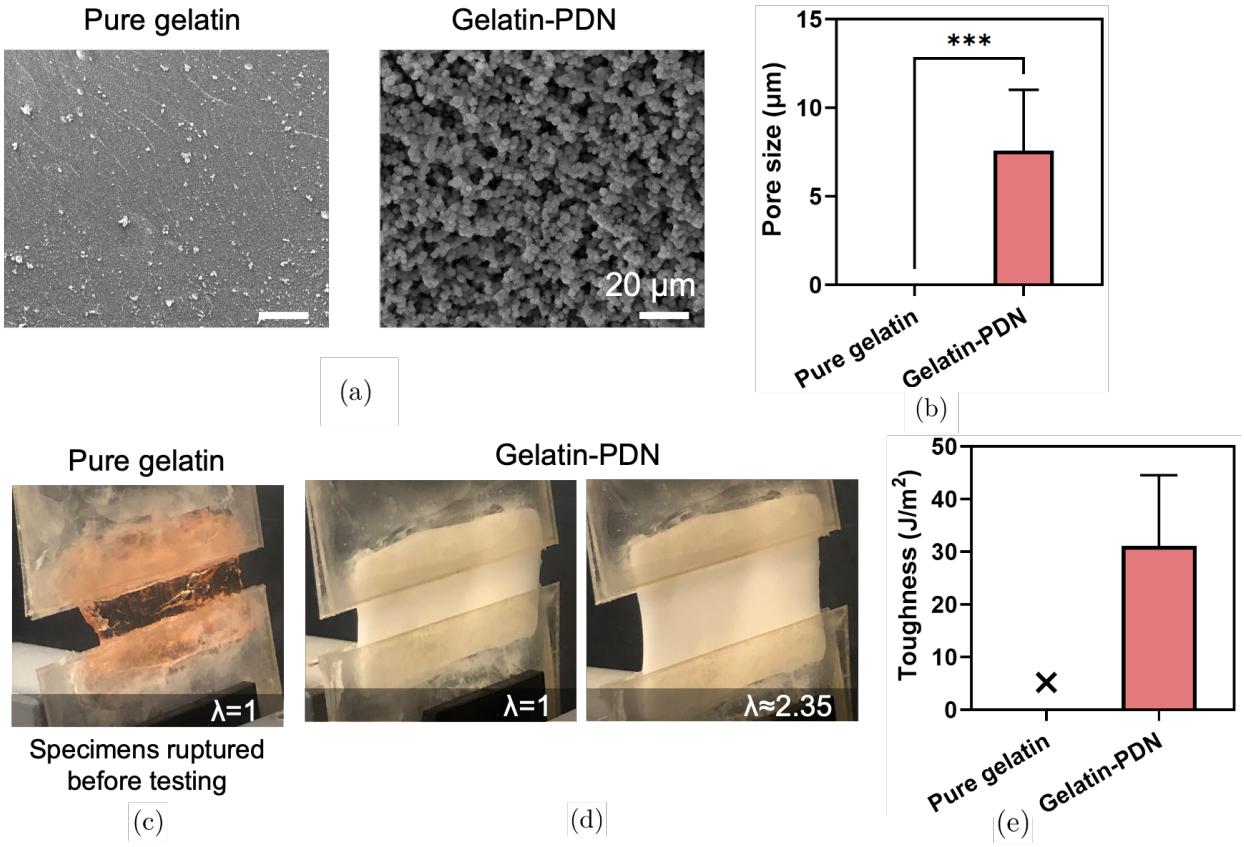

Fig. 4.14. Pore size and toughness of gelatin-based PDN. "(a) scanning electron microscopy (SEM) images showing the structures of pure gelatin and gelatin-PDN. (b) Pore size comparison. (c) Photos showing the pure gelatin specimens ruptured during sample preparation steps due to the brittleness of the hydrogel matrix. (d) Stretchability and (e) toughness of gelatin-PDN hydrogels. Toughness of pure gelatin hydrogels was not measured due to specimen rupture before testing and denoted with a cross sign. Sample size, N = 3."

4.5 Discussion

PDNs showed a great potential for the use in cell-culture perfusion microfluidics and VF mimetic perfusion bioreactors. It was demonstrated that the precise prefabrication of microfluidic devices tight fitting inserts will be removed owing to the PDN injectability

characteristics. PDNs can be great candidates for modeling multiple organs on a chip as they allow a modular design for co-cluture of different cells. Additionally, it was shown that the PDNs can be taken out from the channels without any breakage thanks to their high toughness. Overall, PDNs demonstrated potential in facilitating the design and operation of 3D cell culture while other existing microfluidc devices can be only operated for the 2D cell culture.

Moreover, a perfusion bioreactor was used to investigate the biological and mechanical behavior of PDNs under mimetic condition. Before the injection of PDN within the bioreactor, the phonatory characteristics of the bioreactor were analyzed and the results were within the range of human phonation. The PDN, PSN and NSN were then injected in the bioreactor separately and subjected to more than 6 milion cycles of vibration. After 7 days of phonation, on a 2 hour/day basis, the hydrogels were harvested. It was observed that PSN fractured into small fragments while NSN were disintegrated and washed away owing to its nanporous structure. However, PDN remained intact, proving the high mechanical stability and toughness of the gel. The pore stability of the gel were also analyzed using SEM and the pores were found similar to the those of the unphonated samples. In addition, the stiffness of the PDN after phonation was also measured using the compression test and we found that the PDN's stiffness was not affected by the intense mechanical stimuli. In general, the PDN showed great mechanical performance under the intense bio-mechanical environment without any failure. We also simulated he bioreactor environment using COMSOL and realized that the maximum von Mises stress was at its lowest value for the PDN model with the most homogeneous stress distribution compared to NSN and PSN, thanks to its great energy dissipation under loading.

Last but not least, the biological performance of the PDN under biomemtic stimulations

was studied. First. the viability of cells after 7 days of phonation was investigated and we found a higher viability and proliferation rate for the phonated PDN compared to the nonphonated control. These results confirmed the excellent permeability of the PDN which allow the cell culture medium perfuse properly through the entire 6 cm-thick scaffold. To our knowledge, this is the first time reported in literature that a biomaterial in a a centimeter-scale provides such a high viability rate. Also, collogen synthesis of encapsulated HVFFs increased noticeably under phonated condition compared to the NSN and static samples. This proved the stability of the PDN which enabled the cells to synthesize a functionalized tissue. On a pilot study, the PDN was also injected into animals and was able to form a porous gel in situ without any leakage and swelling.

One interesting finding about the PDN design strategy was its generalizability. We showed that the methodology can be extended to other material systems. In other words, any material that doesn't affect the phase separation behaviour of the chitosan can be used instead of GC. As an example, GC was replaced with gelatin and we found that the new PDN also has interconnected pores as well as high mechanical stability and toughness.

CHAPTER 5

Conclusions and perspectives

The main focus of this chapter is to summarize the key points and findings of the thesis in terms of the design and biofabrication of biomaterials for tissue engineering applications. Firstly, the outcome of the developed methodology in fabrication of the macro-porous hyrogels is discussed and then the transnational applications of the PDNs are explored. The last section of this chapter outlines the potential future directions of the studies.

5.1 Conclusions

5.1.1 PDNs Fabrication

To fabricate porous double-network (PDN)s, we used different concentrations of polymer precursor and gelling agent separately. It was observed that upon mixing of the PDN precursor with the gelling agent, the sodium bicarbonate in the latter raised the pH of the mixture from acidic to neutral and acted as a phase separation inducer to initiate the formation of

the dissipative network. We found that the formation of interconnected pores stems from the phase separation behavior of the chitosan. Following that, glyoxal (GY) chemically crosslinked the glycol chitosan (GC) to form the secondary network.

5.1.2 Characteristics of PDNs

Different mechanical and physical characteristics of the PDN were studied in chapter 3. The gelation of PDN was found to be temperature dependant and followed three coordinated steps including initial solidification, phase separation and further crosslinking, which is similar to the gelation of existing injectable pore-forming hydorgels. The stiffness of the developed PDNs were found to be within the range of soft biological tissues. It was also observed that the Young's moduli of PDN's were noticeably higher than that of non-porous single-network (NSN) and porous single-network (PSN), which can be justified by several reasons. Additionally, the PDNs showed a fast relaxation behavior comparable to the native tissues. This was explained by the stress-induced rupture of hydrogen bonds in the dissipative network and also the quick water migration stemed from the interconnected pores. Using imaging techniques, we illustrated that PDNs have interconnected pores, owing to the phase separation behavior of chitosan. The pore size was within the range of cell size and it decreased by increasing the GC concentration. A customized setup was designed and fabricated to characterize the permeability of the PDNs and it was found that the permeability of PDNs significantly increased compared to the other existing hyrogels. The PDNs were, however; pore-insensitive and mechanically tough. There was a 20 to 40 fold increase in the fracture toughness of PDN compared to NSN as well as other in use single network hyrogels. The stretchibility of PDNs also improved noticeably in comparison with NSN. This

can be attributed to the double-network configuration. Lastly, the physical characteristic of the hydrogels including its swelling and degradatin behavior were investigated. The PDN exhibited a great physical stability in a liquid environment as they maintained their shape and size after 7 days of embedding in phosphate-buffered saline (PBS). This behavior is crucial to ensure that surrounding organs do-not undergo compressive stresses. PDNs also showed a slow degradation rate over 28 days, which is helpful for the encapsulated cells to grow while they secrete their own matrix to generate a new tissue.

5.1.3 Cell-biomaterial Interactions of PDNs

As a vital step, the cytocompatibility of the PDNs were investigated and they showed a high viability rate over a 7 day of culture (higher than 85%). Cell proliferation also improved noticeably compare to the NSN, thanks to the porous structure of the PDNs. Moreover, we found that the human vocal fold fibroblast (HVFF)s elongated within the PDN's porous scaffolds while they remained rounded in NSN, proving the role of interconnected pores in enhancing the cell spreading. Additionally, we illustrated that the HVFFs cells penetrated into the PDN after 2 days of culture while they remained on the surface of the NSN, supporting the role of pores in promoting cell recruitment and migration.

5.1.4 PDNs Applications

In chapter 4, we showed the application of PDN in microfluidics and a perfusion vocal fold (VF) bioreactor. The PDNs showed great potential for the use in cell-culture perfusion microfluidics as their injectability facilitates the fabrication process of the devices. The PDNs can be used in well plates and they also enable the co-culture of different types of cells owing

to their modular design capacity. We also injected the PDNs in a perfusion VF bioreactor to assess their mechanical stability and biological performance under intense cyclic loading. We observed that PDNs withstood the highly dynamic bio-mechanical environment while the NSN was washed away by the cell culture medium and PSN was fractured into small chunks. It was observed that the stiffness of the PDN wasn't affected by the dynamic stresses. The pore stability of the PDN was also evaluated and it was illustrated that the porous structure remained similar to the pristine state. Additionally, the effect of phonation on the cellular behavior of the PDNs was studied. We found that phonation increased the cell proliferation and also secretion of the Collagen type I in PDNs compared to the PDNs in static condition, supporting the idea that stability of PDN could activate the HVFFs to form a functionalized tissue. To the author's knowledge, it is the first time that a scaffold in a centimeter-scale can provide a cell friendly environment. It was also found that the PDNs can be injected into animals without any swelling and/or leakage.

Lastly, we showed that our proposed methods can be generalized and other materials and polymer cross-linking strategies could be use as the phase separation behavior of chitosan happens in mild condition. In a nutshell, thanks to an unprecedented combination of mechanical, structural, and biological properties, the proposed PDNs and technology are expected to impact broadly the repair and regeneration of mechanically dynamic tissues and benefit the development of drug delivery, microfluidics, cell culture, and disease modeling

5.2 Perspectives and Future Work

5.2.1 Long-term Studies on PDNs

One possible future direction of this study that can be the followed is to investigate the long term outcome of the developed PDNs over varying time frames. Long term study is required since functional tissue construction may take up to 3-4 months under aseptic conditions. The bioreactor study can be also extended and the effect of phonation-induced biomechanical stimulation on cellular behavior of the PDNs can be studied on a longer period of time. In other words, the cellular behavior namely, cell viability, cell proliferation, cell morphology and extracellular matrix (ECM) synthesis, will be will be initially captured over a short period of time (2 week), i.e. longer than what explored in the current thesis. Then, the study will be repeated over a one-month and two-months time frames to ensure the functionality of the bioreactor over long term.

Additionally, as it was shown in Fig. 2.4b, the bioreactor systems benefited from a secondary control loop. With this perfusion system, a proportion of drained used medium is mixed with fresh medium and perfuses through the cell-seeded scaffold and the remaining cell culture medium (CCM) is collected as the waste byproduct. As the cells continue to grow and divide, they communicate with one another through the production of a combination of chemical signals. Therefore, as another future phase of this project, it would be noteworthy to study the waste products and come up with a perfusion system capable of feeding, dispose of metabolic products, and discriminating between signals and waste products.

5.2.2 Animal studies of PDNs

Although *in vitro* studies including petri-dishes and bioreactors offer precious information to characterize the accurate compositions of the injectable hydrogels, they cannot completely replicate the native tissue environment with its complex physiological conditions. Animal studies are, therefore, needed for translating injectable hydrogels to clinical use [220]. In a study by Bouhabel et al. [221], the functional effect of the immediate injection treatment of hylauronic acid (HA)/gelatin hydrogels and GC solution on phonatory function of rabbit larynges after surgical injury of the VFs has been evaluated using high-speed videoendoscopy (HSV) and acoustic analysis techniques [221]. Quantitative analyses of acoustic and aerodynamic data obtained from laryngeal HSV was used to assess the VF function and vibratory characteristics.

In the current study, the injection of PDN into a rat cadaver subcutaneously is demonstrated, however; a detailed animal study can be conducted for further clinical purposes. Animal studies of PDNs are planned in the near future as the animal ethics protocol (2014-7556) is already approved by the McGill Board of Ethics. The proposed use of animals is explained below.

Animals will undergo unilateral VF modified microflap surgery, and then will be immediately injected with PDN. A 5-mm long incision will be made to the vocal fold through the epithelium and mucosal cover using routine microlaryngeal instruments, creating a microflap. The microflap will be elevated so the injury can be exacerbated by anteroposterior movements of a microlaryngeal fine angled spatula inside the incision. This will result in a pocket for PDN injection. The PDN will then be injected into the pocket with an injection needle.

The contralateral vocal fold will be preserved as an uninjured control. To ascertain material retention in the injured VF, the modified microflap procedure will be performed on excised rabbit larynges immediately followed by injection of fluorescein isothiocyanate (FITC)-labeled chitosan. The animal studies procedure is shown in Fig. 5.1.

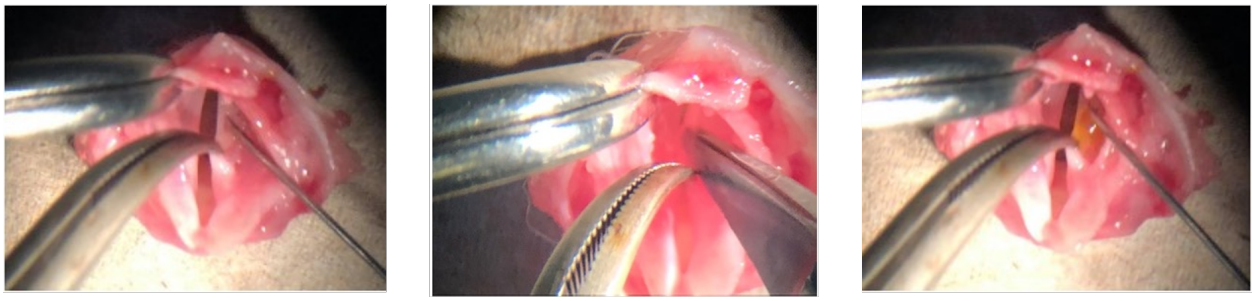

Fig. 5.1. Animal studies procedure. (a) Elevation of microflap and exacerbate the injury, (b) injection of the biomaterial and, (c) ensuring biomaterial retention within the modified microflap.

Animals will be sacrificed either at 1 week or 12 weeks after the procedures. The larynges will be excised for evaluation of histology, biochemistry, immunology, tissue viscoelasticity, and phonatory function. In addition, animals will be used for surgical practice to ensure that the surgical and injection procedures are consistent and repeatable throughout the study. The choice of rabbit animals is justified by cost and ethical considerations, in view of the fact that statistical analysis of quantitative data is required. The proposed experimental design calls for for criterias including: 1) Four groups including controls to investigate the effects of PDN biomaterials: no injury/ no injectable controls; saline placebo controls; NSN; and PSN. 2. Two time points (1 and 12 weeks) to obtain the early host response and the late tissue remodeling

phases. 3. Two biological sexes, males and females, as a biological variable to understand sex influences on vocal health processes and outcomes. 4. Five measurements: macrophage and myofibroblast accumulation, ECM organization, bulk viscoelastic properties, local mechanical properties, and phonatory function. The efficacy of the PDN on the functional outcome of VF will be compared with the control groups to prove PDN's potential as an effective injectable treatment.

5.2.3 PDN-based three-dimensional cell culture for organ-on-a-chip applications

PDNs showed great potential to simulate ECM environment owing to their physical, chemical, and biological characteristics. A combination of PDNs and microtechologies for organ-on-a-chip applications will more closely recapitulate the in vivo micro-environment. Depending on the type of organs, different types of cells will be selected with the appropriate scaffold's porosity to control the oxyegn and medium perfusion. A variety of loading can be simulated and applied to the encapsulated cells within PDNs, injected into the micro-channels, and their mechanical and cellular behavior will be evaluated [222].

Bibliography

[1] S. Taheri, G. Bao, Z. He, S. Mohammadi, H. Ravanbakhsh, L. Lessard, J. Li, L. Mongeau, Injectable, pore-forming, perfusable double-network hydrogels resilient to extreme biomechanical stimulations, Advanced Science (2021) 2102627.

[2] R. Langer, J. Vacanti, Tissue eng, Molecular therapy 1 (2000) 12.

[3] J. P. Vacanti, R. Langer, Tissue engineering: the design and fabrication of living replacement devices for surgical reconstruction and transplantation, The lancet 354 (1999) S32–S34.

[4] M. J. Lysaght, J. A. O'Loughlin, Demographic scope and economic magnitude of contemporary organ replacement therapies, ASAIO journal 46 (2000) 515–521.

[5] R. Pörtner, S. Nagel-Heyer, C. Goepfert, P. Adamietz, N. M. Meenen, Bioreactor design for tissue engineering, Journal of bioscience and bioengineering 100 (2005) 235–245.

[6] M. Liu, X. Zeng, C. Ma, H. Yi, Z. Ali, X. Mou, S. Li, Y. Deng, N. He, Injectable hydrogels for cartilage and bone tissue engineering, Bone research 5 (2017) 1–20.

[7] S. Mohammadi, H. Ravanbakhsh, S. Taheri, G. Bao, L. Mongeau, Immunomodulatory

microgels support pro-regenerative macrophage activation and attenuate fibroblast collagen synthesis, Advanced Healthcare Materials (????) 2102366.

[8] L. G. Griffith, G. Naughton, Tissue engineering–current challenges and expanding opportunities, science 295 (2002) 1009–1014.

[9] R. Y. Kannan, H. J. Salacinski, K. Sales, P. Butler, A. M. Seifalian, The roles of tissue engineering and vascularisation in the development of micro-vascular networks: a review, Biomaterials 26 (2005) 1857–1875.

[10] B. Alberts, D. Bray, K. Hopkin, A. D. Johnson, J. Lewis, M. Raff, K. Roberts, P. Walter, Essential cell biology, Garland Science, 2015.

[11] H. Sekine, T. Shimizu, K. Sakaguchi, I. Dobashi, M. Wada, M. Yamato, E. Kobayashi, M. Umezu, T. Okano, In vitro fabrication of functional three-dimensional tissues with perfusable blood vessels, Nature communications 4 (2013) 1–10.

[12] V. K. Lee, A. M. Lanzi, H. Ngo, S.-S. Yoo, P. A. Vincent, G. Dai, Generation of multi-scale vascular network system within 3d hydrogel using 3d bio-printing technology, Cellular and molecular bioengineering 7 (2014) 460–472.

[13] D. Fassnacht, R. Pörtner, Experimental and theoretical considerations on oxygen supply for animal cell growth in fixed-bed reactors, Journal of biotechnology 72 (1999) 169–184.

[14] K. J. De France, F. Xu, T. Hoare, Structured macroporous hydrogels: Progress, challenges, and opportunities, Advanced healthcare materials 7 (2018) 1700927.

[15] D. L. Butler, S. A. Goldstein, F. Guilak, Functional tissue engineering: the role of biomechanics, J. Biomech. Eng. 122 (2000) 570–575.

[16] A. K. Miri, Mechanical characterization of vocal fold tissue: a review study, Journal of Voice 28 (2014) 657–667.

[17] N. Sahiner, A. K. Jha, D. Nguyen, X. Jia, Fabrication and characterization of cross-linkable hydrogel particles based on hyaluronic acid: potential application in vocal fold regeneration, Journal of Biomaterials Science, Polymer Edition 19 (2008) 223–243.

[18] Z. Ma, G. Bao, J. Li, Multifaceted design and emerging applications of tissue adhesives, Advanced Materials (2021) 2007663.

[19] H. Yang, M. Ji, M. Yang, M. Shi, Y. Pan, Y. Zhou, H. J. Qi, Z. Suo, J. Tang, Fabricating hydrogels to mimic biological tissues of complex shapes and high fatigue resistance, Matter 4 (2021) 1935–1946.

[20] T. I. Croll, S. Gentz, K. Mueller, M. Davidson, A. J. O'Connor, G. W. Stevens, J. J. Cooper-White, Modelling oxygen diffusion and cell growth in a porous, vascularising scaffold for soft tissue engineering applications, Chemical Engineering Science 60 (2005) 4924–4934.

[21] J. Nikolovski, D. J. Mooney, Smooth muscle cell adhesion to tissue engineering scaffolds, Biomaterials 21 (2000) 2025–2032.

[22] L. Flynn, G. D. Prestwich, J. L. Semple, K. A. Woodhouse, Adipose tissue engineering with naturally derived scaffolds and adipose-derived stem cells, Biomaterials 28 (2007) 3834–3842.

[23] D. Seliktar, Designing cell-compatible hydrogels for biomedical applications, Science 336 (2012) 1124–1128.

[24] S. Ahadian, R. B. Sadeghian, S. Salehi, S. Ostrovidov, H. Bae, M. Ramalingam, A. Khademhosseini, Bioconjugated hydrogels for tissue engineering and regenerative medicine, Bioconjugate Chemistry 26 (2015) 1984–2001.

[25] Z. Hao, Z. Song, J. Huang, K. Huang, A. Panetta, Z. Gu, J. Wu, The scaffold microenvironment for stem cell based bone tissue engineering, Biomaterials science 5 (2017) 1382–1392.

[26] K. Haraguchi, T. Takehisa, Nanocomposite hydrogels: A unique organic–inorganic network structure with extraordinary mechanical, optical, and swelling/de-swelling properties, Advanced materials 14 (2002) 1120–1124.

[27] Z. Gu, K. Huang, Y. Luo, L. Zhang, T. Kuang, Z. Chen, G. Liao, Double network hydrogel for tissue engineering, Wiley Interdisciplinary Reviews: Nanomedicine and Nanobiotechnology 10 (2018) e1520.

[28] L. Yu, J. Ding, Injectable hydrogels as unique biomedical materials, Chemical Society Reviews 37 (2008) 1473–1481.

[29] H. Blanco-Fuente, S. Anguiano-Igea, F. Otero-Espinar, J. Blanco-Méndez, In-vitro bioadhesion of carbopol hydrogels, International journal of pharmaceutics 142 (1996) 169–174.

[30] W. E. Hennink, C. F. van Nostrum, Novel crosslinking methods to design hydrogels, Advanced drug delivery reviews 64 (2012) 223–236.

[31] C. K. Kuo, P. X. Ma, Ionically crosslinked alginate hydrogels as scaffolds for tissue engineering: Part 1. structure, gelation rate and mechanical properties, Biomaterials 22 (2001) 511–521.

[32] H. Tan, K. G. Marra, Injectable, biodegradable hydrogels for tissue engineering applications, Materials 3 (2010) 1746–1767.

[33] Y. Hu, W. Dan, S. Xiong, Y. Kang, A. Dhinakar, J. Wu, Z. Gu, Development of collagen/polydopamine complexed matrix as mechanically enhanced and highly biocompatible semi-natural tissue engineering scaffold, Acta biomaterialia 47 (2017) 135–148.

[34] P. Miao, Y. Tang, B. Wang, F. Meng, Near-infrared ag2s quantum dots-based dna logic gate platform for mirna diagnostics, Analytical chemistry 88 (2016) 7567–7573.

[35] H. Xie, J. Wang, Y. He, Z. Gu, J. Xu, L. Li, Q. Ye, Biocompatibility and safety evaluation of a silk fibroin-doped calcium polyphosphate scaffold copolymer in vitro and in vivo, RSC advances 7 (2017) 46036–46044.

[36] J. L. Drury, D. J. Mooney, Hydrogels for tissue engineering: scaffold design variables and applications, Biomaterials 24 (2003) 4337–4351.

[37] J. Fu, F. Yang, Z. Guo, The chitosan hydrogels: from structure to function, New Journal of Chemistry 42 (2018) 17162–17180.

[38] G. Bao, T. Jiang, H. Ravanbakhsh, A. Reyes, Z. Ma, M. Strong, H. Wang, J. M. Kinsella, J. Li, L. Mongeau, Triggered micropore-forming bioprinting of porous viscoelastic hydrogels, Materials Horizons 7 (2020) 2336–2347.

[39] H. Ravanbakhsh, G. Bao, N. Latifi, L. G. Mongeau, Carbon nanotube composite hydrogels for vocal fold tissue engineering: biocompatibility, rheology, and porosity, Materials Science and Engineering: C 103 (2019) 109861.

[40] S. Lü, B. Li, B. Ni, Z. Sun, M. Liu, Q. Wang, Thermoresponsive injectable hydrogel for three-dimensional cell culture: chondroitin sulfate bioconjugated with poly (n-isopropylacrylamide) synthesized by raft polymerization, Soft Matter 7 (2011) 10763–10772.

[41] D. B. Pike, S. Cai, K. R. Pomraning, M. A. Firpo, R. J. Fisher, X. Z. Shu, G. D. Prestwich, R. A. Peattie, Heparin-regulated release of growth factors in vitro and angiogenic response in vivo to implanted hyaluronan hydrogels containing vegf and bfgf, Biomaterials 27 (2006) 5242–5251.

[42] N. Yamaguchi, L. Zhang, B.-S. Chae, C. S. Palla, E. M. Furst, K. L. Kiick, Growth factor mediated assembly of cell receptor-responsive hydrogels, Journal of the American Chemical Society 129 (2007) 3040–3041.

[43] J. Zhu, Bioactive modification of poly (ethylene glycol) hydrogels for tissue engineering, Biomaterials 31 (2010) 4639–4656.

[44] E. S. Place, J. H. George, C. K. Williams, M. M. Stevens, Synthetic polymer scaffolds for tissue engineering, Chemical society reviews 38 (2009) 1139–1151.

[45] R. J. Mart, R. D. Osborne, M. M. Stevens, R. V. Ulijn, Peptide-based stimuli-responsive biomaterials, Soft Matter 2 (2006) 822–835.

[46] A. S. Hoffman, Hydrogels for biomedical applications, Advanced drug delivery reviews 64 (2012) 18–23.

[47] Y. Li, J. Rodrigues, H. Tomas, Injectable and biodegradable hydrogels: gelation, biodegradation and biomedical applications, Chemical Society Reviews 41 (2012) 2193–2221.

[48] F. A. Auger, F. Berthod, V. Moulin, R. Pouliot, L. Germain, Tissue-engineered skin substitutes: from in vitro constructs to in vivo applications, Biotechnology and applied biochemistry 39 (2004) 263–275.

[49] X. Zhang, J. Li, P. Ye, G. Gao, K. Hubbell, X. Cui, Coculture of mesenchymal stem cells and endothelial cells enhances host tissue integration and epidermis maturation through akt activation in gelatin methacryloyl hydrogel-based skin model, Acta biomaterialia 59 (2017) 317–326.

[50] N. Boucard, C. Viton, D. Agay, E. Mari, T. Roger, Y. Chancerelle, A. Domard, The use of physical hydrogels of chitosan for skin regeneration following third-degree burns, Biomaterials 28 (2007) 3478–3488.

[51] T. Wong, J. McGrath, H. Navsaria, The role of fibroblasts in tissue engineering and regeneration, British Journal of Dermatology 156 (2007) 1149–1155.

[52] H. R. Moreira, A. P. Marques, Vascularization in skin wound healing: where do we stand and where do we go?, Current Opinion in Biotechnology 73 (2022) 253–262.

[53] K. M. Malinda, A. B. Wysocki, J. E. Koblinski, H. K. Kleinman, M. L. Ponce, Angio-

genic laminin-derived peptides stimulate wound healing, The international journal of biochemistry & cell biology 40 (2008) 2771–2780.

[54] M. M. Martino, P. S. Briquez, A. Ranga, M. P. Lutolf, J. A. Hubbell, Heparin-binding domain of fibrin (ogen) binds growth factors and promotes tissue repair when incorporated within a synthetic matrix, Proceedings of the National Academy of Sciences 110 (2013) 4563–4568.

[55] W. Wang, L. Guo, Y. Yu, Z. Chen, R. Zhou, Z. Yuan, Peptide redv-modified polysaccharide hydrogel with endothelial cell selectivity for the promotion of angiogenesis, Journal of Biomedical Materials Research Part A 103 (2015) 1703–1712.

[56] S. Li, L. R. Nih, H. Bachman, P. Fei, Y. Li, E. Nam, R. Dimatteo, S. T. Carmichael, T. H. Barker, T. Segura, Hydrogels with precisely controlled integrin activation dictate vascular patterning and permeability, Nature materials 16 (2017) 953–961.

[57] L. P. d. Silva, R. P. Pirraco, T. C. Santos, R. Novoa-Carballal, M. T. Cerqueira, R. L. Reis, V. M. Correlo, A. P. Marques, Neovascularization induced by the hyaluronic acid-based spongy-like hydrogels degradation products, ACS Applied Materials & Interfaces 8 (2016) 33464–33474.

[58] F. Rowland, M. Donovan, P. Picciano, G. Wilner, D. Kreutzer, Fibrin-mediated vascular injury. identification of fibrin peptides that mediate endothelial cell retraction., The American journal of pathology 117 (1984) 418.

[59] M. Ge, T. J. Ryan, H. Lum, A. B. Malik, Fibrinogen degradation product fragment d

increases endothelial monolayer permeability, American Journal of Physiology-Lung Cellular and Molecular Physiology 261 (1991) L283–L289.

[60] D. K. Jarrell, E. J. Vanderslice, M. L. Lennon, A. C. Lyons, M. C. VeDepo, J. G. Jacot, Increasing salinity of fibrinogen solvent generates stable fibrin hydrogels for cell delivery or tissue engineering, Plos one 16 (2021) e0239242.

[61] T. Segura, B. C. Anderson, P. H. Chung, R. E. Webber, K. R. Shull, L. D. Shea, Crosslinked hyaluronic acid hydrogels: a strategy to functionalize and pattern, Biomaterials 26 (2005) 359–371.

[62] A. Amirsadeghi, A. Jafari, L. J. Eggermont, S.-S. Hashemi, S. A. Bencherif, M. Khorram, Vascularization strategies for skin tissue engineering, Biomaterials Science 8 (2020) 4073–4094.

[63] N. J. Blackburn, T. Sofrenovic, D. Kuraitis, A. Ahmadi, B. McNeill, C. Deng, K. J. Rayner, Z. Zhong, M. Ruel, E. J. Suuronen, Timing underpins the benefits associated with injectable collagen biomaterial therapy for the treatment of myocardial infarction, Biomaterials 39 (2015) 182–192.

[64] B. Peña, M. Laughter, S. Jett, T. J. Rowland, M. R. Taylor, L. Mestroni, D. Park, Injectable hydrogels for cardiac tissue engineering, Macromolecular bioscience 18 (2018) 1800079.

[65] M. D. Brigham, A. Bick, E. Lo, A. Bendali, J. A. Burdick, A. Khademhosseini, Mechanically robust and bioadhesive collagen and photocrosslinkable hyaluronic acid semi-interpenetrating networks, Tissue Engineering Part A 15 (2009) 1645–1653.

[66] K. Hu, H. Shi, J. Zhu, D. Deng, G. Zhou, W. Zhang, Y. Cao, W. Liu, Compressed collagen gel as the scaffold for skin engineering, Biomedical microdevices 12 (2010) 627–635.

[67] K. L. Christman, A. J. Vardanian, Q. Fang, R. E. Sievers, H. H. Fok, R. J. Lee, Injectable fibrin scaffold improves cell transplant survival, reduces infarct expansion, and induces neovasculature formation in ischemic myocardium, Journal of the American College of Cardiology 44 (2004) 654–660.

[68] J. H. Ryu, I.-K. Kim, S.-W. Cho, M.-C. Cho, K.-K. Hwang, H. Piao, S. Piao, S. H. Lim, Y. S. Hong, C. Y. Choi, et al., Implantation of bone marrow mononuclear cells using injectable fibrin matrix enhances neovascularization in infarcted myocardium, Biomaterials 26 (2005) 319–326.

[69] C. M. Brougham, T. J. Levingstone, S. Jockenhoevel, T. C. Flanagan, F. J. O'Brien, Incorporation of fibrin into a collagen–glycosaminoglycan matrix results in a scaffold with improved mechanical properties and enhanced capacity to resist cell-mediated contraction, Acta biomaterialia 26 (2015) 205–214.

[70] X. Zhang, B. Xu, D. S. Puperi, Y. Wu, J. L. West, K. J. Grande-Allen, Application of hydrogels in heart valve tissue engineering, Journal of long-term effects of medical implants 25 (2015).

[71] F. Alimirzaei, E. Vasheghani-Farahani, A. Ghiaseddin, M. Soleimani, et al., ph-sensitive chitosan hydrogel with instant gelation for myocardial regeneration, J. Tissue Sci. Eng 8 (2017).

[72] B. W. Lee, B. Liu, A. Pluchinsky, N. Kim, G. Eng, G. Vunjak-Novakovic, Modular assembly approach to engineer geometrically precise cardiovascular tissue, Advanced healthcare materials 5 (2016) 900–906.

[73] R. Waters, S. Pacelli, R. Maloney, I. Medhi, R. P. Ahmed, A. Paul, Stem cell secretome-rich nanoclay hydrogel: a dual action therapy for cardiovascular regeneration, Nanoscale 8 (2016) 7371–7376.

[74] A. Chow, D. J. Stuckey, E. Kidher, M. Rocco, R. J. Jabbour, C. A. Mansfield, A. Darzi, S. E. Harding, M. M. Stevens, T. Athanasiou, Human induced pluripotent stem cell-derived cardiomyocyte encapsulating bioactive hydrogels improve rat heart function post myocardial infarction, Stem Cell Reports 9 (2017) 1415–1422.

[75] A. Navaei, D. Truong, J. Heffernan, J. Cutts, D. Brafman, R. W. Sirianni, B. Vernon, M. Nikkhah, Pnipaam-based biohybrid injectable hydrogel for cardiac tissue engineering, Acta biomaterialia 32 (2016) 10–23.

[76] L. R. Geuss, A. C. Allen, D. Ramamoorthy, L. J. Suggs, Maintenance of hl-1 cardiomyocyte functional activity in pegylated fibrin gels, Biotechnology and Bioengineering 112 (2015) 1446–1456.

[77] Z. Fan, M. Fu, Z. Xu, B. Zhang, Z. Li, H. Li, X. Zhou, X. Liu, Y. Duan, P.-H. Lin, et al., Sustained release of a peptide-based matrix metalloproteinase-2 inhibitor to attenuate adverse cardiac remodeling and improve cardiac function following myocardial infarction, Biomacromolecules 18 (2017) 2820–2829.

[78] Y. Xia, K. Zhu, H. Lai, M. Lang, Y. Xiao, S. Lian, C. Guo, C. Wang, Enhanced infarct

myocardium repair mediated by thermosensitive copolymer hydrogel-based stem cell transplantation, Experimental Biology and Medicine 240 (2015) 593–600.

[79] Y.-C. Chang, G. Mirhaidari, J. Kelly, C. Breuer, Current challenges and solutions to tissue engineering of large-scale cardiac constructs, Current Cardiology Reports 23 (2021) 1–6.

[80] G. Vunjak-Novakovic, N. Tandon, A. Godier, R. Maidhof, A. Marsano, T. P. Martens, M. Radisic, Challenges in cardiac tissue engineering, Tissue Engineering Part B: Reviews 16 (2010) 169–187.

[81] N. Williams, Occupational groups at risk of voice disorders: a review of the literature, Occupational medicine 62 (2012) 588–588.

[82] K. Ishii, M. Akita, K. Yamashita, H. Hirose, Age-related development of the arrangement of connective tissue fibers in the lamina propria of the human vocal fold, Annals of Otology, Rhinology & Laryngology 109 (2000) 1055–1064.

[83] C. J. Hartnick, R. Rehbar, V. Prasad, Development and maturation of the pediatric human vocal fold lamina propria, The Laryngoscope 115 (2005) 4–15.

[84] M. Hirano, Growth, development and aging of human vocal fold, Vocal fold physiology (1983) 3–21.

[85] S. Krischke, S. Weigelt, U. Hoppe, V. Köllner, M. Klotz, U. Eysholdt, F. Rosanowski, Quality of life in dysphonic patients, Journal of Voice 19 (2005) 132–137.

[86] L. Li, J. M. Stiadle, H. K. Lau, A. B. Zerdoum, X. Jia, S. L. Thibeault, K. L. Kiick, Tissue engineering-based therapeutic strategies for vocal fold repair and regeneration, Biomaterials 108 (2016) 91–110.

[87] T. Walimbe, A. Panitch, P. M. Sivasankar, A review of hyaluronic acid and hyaluronic acid-based hydrogels for vocal fold tissue engineering, Journal of Voice 31 (2017) 416–423.

[88] N. Latifi, Nano-Fibrillar Hybrid Biomaterials and Phono-Mimetic Perfusion Bioreactor for Vocal Fold Tissue Engineering, McGill University (Canada), 2018.

[89] A. Schindler, F. Mozzanica, D. Ginocchio, P. Maruzzi, M. Atac, F. Ottaviani, Vocal improvement after voice therapy in the treatment of benign vocal fold lesions, Acta Otorhinolaryngologica Italica 32 (2012) 304.

[90] A. J. Farran, Z. Tong, R. L. Witt, X. Jia, Tissue engineering strategies for vocal fold repair and regeneration, in: Engineering Biomaterials for Regenerative Medicine, Springer, 2012, pp. 253–284.

[91] J. A. Burdick, G. D. Prestwich, Hyaluronic acid hydrogels for biomedical applications, Advanced materials 23 (2011) H41–H56.

[92] J. Gaston, S. L. Thibeault, Hyaluronic acid hydrogels for vocal fold wound healing, Biomatter 3 (2013) e23799.

[93] H. K. Heris, M. Rahmat, L. Mongeau, Characterization of a hierarchical network of hyaluronic acid/gelatin composite for use as a smart injectable biomaterial, Macromolecular bioscience 12 (2012) 202–210.

[94] S. Duflo, S. L. Thibeault, W. Li, X. Z. Shu, G. D. Prestwich, Vocal fold tissue repair in vivo using a synthetic extracellular matrix, Tissue engineering 12 (2006) 2171–2180.

[95] X. Z. Shu, Y. Liu, F. Palumbo, G. D. Prestwich, Disulfide-crosslinked hyaluronan-gelatin hydrogel films: a covalent mimic of the extracellular matrix for in vitro cell growth, Biomaterials 24 (2003) 3825–3834.

[96] J. J. Rice, M. M. Martino, L. De Laporte, F. Tortelli, P. S. Briquez, J. A. Hubbell, Engineering the regenerative microenvironment with biomaterials, Advanced healthcare materials 2 (2013) 57–71.

[97] R. Langer, D. A. Tirrell, Designing materials for biology and medicine, Nature 428 (2004) 487–492.

[98] J. A. Hubbell, Biomaterials in tissue engineering, Bio/technology 13 (1995) 565–576.

[99] S.-I. Kanemaru, H. Kojima, S. Hirano, T. Nakamura, A. Magrufov, J. Ito, K. Omori, Y. Hiratsuka, Y. Shimizu, Regeneration of the vocal fold using autologous mesenchymal stem cells, Annals of Otology, Rhinology & Laryngology 112 (2003) 915–920.

[100] Y. Kishimoto, N. V. Welham, S. Hirano, Implantation of atelocollagen sheet for vocal fold scar, Current opinion in otolaryngology & head and neck surgery 18 (2010) 507.

[101] Y. Kishimoto, S. Hirano, T. Kojima, S.-I. Kanemaru, J. Ito, Implantation of an atelocollagen sheet for the treatment of vocal fold scarring and sulcus vocalis, Annals of Otology, Rhinology & Laryngology 118 (2009) 613–620.

[102] M. S. Benninger, D. Alessi, S. Archer, R. Bastian, C. Ford, J. Koufman, R. T. Sataloff, J. R. Spiegel, P. Woo, Vocal fold scarring: current concepts and management, Otolaryngology—head and neck surgery 115 (1996) 474–482.

[103] T. Caton, S. L. Thibeault, S. Klemuk, M. E. Smith, Viscoelasticity of hyaluronan and nonhyaluronan based vocal fold injectables: implications for mucosal versus muscle use, The Laryngoscope 117 (2007) 516–521.

[104] C. N. Ford, D. M. Bless, Collagen injection in the scarred vocal fold, Journal of Voice 1 (1987) 116–118.

[105] M. S. Hahn, B. A. Teply, M. M. Stevens, S. M. Zeitels, R. Langer, Collagen composite hydrogels for vocal fold lamina propria restoration, Biomaterials 27 (2006) 1104–1109.

[106] A. D. Augst, H. J. Kong, D. J. Mooney, Alginate hydrogels as biomaterials, Macromolecular bioscience 6 (2006) 623–633.

[107] H. K. Heris, N. Latifi, H. Vali, N. Li, L. Mongeau, Investigation of chitosan-glycol/glyoxal as an injectable biomaterial for vocal fold tissue engineering, Procedia Engineering 110 (2015) 143–150.

[108] C. H. Lee, A. Singla, Y. Lee, Biomedical applications of collagen, International journal of pharmaceutics 221 (2001) 1–22.

[109] P. Balasubramanian, M. P. Prabhakaran, M. Sireesha, S. Ramakrishna, Collagen in human tissues: structure, function, and biomedical implications from a tissue engineering perspective, in: Polymer Composites–Polyolefin Fractionation–Polymeric Peptidomimetics–Collagens, Springer, 2012, pp. 173–206.

[110] L. Cen, W. Liu, L. Cui, W. Zhang, Y. Cao, Collagen tissue engineering: development of novel biomaterials and applications, Pediatric research 63 (2008) 492–496.

[111] B. Chevallay, D. Herbage, Collagen-based biomaterials as 3d scaffold for cell cultures: applications for tissue engineering and gene therapy, Medical and Biological Engineering and Computing 38 (2000) 211–218.

[112] R. Parenteau-Bareil, R. Gauvin, F. Berthod, Collagen-based biomaterials for tissue engineering applications, Materials 3 (2010) 1863–1887.

[113] A. K. Miri, H. G. Hosseinabadi, B. Cecen, S. Hassan, Y. S. Zhang, Permeability mapping of gelatin methacryloyl hydrogels, Acta biomaterialia 77 (2018) 38–47.

[114] J. Zhang, L. Wu, D. Jing, J. Ding, A comparative study of porous scaffolds with cubic and spherical macropores, Polymer 46 (2005) 4979–4985.

[115] V. Keskar, N. W. Marion, J. J. Mao, R. A. Gemeinhart, In vitro evaluation of macroporous hydrogels to facilitate stem cell infiltration, growth, and mineralization, Tissue Engineering Part A 15 (2009) 1695–1707.

[116] B. H. Oh, A. Bismarck, M. B. Chan-Park, Injectable, interconnected, high-porosity macroporous biocompatible gelatin scaffolds made by surfactant-free emulsion templating, Macromolecular rapid communications 36 (2015) 364–372.

[117] H.-W. Kang, Y. Tabata, Y. Ikada, Fabrication of porous gelatin scaffolds for tissue engineering, Biomaterials 20 (1999) 1339–1344.

[118] G. M. Cruise, D. S. Scharp, J. A. Hubbell, Characterization of permeability and network structure of interfacially photopolymerized poly (ethylene glycol) diacrylate hydrogels, Biomaterials 19 (1998) 1287–1294.

[119] E. M. Johnson, W. M. Deen, Hydraulic permeability of agarose gels, AIChE Journal 42 (1996) 1220–1224.

[120] W. Gu, H. Yao, C. Huang, H. Cheung, New insight into deformation-dependent hydraulic permeability of gels and cartilage, and dynamic behavior of agarose gels in confined compression, Journal of biomechanics 36 (2003) 593–598.

[121] G. A. Busby, M. H. Grant, S. P. MacKay, P. E. Riches, Confined compression of collagen hydrogels, Journal of biomechanics 46 (2013) 837–840.

[122] M. F. Refojo, Permeation of water through some hydrogels, Journal of Applied Polymer Science 9 (1965) 3417–3426.

[123] V. Kapur, J. C. Charkoudian, S. B. Kessler, J. L. Anderson, Hydrodynamic permeability of hydrogels stabilized within porous membranes, Industrial & engineering chemistry research 35 (1996) 3179–3185.

[124] D. G. Strange, T. L. Fletcher, K. Tonsomboon, H. Brawn, X. Zhao, M. L. Oyen, Separating poroviscoelastic deformation mechanisms in hydrogels, Applied Physics Letters 102 (2013) 031913.

[125] S. A. Bencherif, R. W. Sands, D. Bhatta, P. Arany, C. S. Verbeke, D. A. Edwards, D. J. Mooney, Injectable preformed scaffolds with shape-memory properties, Proceedings of the National Academy of Sciences 109 (2012) 19590–19595.

[126] H. Ravanbakhsh, G. Bao, Z. Luo, L. G. Mongeau, Y. S. Zhang, Composite inks for extrusion printing of biological and biomedical constructs, ACS Biomaterials Science & Engineering 7 (2020) 4009–4026.

[127] G. Bao, Biofabrication in tissue engineering, Racing for the Surface (2020) 289–312.

[128] H. Ravanbakhsh, V. Karamzadeh, G. Bao, L. Mongeau, D. Juncker, Y. S. Zhang, Emerging technologies in multi-material bioprinting, Advanced Materials 33 (2021) 2104730.

[129] G. Ying, N. Jiang, C. Parra-Cantu, G. Tang, J. Zhang, H. Wang, S. Chen, N.-P. Huang, J. Xie, Y. S. Zhang, Bioprinted injectable hierarchically porous gelatin methacryloyl hydrogel constructs with shape-memory properties, Advanced Functional Materials 30 (2020) 2003740.

[130] P. Eiselt, J. Yeh, R. K. Latvala, L. D. Shea, D. J. Mooney, Porous carriers for biomedical applications based on alginate hydrogels, Biomaterials 21 (2000) 1921–1927.

[131] L. Wang, S. Dong, Y. Liu, Y. Ma, J. Zhang, Z. Yang, W. Jiang, Y. Yuan, Fabrication of injectable, porous hyaluronic acid hydrogel based on an in-situ bubble-forming hydrogel entrapment process, Polymers 12 (2020) 1138.

[132] Y. Tang, S. Lin, S. Yin, F. Jiang, M. Zhou, G. Yang, N. Sun, W. Zhang, X. Jiang, In situ gas foaming based on magnesium particle degradation: A novel approach to fabricate injectable macroporous hydrogels, Biomaterials 232 (2020) 119727.

[133] M. Goh, Y. Kim, K. Gwon, K. Min, Y. Hwang, G. Tae, In situ formation of injectable and porous heparin-based hydrogel, Carbohydrate polymers 174 (2017) 990–998.

[134] Z.-K. Cui, S. Kim, J. J. Baljon, B. M. Wu, T. Aghaloo, M. Lee, Microporous methacrylated glycol chitosan-montmorillonite nanocomposite hydrogel for bone tissue engineering, Nature communications 10 (2019) 1–10.

[135] R.-S. Hsu, P.-Y. Chen, J.-H. Fang, Y.-Y. Chen, C.-W. Chang, Y.-J. Lu, S.-H. Hu, Adaptable microporous hydrogels of propagating ngf-gradient by injectable building blocks for accelerated axonal outgrowth, Advanced Science 6 (2019) 1900520.

[136] H. T. T. Duong, T. Thambi, Y. Yin, S. H. Kim, T. L. Nguyen, V. G. Phan, J. Kim, J. H. Jeong, D. S. Lee, Degradation-regulated architecture of injectable smart hydrogels enhances humoral immune response and potentiates antitumor activity in human lung carcinoma, Biomaterials 230 (2020) 119599.

[137] J. Kim, W. A. Li, Y. Choi, S. A. Lewin, C. S. Verbeke, G. Dranoff, D. J. Mooney, Injectable, spontaneously assembling, inorganic scaffolds modulate immune cells in vivo and increase vaccine efficacy, Nature biotechnology 33 (2015) 64–72.

[138] N. Huebsch, E. Lippens, K. Lee, M. Mehta, S. T. Koshy, M. C. Darnell, R. M. Desai, C. M. Madl, M. Xu, X. Zhao, et al., Matrix elasticity of void-forming hydrogels controls transplanted-stem-cell-mediated bone formation, Nature materials 14 (2015) 1269–1277.

[139] G.-L. Ying, N. Jiang, S. Maharjan, Y.-X. Yin, R.-R. Chai, X. Cao, J.-Z. Yang, A. K. Miri, S. Hassan, Y. S. Zhang, Aqueous two-phase emulsion bioink-enabled 3d bioprinting of porous hydrogels, Advanced Materials 30 (2018) 1805460.

[140] G. Ying, J. Manríquez, D. Wu, J. Zhang, N. Jiang, S. Maharjan, D. H. Medina,

Y. Zhang, An open-source handheld extruder loaded with pore-forming bioink for in situ wound dressing, Materials Today Bio 8 (2020) 100074.

[141] B. Kessel, M. Lee, A. Bonato, Y. Tinguely, E. Tosoratti, M. Zenobi-Wong, 3d bioprinting of macroporous materials based on entangled hydrogel microstrands, Advanced Science 7 (2020) 2001419.

[142] X. Zhao, X. Chen, H. Yuk, S. Lin, X. Liu, G. Parada, Soft materials by design: Unconventional polymer networks give extreme properties, Chemical Reviews 121 (2021) 4309–4372.

[143] J. P. Gong, Why are double network hydrogels so tough?, Soft Matter 6 (2010) 2583–2590.

[144] J. P. Gong, Y. Katsuyama, T. Kurokawa, Y. Osada, Double-network hydrogels with extremely high mechanical strength, Advanced materials 15 (2003) 1155–1158.

[145] K. Yasuda, J. P. Gong, Y. Katsuyama, A. Nakayama, Y. Tanabe, E. Kondo, M. Ueno, Y. Osada, Biomechanical properties of high-toughness double network hydrogels, Biomaterials 26 (2005) 4468–4475.

[146] T. Nakajima, H. Sato, Y. Zhao, S. Kawahara, T. Kurokawa, K. Sugahara, J. P. Gong, A universal molecular stent method to toughen any hydrogels based on double network concept, Advanced functional materials 22 (2012) 4426–4432.

[147] X. J. Liu, X. Y. Ren, S. Guan, H. Q. Li, Z. K. Song, G. H. Gao, Highly stretchable and tough double network hydrogels via molecular stent, European Polymer Journal 73 (2015) 149–161.

[148] T. Nakajima, Y. Fukuda, T. Kurokawa, T. Sakai, U.-i. Chung, J. P. Gong, Synthesis and fracture process analysis of double network hydrogels with a well-defined first network, ACS Macro Letters 2 (2013) 518–521.

[149] H. Tsukeshiba, M. Huang, Y.-H. Na, T. Kurokawa, R. Kuwabara, Y. Tanaka, H. Furukawa, Y. Osada, J. P. Gong, Effect of polymer entanglement on the toughening of double network hydrogels, The Journal of Physical Chemistry B 109 (2005) 16304–16309.

[150] Y.-H. Na, Y. Tanaka, Y. Kawauchi, H. Furukawa, T. Sumiyoshi, J. P. Gong, Y. Osada, Necking phenomenon of double-network gels, Macromolecules 39 (2006) 4641–4645.

[151] M. Huang, H. Furukawa, Y. Tanaka, T. Nakajima, Y. Osada, J. P. Gong, Importance of entanglement between first and second components in high-strength double network gels, Macromolecules 40 (2007) 6658–6664.

[152] Y. Tanaka, R. Kuwabara, Y.-H. Na, T. Kurokawa, J. P. Gong, Y. Osada, Determination of fracture energy of high strength double network hydrogels, The Journal of Physical Chemistry B 109 (2005) 11559–11562.

[153] T. Nakajima, H. Furukawa, Y. Tanaka, T. Kurokawa, Y. Osada, J. P. Gong, True chemical structure of double network hydrogels, Macromolecules 42 (2009) 2184–2189.

[154] E. Raphael, P. De Gennes, Rubber-rubber adhesion with connector molecules, The Journal of Physical Chemistry 96 (1992) 4002–4007.

[155] H. R. Brown, Effects of chain pull-out on adhesion of elastomers, Macromolecules 26 (1993) 1666–1670.

[156] K. Okumura, Toughness of double elastic networks, EPL (Europhysics Letters) 67 (2004) 470.

[157] H. R. Brown, A model of the fracture of double network gels, Macromolecules 40 (2007) 3815–3818.

[158] Y. Tanaka, A local damage model for anomalous high toughness of double-network gels, EPL (Europhysics Letters) 78 (2007) 56005.

[159] V. R. Tirumala, T. Tominaga, S. Lee, P. D. Butler, E. K. Lin, J. P. Gong, W.-l. Wu, Molecular model for toughening in double-network hydrogels, The Journal of Physical Chemistry B 112 (2008) 8024–8031.

[160] S. S. Jang, W. A. Goddard, M. Y. S. Kalani, Mechanical and transport properties of the poly (ethylene oxide)- poly (acrylic acid) double network hydrogel from molecular dynamic simulations, The Journal of Physical Chemistry B 111 (2007) 1729–1737.

[161] V. X. Truong, M. P. Ablett, S. M. Richardson, J. A. Hoyland, A. P. Dove, Simultaneous orthogonal dual-click approach to tough, in-situ-forming hydrogels for cell encapsulation, Journal of the American Chemical Society 137 (2015) 1618–1622.

[162] C. B. Rodell, N. N. Dusaj, C. B. Highley, J. A. Burdick, Injectable and cytocompatible tough double-network hydrogels through tandem supramolecular and covalent crosslinking, Advanced materials 28 (2016) 8419–8424.

[163] G. Jalani, D. H. Rosenzweig, G. Makhoul, S. Abdalla, R. Cecere, F. Vetrone, L. Haglund, M. Cerruti, Tough, in-situ thermogelling, injectable hydrogels for biomedical applications, Macromolecular bioscience 15 (2015) 473–480.

[164] Y. Zhao, M. Li, B. Liu, J. Xiang, Z. Cui, X. Qu, D. Qiu, Y. Tian, Z. Yang, Ultra-tough injectable cytocompatible hydrogel for 3d cell culture and cartilage repair, Journal of Materials Chemistry B 6 (2018) 1351–1358.

[165] Z. Guo, H. Gu, Y. He, Y. Zhang, W. Xu, J. Zhang, Y. Liu, L. Xiong, A. Chen, Y. Feng, Dual dynamic bonds enable biocompatible and tough hydrogels with fast self-recoverable, self-healable and injectable properties, Chemical Engineering Journal 388 (2020) 124282.

[166] Z. Mu, K. Chen, S. Yuan, Y. Li, Y. Huang, C. Wang, Y. Zhang, W. Liu, W. Luo, P. Liang, et al., Gelatin nanoparticle-injectable platelet-rich fibrin double network hydrogels with local adaptability and bioactivity for enhanced osteogenesis, Advanced healthcare materials 9 (2020) 1901469.

[167] S. Hong, D. Sycks, H. F. Chan, S. Lin, G. P. Lopez, F. Guilak, K. W. Leong, X. Zhao, 3d printing of highly stretchable and tough hydrogels into complex, cellularized structures, Advanced materials 27 (2015) 4035–4040.

[168] A. M. Gracioso Martins, A. Biehl, D. Sze, D. O. Freytes, Bioreactors for vocal fold tissue engineering, Tissue Engineering Part B: Reviews (2021).

[169] I. Martin, D. Wendt, M. Heberer, The role of bioreactors in tissue engineering, TRENDS in Biotechnology 22 (2004) 80–86.

[170] I. R. Titze, R. W. Hitchcock, K. Broadhead, K. Webb, W. Li, S. D. Gray, P. A. Tresco, Design and validation of a bioreactor for engineering vocal fold tissues under combined tensile and vibrational stresses, Journal of Biomechanics 37 (2004) 1521–1529.

[171] J. C. Wolchok, C. Brokopp, C. J. Underwood, P. A. Tresco, The effect of bioreactor induced vibrational stimulation on extracellular matrix production from human derived fibroblasts, Biomaterials 30 (2009) 327–335.

[172] R. C. Branski, P. Perera, K. Verdolini, C. A. Rosen, P. A. Hebda, S. Agarwal, Dynamic biomechanical strain inhibits il-1β–induced inflammation in vocal fold fibroblasts, Journal of Voice 21 (2007) 651–660.

[173] A. J. Farran, S. S. Teller, F. Jia, R. J. Clifton, R. L. Duncan, X. Jia, Design and characterization of a dynamic vibrational culture system, Journal of tissue engineering and regenerative medicine 7 (2013) 213–225.

[174] N. Latifi, H. K. Heris, S. L. Thomson, R. Taher, S. Kazemirad, S. Sheibani, N. Y. Li-Jessen, H. Vali, L. Mongeau, A flow perfusion bioreactor system for vocal fold tissue engineering applications, Tissue Engineering Part C: Methods 22 (2016) 823–838.

[175] A. Kirsch, D. Hortobagyi, T. Stachl, M. Karbiener, T. Grossmann, C. Gerstenberger, M. Gugatschka, Development and validation of a novel phonomimetic bioreactor, Plos one 14 (2019) e0213788.

[176] Y.-W. Jiang, H.-Y. Guo, Z. Chen, Z.-W. Yu, Z. Wang, F.-G. Wu, In situ visualization of lipid raft domains by fluorescent glycol chitosan derivatives, Langmuir 32 (2016) 6739–6745.

[177] A. São Pedro, E. Cabral-Albuquerque, D. Ferreira, B. Sarmento, Chitosan: an option for development of essential oil delivery systems for oral cavity care?, Carbohydrate polymers 76 (2009) 501–508.

[178] R. C. Scherer, D. Shinwari, K. J. De Witt, C. Zhang, B. R. Kucinschi, A. A. Afjeh, Intraglottal pressure profiles for a symmetric and oblique glottis with a divergence angle of 10 degrees, The Journal of the Acoustical Society of America 109 (2001) 1616–1630.

[179] A. Monette, C. Ceccaldi, E. Assaad, S. Lerouge, R. Lapointe, Chitosan thermogels for local expansion and delivery of tumor-specific t lymphocytes towards enhanced cancer immunotherapies, Biomaterials 75 (2016) 237–249.

[180] G. Bao, R. Huo, Z. Ma, M. Strong, A. Valiei, S. Jiang, S. Liu, L. Mongeau, J. Li, Ionotronic tough adhesives with intrinsic multifunctionality, ACS Applied Materials & Interfaces 13 (2021) 37849–37861.

[181] O. Chaudhuri, J. Cooper-White, P. A. Janmey, D. J. Mooney, V. B. Shenoy, Effects of extracellular matrix viscoelasticity on cellular behaviour, Nature 584 (2020) 535–546.

[182] K. H. Vining, D. J. Mooney, Mechanical forces direct stem cell behaviour in development and regeneration, Nature reviews Molecular cell biology 18 (2017) 728–742.

[183] J.-Y. Sun, X. Zhao, W. R. Illeperuma, O. Chaudhuri, K. H. Oh, D. J. Mooney, J. J. Vlassak, Z. Suo, Highly stretchable and tough hydrogels, Nature 489 (2012) 133–136.

[184] O. Chaudhuri, L. Gu, D. Klumpers, M. Darnell, S. Bencherif, J. Weaver, N. Huebsch, H. Lee, p., lippens e., duda gn, mooney dj, Nat. Mater 15 (2016) 326.

[185] H. Kwon, A. D. Rogalsky, D.-W. Kim, On the measurement of fracture toughness of soft biogel, Polymer Engineering & Science 51 (2011) 1078–1086.

[186] P. G. Righetti, B. C. Brost, R. S. Snyder, On the limiting pore size of hydrophilic gels for electrophoresis and isoelectric focussing, Journal of biochemical and biophysical methods 4 (1981) 347–363.

[187] A. A. Thakre, A. K. Singh, Energy release rate of gelatin hydrogels on glass surface in direct shear sliding experiments, Journal of adhesion science and Technology 32 (2018) 1899–1910.

[188] M. Miller, J. D. Ferry, F. W. Schremp, J. E. Eldridge, Studies of the cross-linking process in gelatin gels. ii. static rigidity and stress relaxation., The Journal of Physical Chemistry 55 (1951) 1387–1400.

[189] S. Koshy, R. Desai, P. Joly, J. Li, R. Bagrodia, S. Lewin, N. Joshi, D. Mooney, Click-crosslinked injectable gelatin hydrogels, adv. healthc. mater. 5 (2016) 541–547, ????

[190] X. Xu, A. K. Jha, D. A. Harrington, M. C. Farach-Carson, X. Jia, Hyaluronic acid-based hydrogels: from a natural polysaccharide to complex networks, Soft matter 8 (2012) 3280–3294.

[191] J. Lou, R. Stowers, S. Nam, Y. Xia, O. Chaudhuri, Stress relaxing hyaluronic acid-collagen hydrogels promote cell spreading, fiber remodeling, and focal adhesion formation in 3d cell culture, Biomaterials 154 (2018) 213–222.

[192] G. Offeddu, E. Axpe, B. Harley, M. Oyen, Relationship between permeability and diffusivity in polyethylene glycol hydrogels, AIP advances 8 (2018) 105006.

[193] Y.-C. Chiu, M.-H. Cheng, H. Engel, S.-W. Kao, J. C. Larson, S. Gupta, E. M. Brey, The role of pore size on vascularization and tissue remodeling in peg hydrogels, Biomaterials 32 (2011) 6045–6051.

[194] S. Ramanujan, A. Pluen, T. D. McKee, E. B. Brown, Y. Boucher, R. K. Jain, Diffusion and convection in collagen gels: implications for transport in the tumor interstitium, Biophysical journal 83 (2002) 1650–1660.

[195] S. Campbell, B. Watson, A. Gibson, G. Husband, K. Bremner, Comprehensive service and practice development: city hospitals sunderland's experience of patient journeys, Practice Development in Health Care 3 (2004) 15–26.

[196] I. Ochoa, J. A. Sanz-Herrera, J. M. García-Aznar, M. Doblaré, D. M. Yunos, A. R. Boccaccini, Permeability evaluation of 45s5 bioglass®-based scaffolds for bone tissue engineering, Journal of biomechanics 42 (2009) 257–260.

[197] A. G. Mitsak, J. M. Kemppainen, M. T. Harris, S. J. Hollister, Effect of polycaprolactone scaffold permeability on bone regeneration in vivo, Tissue Engineering Part A 17 (2011) 1831–1839.

[198] M. Dias, P. Fernandes, J. Guedes, S. Hollister, Permeability analysis of scaffolds for bone tissue engineering, Journal of biomechanics 45 (2012) 938–944.

[199] C. C. Xu, R. W. Chan, Pore architecture of a bovine acellular vocal fold scaffold, Tissue engineering Part A 14 (2008) 1893–1903.

[200] A. K. Miri, L. X. Chen, R. Mongrain, L. Mongeau, Fracture toughness of vocal fold tissue: A preliminary study, Journal of Voice 30 (2016) 251–254.

[201] C. Gokgol, C. Basdogan, D. Canadinc, Estimation of fracture toughness of liver tissue: Experiments and validation, Medical engineering & physics 34 (2012) 882–891.

[202] S. Raghunathan, D. Evans, J. L. Sparks, Poroviscoelastic modeling of liver biomechanical response in unconfined compression, Annals of biomedical engineering 38 (2010) 1789–1800.

[203] Q. Zhang, J. A. Johnson, L. W. Dunne, Y. Chen, T. Iyyanki, Y. Wu, E. I. Chang, C. D. Branch-Brooks, G. L. Robb, C. E. Butler, Decellularized skin/adipose tissue flap matrix for engineering vascularized composite soft tissue flaps, Acta biomaterialia 35 (2016) 166–184.

[204] J. B. Holyoke, W. C. Lobitz Jr, Histologic variations in the structure of human eccrine sweat glands, Journal of Investigative Dermatology 18 (1952) 147–167.

[205] R. Oftadeh, B. K. Connizzo, H. T. Nia, C. Ortiz, A. J. Grodzinsky, Biological connective tissues exhibit viscoelastic and poroelastic behavior at different frequency regimes: application to tendon and skin biophysics, Acta biomaterialia 70 (2018) 249–259.

[206] H. Ramakrishna, Biodegradable Biphasic Scaffolds using Braiding Technology and Surface Treatments for Regeneration of Tendon-Bone Junction Tissue, North Carolina State University, 2019.

[207] S. Butler, S. Kohles, R. Thielke, C. Chen, R. Vanderby, Interstitial fluid flow in tendons or ligaments: a porous medium finite element simulation, Medical and Biological Engineering and Computing 35 (1997) 742–746.

[208] D. H. Cortes, N. T. Jacobs, J. F. DeLucca, D. M. Elliott, Elastic, permeability and swelling properties of human intervertebral disc tissues: A benchmark for tissue engineering, Journal of biomechanics 47 (2014) 2088–2094.

[209] L. Cardoso, S. P. Fritton, G. Gailani, M. Benalla, S. C. Cowin, Advances in assessment of bone porosity, permeability and interstitial fluid flow, Journal of biomechanics 46 (2013) 253–265.

[210] G. Renders, L. Mulder, L. Van Ruijven, T. Van Eijden, Porosity of human mandibular condylar bone, Journal of anatomy 210 (2007) 239–248.

[211] M. W. Beatty, A. K. Ojha, J. L. Cook, L. R. Alberts, G. K. Mahanna, L. R. Iwasaki, J. C. Nickel, Small intestinal submucosa versus salt-extracted polyglycolic acid-poly-l-lactic acid: a comparison of neocartilage formed in two scaffold materials, Tissue engineering 8 (2002) 955–968.

[212] C. D. DiDomenico, M. Lintz, L. J. Bonassar, Molecular transport in articular cartilage—what have we learned from the past 50 years?, Nature Reviews Rheumatology 14 (2018) 393–403.

[213] A. Reyes Valenzuela, G. Bao, A. Vikstrom, K. M. Kost, S. Prakash, L. Mongeau, Polymeric microspheres containing human vocal fold fibroblasts for vocal fold regeneration, The Laryngoscope 131 (2021) 1828–1834.

[214] Y.-L. Chiu, S.-C. Chen, C.-J. Su, C.-W. Hsiao, Y.-M. Chen, H.-L. Chen, H.-W. Sung, ph-triggered injectable hydrogels prepared from aqueous n-palmitoyl chitosan: in vitro characteristics and in vivo biocompatibility, Biomaterials 30 (2009) 4877–4888.

[215] M. Mahmoudzadeh, A. Fassihi, J. Emami, N. M. Davies, F. Dorkoosh, Physicochemical, pharmaceutical and biological approaches toward designing optimized and efficient hydrophobically modified chitosan-based polymeric micelles as a nanocarrier system for targeted delivery of anticancer drugs, Journal of drug targeting 21 (2013) 693–709.

[216] H. Ravanbakhsh, G. Bao, L. Mongeau, Carbon nanotubes promote cell migration in hydrogels, Scientific reports 10 (2020) 1–10.

[217] J. Sundberg, R. Scherer, M. Hess, F. Müller, S. Granqvist, Subglottal pressure oscillations accompanying phonation, Journal of Voice 27 (2013) 411–421.

[218] J. C. Lucero, A theoretical study of the hysteresis phenomenon at vocal fold oscillation onset–offset, The Journal of the Acoustical Society of America 105 (1999) 423–431.

[219] Y. Alsaid, S. Wu, D. Wu, Y. Du, L. Shi, R. Khodambashi, R. Rico, M. Hua, Y. Yan, Y. Zhao, et al., Tunable sponge-like hierarchically porous hydrogels with simultaneously enhanced diffusivity and mechanical properties, Advanced Materials 33 (2021) 2008235.

[220] D. M. Bless, N. V. Welham, Characterization of vocal fold scar formation, prophylaxis and treatment using animal models, Current opinion in otolaryngology & head and neck surgery 18 (2010) 481.

[221] S. Bouhabel, S. Park, K. Kolosova, N. Latifi, K. Kost, N. Y. Li-Jessen, L. Mongeau, Functional analysis of injectable substance treatment on surgically injured rabbit vocal folds, Journal of Voice (2021).

[222] S. H. Lee, K. Y. Shim, B. Kim, J. H. Sung, Hydrogel-based three-dimensional cell culture for organ-on-a-chip applications, Biotechnology progress 33 (2017) 580–589.